NOV 3 1958

Journal of Research

of the

National Bureau of Standards

UNIVERSITY OF MICHIGAN
OCT 29 1958
PHYSICS LIBRARY

AUGUST 1958

VOLUME 61 NUMBER 2

U. S. DEPARTMENT OF COMMERCE
Sinclair Weeks, Secretary
NATIONAL BUREAU OF STANDARDS
A. V. Astin, Director

AUGUST • 1958
VOLUME • 61
NUMBER • 2

JOURNAL OF RESEARCH
of the
NATIONAL BUREAU OF STANDARDS

The National Bureau of Standards

Functions and Activities

The functions of the National Bureau of Standards are set forth in the Act of Congress, March 3, 1901, as amended by Congress in Public Law 619, 1950. These include the development and maintenance of the national standards of measurement and the provision of means and methods for making measurements consistent with these standards; the determination of physical constants and properties of materials; the development of methods and instruments for testing materials, devices, and structures; advisory services to government agencies on scientific and technical problems; invention and development of devices to serve special needs of the Government; and the development of standard practices, codes, and specifications. The work includes basic and applied research, development, engineering, instrumentation, testing, evaluation, calibration services, and various consultation and information services. Research projects are also performed for other government agencies when the work relates to and supplements the basic program of the Bureau or when the Bureau's unique competence is required. The scope of activities is suggested by the listing of divisions and sections on the inside of the back cover.

Publications

The results of the Bureau's work take the form of either actual equipment and devices or published papers. These papers appear either in the Bureau's own series of publications or in the journals of professional and scientific societies. The Bureau itself publishes three monthly periodicals, available from the Government Printing Office: The Journal of Research, which presents complete papers reporting technical investigations; the Technical News Bulletin, which presents summary and preliminary reports on work in progress; and Basic Radio Propagation Predictions, which provides data for determining the best frequencies to use for radio communications throughout the world. There are also five series of nonperiodical publications: The Applied Mathematics Series, Circulars, Handbooks, Building Materials and Structures Reports, and Miscellaneous Publications.

Information on the Bureau's publications can be found in NBS Circular 460, Publications of the National Bureau of Standards ($1.25) and its Supplement ($1.50), available from the Superintendent of Documents, Government Printing Office, Washington 25, D. C.

Order all publications from the Superintendent of Documents
U. S. Government Printing Office, Washington 25, D. C.

Use of funds for printing this publication approved by the Director of the Bureau of the Budget (May 14, 1956)

Journal of Research of the National Bureau of Standards Vol. 61, No. 2, August 1958 Research Paper 2886

Carbon-14 Carboxy-Labeled Polysaccharides[1]

Joseph D. Moyer and Horace S. Isbell

Procedures are given for the preparation of C^{14} carboxydextran and C^{14} carboxyinulin. These materials have C^{14}-labeled carboxyl groups in place of the reducing end groups present in the parent polysaccharides. The substances can be prepared cheaply and should find many applications as tracers in biological and chemical research.

1. Introduction

A process for labeling polysaccharides with carbon-14 was described briefly in a prior note [1][2] and in a patent assigned to the United States Secretary of Commerce [2]. Subsequently, the labeled products have been furnished to research workers in other laboratories, but the procedures for making the compounds have not been described in detail.

The present paper reports the methods used for the production of C^{14} carboxydextran and of C^{14} carboxyinulin. These materials have already found use in the study of adsorption on blood platelets and cells, as well as for the study of kidney function [3, 4]. Other applications can be envisioned and will be realized in the future.

In the labeling process, reducing end groups present in the polysaccharide combine with C^{14}-labeled cyanide; the resulting cyanohydrin, on hydrolysis, yields a polysaccharide having a radioactive carboxyl group. The activity of the labeled product depends on the equivalent weight of the polysaccharide and on the activity of the cyanide used in the synthesis. The radioactive product differs from the parent polysaccharide in that it has a C^{14}-labeled carboxyl group in place of the reducing end group. The presence of a single carboxyl group in a large molecule has little effect on the biological behavior of the substance. Hence the carboxy-labeled polysaccharides can be used as tracers in biological and chemical research. Prior to starting the synthesis, the combining weight of the polysaccharide is determined by reaction with radioactive cyanide by the method already described [5]. The polysaccharide is then treated with C^{14}-labeled cyanide and, after removal of the excess cyanide, the product is isolated. The methods used for purification and isolation of the product depend on the properties of the material being labeled. The procedures described here can be used, with small changes, for almost any water-soluble polysaccharide.

2. Experimental Procedures

2.1. Materials

Carbon-14-labeled cyanide was prepared by the previously described method [6]. The solution used contained 0.065 mM of sodium cyanide plus 0.15 mM of sodium hydroxide per milliliter and had an activity of 1 mc/ml.

The ion-exchange resins used for release of hydrogen cyanide from the reaction mixtures were conditioned by successive treatment with 5-percent aqueous sodium hydroxide, 5-percent aqueous sodium cyanide, water, 5-percent aqueous hydrochloric acid, and water until the wash liquor was neutral and free from chloride.

The clinical dextran was supplied by the Committee on Shock, National Research Council. The sample, designated NRC–3, was part of a supply made for experimental studies by the Commercial Solvents Corporation.

The inulin used was a commercial product. Before labeling, it was recrystallized from water [7].

2.2. Determination of Cyanide-Combining Power

Approximately 5 mg of the lyophilized polysaccharide was placed in a weighed test tube which had been constricted near the middle for sealing in a flame. The sample and tube were dried at 80°C under a pressure of less than 0.1 mm, and the weight of the sample was ascertained. The analyses were set up in triplicate, with controls containing 0.02 mg of D-glucose and with blank determinations having like quantities of the reagents only.

A buffered sodium cyanide–C^{14} solution was prepared from the 0.005 N carbon-14-labeled cyanide solution by adding crystalline sodium bicarbonate equivalent to the excess sodium hydroxide. A three- to five-fold excess of the cyanide solution (approximately 0.1 ml of the solution, containing about 0.2 μc of carbon–14) and 1 drop of toluene were added to each tube. The tube was sealed and stored at room temperature. After 10 days the tube was opened, a few drops of 10 percent aqueous formic acid was added, and the solution was concentrated in a current of air. The residue was dissolved in a few drops of aqueous formic acid, and the solution was frozen and lyophilized to remove the last possible trace of hydrogen cyanide. The material in the tube was dissolved in formamide, and the radioactivity was measured with an internal, gas-flow, proportional counter [8]. The equivalent weight was obtained from the relationship:

$$\text{Equivalent weight}=\frac{(\text{cps})_G \cdot W}{(\text{cps})_W \cdot G}$$

where $(\text{cps})_G$ is the net count of the control containing G millimoles of D-glucose and $(\text{cps})_W$ is the net count for the polysaccharide sample of weight W.

[1] Part of a project on the development of methods for the synthesis of radioactive carbohydrates, sponsored by the Division of Research, Atomic Energy Commission.

[2] Figures in brackets indicate the literature references at the end of this paper.

2.3. Carbon–14 Carboxy-Labeled Carboxydextran

Ten milliliters of a 0.065 *M* sodium cyanide-C^{14} solution was placed in a 100-ml flask containing 2.6 g of lyophilized dextran (NRC–3). The flask was sealed by a glass stopper and a ring of silicone grease. The dextran was dissolved and stored at room temperature.

After 4 days, a 10-μl sample was withdrawn for analysis, and the flask was immediately restoppered. The sample was transferred, together with washings of the pipet, to a small test tube and acidified with 3 drops of 10-percent formic acid. The mixture was evaporated to dryness in a jet of air. To insure complete removal of hydrogen cyanide, the residue was twice dissolved in 0.5 ml of water and reevaporated to dryness. Radioassay of the residue, dissolved in 1 ml of formamide, showed that approximately 0.67 mc of carbon–14 had been fixed. This was 88 percent of the amount expected (0.76 mc) from the specific activity of the cyanide (15.2 mc/mM) and from the cyanide-combining power determined by the method of section 2.2.

The reaction mixture in the 100-ml flask was allowed to stand an additional 3 days to assure completion of the reaction. The liquid was then frozen by immersion of the flask in a liquid-nitrogen bath with gentle swirling. The stopper was removed, 5 ml of conditioned Amberlite IR–120(H) resin [3] was added and the flask, A, was connected to a receiving flask, B, as shown in figure 1. The receiver B contained excess sodium hydroxide solution (1 ml of *N* NaOH). Flasks A and B were immersed in liquid nitrogen and the system was evacuated with an efficient oil pump. Stopcocks E and C were closed, the liquid-nitrogen bath was removed from A, and the contents of the flask were thawed. After thorough mixing, the contents were again frozen in liquid nitrogen. Stopcock E was then opened and the liquid-nitrogen bath was removed from A, but not from B. As the frozen mixture became warmer, water and hydrogen cyanide were transferred to B by lyophilization. After the lyophilization was complete (5 hr), stopcock C was closed, and 10 ml of water was added to A (through funnel D) and mixed with the contents of the flask. The liquid was frozen in liquid nitrogen, the system was evacuated, and the lyophilization process was repeated. Finally, flask A was removed from the apparatus, and flask B, containing the recovered cyanide, was stoppered and set aside for future use.

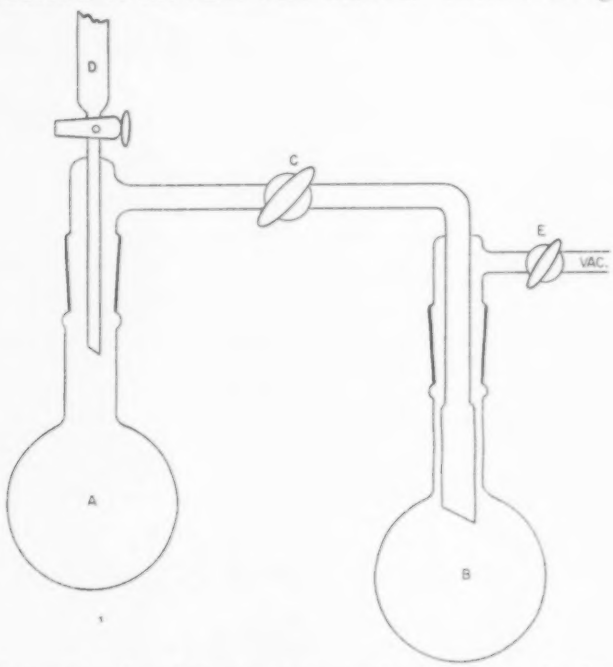

FIGURE 1. *Lyophilization apparatus for the recovery of carbon-14-labeled cyanide.*

The contents of A were passed through a column containing 10 ml of a 1:1 mixture of Amberlite IR–120(H) resin and Duolite A–4 resin.[4] The flask and resin were washed with water. The solution was acidified with a drop of 10-percent acetic acid and lyophilized. The residue was dissolved in 50 ml of water and again lyophilized. (The second lyophilization was to remove the last trace of hydrogen cyanide.) The product weighed 2.29 g and had an activity of 0.28 μc/mg.

2.4. Carbon–14 Carboxy-Labeled Carboxyinulin

Seven grams of finely powdered, lyophilized, recrystallized inulin was added slowly with constant swirling to 43 ml of an ice-cold cyanide solution in a 100-ml flask. The cyanide solution contained 0.47 mM of sodium cyanide–C^{14} (7.2 mc) and 0.3 mM of sodium hydroxide. The flask was capped with an adapter carrying a stopcock for evacuation. The contents were frozen in a liquid-nitrogen bath and the flask was evacuated. The stopcock was closed and the flask was allowed to come to room temperature. It was then heated in a water bath, with constant swirling, until the inulin had dissolved. After two days at room temperature, the inulin that had crystallized from solution was redissolved by warming. This was repeated every other day for 8 days. At this time, an analysis on a 20-μl sample showed that 5.2 mc of carbon–14 had been fixed. This amount corresponds to approximately the activity anticipated from the cyanide-combining power of inulin (previously measured) and the specific activity of the cyanide used.

The contents of the flask were frozen in liquid nitrogen and, after the addition of 5 ml of conditioned Amberlite IRC–50(H) resin, the flask was connected to a second flask (B of fig. 1) containing 1 ml of *N* NaOH. Flasks A and B were immersed in liquid nitrogen, the system was evacuated, and the hydrogen cyanide liberated in A was transferred to B by the procedure described in connection with the preparation of labeled dextran. After removal of all cyanide, the residue in A was extracted at 40° to 50° C with portions of water totaling 150 ml. The solution was filtered and passed through a column containing 5 ml of a 1:1 mixture of Amberlite IRC–50(H) resin and Duolite A–4 resin. The combined

[3] Rohm and Haas Co., Philadelphia, Pa.
[4] Chemical Process Co., Redwood City, Calif

effluent and washing were lyophilized after the addition of 3 drops of acetic acid. The residue was dissolved in 100 ml of warm water. A 20-μl aliquot was removed and counted for radioactivity in 1 ml of formamide; the remainder of the solution was lyophilized. The residue weighed 7.1 g and its radioactivity showed the presence of 5.14 mc.

Elution of the resin column with 5 ml of 5 percent HCl, and washing, resulted in the recovery of 0.16 mc of activity. The cyanide collected in flask B had an activity of 1.08 mc.

The work reported in this paper was part of a thesis submitted by J. D. Moyer to the University of Maryland in partial fulfillment of the requirements for the degree of Doctor of Philosophy. The authors thank Nathan L. Drake of the University of Maryland for helpful advice.

3. References

[1] H. S. Isbell, Science **113,** 2940 (1951).
[2] H. S. Isbell (to United States of America), U. S. Patent 2,653,931 (Sept. 29, 1953).
[3] S. Rothman, E. Adelson, A. Schwebel, and R. D. Langdell, Vox Sanguinis **2,** 104 (1957).
[4] E. Cotlove, M. C. Reder, W. B. Looney, M. Walser, and L. W. Matthews, J. Clin. Invest. **33,** 924 (1954).
[5] J. D. Moyer and H. S. Isbell, Anal Chem. (in press).
[6] J. D. Moyer and H. S. Isbell, Anal. Chem. **29,** 393 (1957).
[7] F. J. Bates and associates, Polarimetry, Saccharimetry and the Sugars, NBS Circ. 440, 397 (1942).
[8] A. Schwebel, H. S. Isbell, and J. D. Moyer, J. Research NBS **53,** 221 (1954), RP2537.

Washington, March 27, 1958.

Journal of Research of the National Bureau of Standards Vol. 61, No. 2, August 1958 Research Paper 2887

Heat of Formation of Sodium Calcium Aluminate

Edwin S. Newman

The compounds $3CaO \cdot Al_2O_3$, Na_2SO_4 V (Thenardite), $Na_2O \cdot 8CaO \cdot 3Al_2O_3$, and $CaSO_4$, anhydrite, were prepared, and their heats of solution in HCl, $26.61H_2O$ were determined. The heat of solution of Na_2SO_4 V in water to form Na_2SO_4, $1000H_2O$ was also measured. From these and other data in the literature the heats of formation of $Na_2O \cdot 8CaO \cdot 3Al_2O_3$ and $NaSO_4$ V were calculated to be -2576 and -330.92 kcal/mole, respectively.

1. Introduction

Investigations of the alkali phases in portland cement clinker, summarized by Newkirk [1],[1] have shown that the compound $Na_2O \cdot 8CaO \cdot 3Al_2O_3$, hereafter abbreviated NC_8A_3,[2] is formed. As part of a continuing investigation of the thermochemical properties of compounds occurring in hydraulic cements and their hydration products, the heat of formation of this compound was determined. No prior thermochemical data on NC_8A_3 have been found. Measurements were made at 25° C of ΔH of the reaction

$$NC_8A_3(c) + CaSO_4(c, \text{anhydrite}) \rightarrow 3C_3A(c) + Na_2SO_4(c.\ V). \quad (1)$$

This reaction occurs spontaneously [4] at high temperatures, where, however, the high-temperature form of calcium sulfate is present and liquid sodium sulfate is formed. The value of ΔH_1 was obtained by measuring the heats of solution of the four substances in hydrochloric acid solution. The heat of formation of NC_8A_2 was calculated from this value of ΔH_1 and the heats of formation of the other three substances taken from the literature.

2. Materials, Apparatus, and Procedure

Tricalcium aluminate was prepared by the method used by Thorvaldson, Brown, and Peaker [2]. The ignition loss of this material after grinding was 0.08 percent, assumed to be water in the compound C_3AH_6 formed by reaction of the anhydrous aluminate with the moisture in the air. Thenardite, Na_2SO_4 V [3], was crystallized from a 50-percent solution of Na_2SO_4 at 50° C by the slow addition of hot alcohol. The mixture was left on the steam bath for 2 hr and then filtered. The crystals were dried overnight at 100° C and ground to pass a No. 100 sieve. They were essentially free from inclusions, as judged by microscopical examination, and the loss in weight on heating for 2½ hr at 950° C was 0.02 percent. In the measurements and calculations, this material was considered to be pure Na_2SO_4. The compound NC_8A_3 was prepared as described by Newkirk [4], except that after heating once at 1,200° C the preparation was autoclaved for several hours at 300 psi before repeated heating at 1,300° C with intervening grinding and sieving. Microscopical examination and chemical analysis indicated that the product was homogenous and of the proper composition. Anhydrite was prepared by first precipitating gypsum from a hot solution of $CaSO_4$ prepared from the hemihydrate and then converting the gypsum to anhydrite by heating for 2 hr at 1,000° C [5].

Details of the calorimetric apparatus and procedure have been given elsewhere [6]. The calorimeter used in this work was a 1-pt wide-mouthed vacuum flask cemented to a metal flange. A brass cover with tubes for stirrer, thermometer, heater, and introduction of the sample was bolted to this flange, and the calorimeter was submerged 4 in. below the surface of a water bath controlled at 25.0° C. The cover was made watertight by means of an O-ring seal. The temperature of the bath remained constant to better than ±0.002° C during a determination. The calorimeter charge was 425.0 g of HCl, $26.61H_2O$ (2.000 normal at 25° C). The starting conditions were so adjusted that the final temperature of the calorimeter was as close as possible to 25.0° C. This procedure was adopted both to avoid the need for correcting the measured heat of solution to the standard temperature of 25° C and to prevent the distillation of water from a warmer surface of the acid solution to condense on a cooler inner surface of the metal cover. Because there was no other free water surface within the flask, condensation in the reverse direction was unlikely.

The weights of the samples for the heat-of-solution determinations were in the proportions required by the stoichiometry of the equation for a weight of 1.42 g of C_3A. First the NC_8A_3 was dissolved in the calorimeter and the final rate of temperature rise determined to complete the measurement of its heat of solution. This final rate became the initial rate for the $CaSO_4$ experiment. The sample of anhydrite was introduced and the determination was completed. This procedure was followed also with a new acid charge for the products on the right side of the equation. Thus the final calorimeter solution for the measurements with the reactants was of the same composition as that for the products, and no dilution experiments were necessary. The experimentally determined energy equivalent of the calorimeter and acid charge was used in computing the heats of solution of NC_8A_3 and C_3A. For $CaSO_4$ and Na_2SO_4 it was increased by 0.28 cal/deg, the estimated heat capacity of the solid previously added. Since this increase was less than 0.1 percent of the total energy equivalent, the error introduced by this approximation was negligible.

[1] Figures in brackets indicate the literature references at the end of this paper.
[2] As usual in papers dealing with portland-cement compounds, the abbreviations C for CaO, A for Al_2O_3, N for Na_2O, and H for H_2O will be used.

TABLE 1. *Heats of solution in 425.0 g of* $HCl \cdot 26.61H_2O$

Sample number	$Na_2O \cdot 8CaO \cdot 3Al_2O_3$(816.51)[a]		$CaSO_4$(136.15)[a]		$3CaO \cdot Al_2O_3$(270.20)[a]		Na_2SO_4 V(142.06)[a]	
	Sample weight	Heat of solution	Sample weight	Heat of solution	Sample weight	Heat of solution	Sample weight	Heat of solution
	g	*cal/g*	*g*	*cal/g*	*g*	*cal/g*	*g*	*cal/g*
1	1.4220	733.52	0.2415	−13.00	1.4200	736.43	0.2515	−32.43
2	1.4233	733.81	.2382	−12.88	1.4189	735.49	.2518	−33.02
3	1.4254	734.05	.2385	−12.36	1.4220	735.27	.2563	−32.82
4	1.4262	734.11	.2378	−12.83	1.4215	735.92	.2526	−32.66
5	1.4276	734.25	.2407	−12.32	1.4228	735.91	.2549	−32.35
Avg		733.95		−12.69		735.80		−32.66
S. D.[b]		0.13		0.14		0.19		0.12
$-\Delta H$	*kcal/mole* 599.28±0.106		*kcal/mole* −1.728 ±0.019		*kcal/mole* 199.11[c] ±0.051		*kcal/mole* −4.640 ±0.017	

[a] Numbers in parentheses are molecular weights. [b] Standard deviation of the average. [c] Corrected for C_3AH_6.

3. Heats of Solution

The results of the measurements of the heats of solution in hydrochloric acid are given in table 1. The negative sign before values in this table indicates that the heat of solution was endothermic. The value shown there for C_2A when corrected for the calculated C_2AH_6 impurity becomes 736.9 cal/g. This value, which was used in computation, may be compared with some previously obtained results. In 1930, Thorvaldson, Brown, and Peaker [2] obtained 736.0 cal/g[3] for the heat of solution of 2.86 g of C_3A in 600.4 g of HCl, $20H_2O$ at 20° C. In 1939 Cirilli [7] obtained 735.1 cal/g for the heat of solution of C_3A in 3.5 N HCl at 25° C. Recently Coughlin [8] obtained 738.0 cal/g for the heat of solution of 1.43 g of C_3A in 1936.2 g of 4.360 M HCl at 30° C. These four values, including the one obtained in this work, are in reasonably good agreement.

No data were found in the literature on the heat of solution of sodium sulfate in hydrochloric acid. Two determinations in this laboratory with larger samples (1.42 g) than were used for the data in table 1 gave values of −32.38 and −31.87 cal/g, respectively.

Newman and Wells [5] obtained −12.75 cal/g for the heat of solution of $CaSO_4$ in HCl, $26.61H_2O$, and Southard [9] obtained −12.28 cal/g in 2.03 N NCl. These values are in substantial agreement with those in table 1.

4. Heats of Formation

From the heats of solution in table 1, the heat for reaction 1 at 25° C is calculated to be $\Delta H_1 = +4.85 \pm 0.19$ kcal/mole. To determine the heat of formation of NC_8A_3 the heats of formation of the other three members of eq 1 must be known.

The heat of formation of C_3A is given as −861 kcal/mole in Circular 500 of the National Bureau of Standards [10]. This value was used in computations. Although Coughlin [8] gave the value −850.04 ±1.23 or −853.46 ±1.23 kcal/mole depending on the value used for the heat of combustion of calcium, these values appear to be low by 3.18 kcal, twice his value for the heat of formation of C_3A from the oxides.

[3] The value given in 20° calories by Thorvaldson, et al., has been recalculated to the thermochemical calory of 4.1840 absolute joules used in this paper.

The heat of formation of Na_2SO_4 V was obtained by measuring its heat of solution in water to form Na_2SO_4,$1000H_2O$, the heat of formation of which is −331.215 kcal [10]. Five determinations gave −293.0 ±2.9 cal/mole for the enthalpy of solution at 25° C. Coughlin's value at 30° C [11], −628.2 cal/mole, was calculated to be −302.2 cal/mole at 25° C. The heat of formation of Na_2SO_4 V was taken as −331.215+0.293=−330.922 kcal/mole.

The heat of formation of $CaSO_4$, anhydrite, is −342.42 kcal/mole [10]. From these values for the heats of formation of C_3A, Na_2SO_4 V, and anhydrite, and the heat of reaction ΔH_1, the heat of formation of NC_8A_3 from the elements at 25° C is calculated to be −2576 kcal/mole.

5. Summary

The compounds $3CaO \cdot Al_2O_3$, Na_2SO_4 V (thenardite), $Na_2O \cdot 8CaO \cdot 3Al_2O_3$, and $CaSO_4$, anhydrite, were prepared, and their heats of solution in $HCl \cdot 26.61H_2O$ were determined. The heat of solution of Na_2SO_4 V in water to form Na_2SO_4,$1000H_2O$ was also measured. From these and other data in the literature the heats of formation of $Na_2O \cdot 8CaO \cdot 3Al_2O_3$ and Na_2SO_4 V were calculated to be −2576 and −330.92 kcal/mole, respectively.

6. References

[1] T. F. Newkirk, Proc. Intern. Symposium on Chem. Cements. 3d Symposium, p. 151, London, 1952 (1954).
[2] T. Thorvaldson, W. G. Brown, and C. R. Peaker, J. Am. Chem. Soc. **52**, 2972 (1930).
[3] F. C. Kracek and R. E. Gibson, J. Phys. Chem., **34**, 18 (1930).
[4] T. F. Newkirk, J. Research NBS, **47**, 349 (1951) RP2261.
[5] E. S. Newman and L. S. Wells, J. Research NBS, **20**, 82 (1938) RP1107.
[6] E. S. Newman and Roald Hoffmann, J. Research NBS, **56**, 313 (1956) RP2681.
[7] V. Cirilli, Ricerca sci., **10**, 459 (1939).
[8] J. P. Coughlin, J. Am. Chem. Soc., **78**, 5479 (1956).
[9] J. C. Southard, Ind. Eng. Chem., **32**, 442 (1940).
[10] F. D. Rossini, D. D. Wagman, W. H. Evans, S. Levine, and I. Jaffe, Selected values of chemical thermodynamic properties, NBS Circ. 500 (1952).
[11] J. P. Coughlin, J. Am. Chem. Soc., **77**, 868 (1955).

WASHINGTON, March 18, 1958.

Thermal Degradation of Polyacrylonitrile, Polybutadiene, and Copolymers of Butadiene With Acrylonitrile and Styrene[1]

Sidney Straus and Samuel L. Madorsky

Polybutadiene and a copolymer consisting of 76.5 percent butadiene and 23.5 percent of styrene were investigated as to the rates of their thermal degradation. The rates for polybutadiene indicated an activation energy of 60 kilocalories per mole. The copolymer had very high initial rates of degradation, followed by a rapid drop, so that it was not possible to obtain a reliable activation energy.

Polyacrylonitrile and a copolymer consisting of 31 percent of acrylonitrile and 69 percent of butadiene were investigated with regard to the nature and distribution of volatile products, as well as to the rates of their thermal degradation. The rates were very high initially, but dropped rapidly so that it was not possible to determine accurately the activation energy. The acrylonitrile-butadiene copolymer showed a decomposition pattern similar to that of polybutadiene. Here, too, the activation energy could not be deduced accurately from the rate curves. Comparative thermal stability in terms of temperature, at which half of the polymer sample is evaporated in 35 minutes of heating, is as follows: 407°C for polybutadiene, 374°C for SBR, 364° C for polystyrene, 369° C for NBR, and 316° C for polyacrylonitrile.

1. Introduction

The copolymers, styrene-butadiene (GR–S) and acrylonitrile-butadiene (nitrile rubber), currently designated in the technical literature as SBR and NBR, respectively, represent two of the more important synthetic rubbers. This paper describes the results of an investigation of the relative thermal stability and of the products of degradation obtained when these rubbers are pyrolyzed in a vacuum. A similar description is given of the thermal behavior of polyacrylonitrile and polybutadiene.

Details of the method employed in this investigation have been described previously [1–5].[2] The method consists of two parts. In the first part, a sample weighing 25 to 50 mg is heated in a vacuum, first for 5 min during a heating-up period, then for 30 min at a constant temperature; the residue is weighed, and the volatile products fractionated. The fractions are then weighed and analyzed in the mass spectrometer or tested for average molecular weight by a microcryoscopic method. In the second part, a 4 to 5 mg sample in a platinum crucible suspended from a very sensitive tungsten spring balance [3] is heated in a vacuum, and the rate of loss of weight of the sample is observed at intervals. The activation energy of degradation is calculated from the initial rates by using the Arrhenius equation.

2. Thermal Degradation of Polybutadiene and SBR

A study of the relative thermal stability of polybutadiene and the copolymer SBR, and of yields and chemical nature of the products resulting from pyrolysis of these two materials, has been reported previously [2,4]. Polybutadiene was found to be more stable than the copolymer. The ratios of small molecular fragments to large ones were 14:84 for polybutadiene and 12:88 for SBR.

In this investigation a study was made of rates of thermal degradation of these two substances by the loss-of-weight method, using a very sensitive tungsten spring balance enclosed in a vacuum [3]. Samples of polybutadiene and of SBR (76.5% of butadiene and 23.5% of styrene), weighing about 5 mg, were used. The materials were prepared by purifying commercial products using a method which has been described previously [2].

Results of rate studies for polybutadiene are shown in figure 1. About 12 to 16 percent of the samples was vaporized at zero time; this vaporization took place during the approximately 15 min heating-up period. Zero time in these experiments was reckoned from the moment the sample had reached the operat-

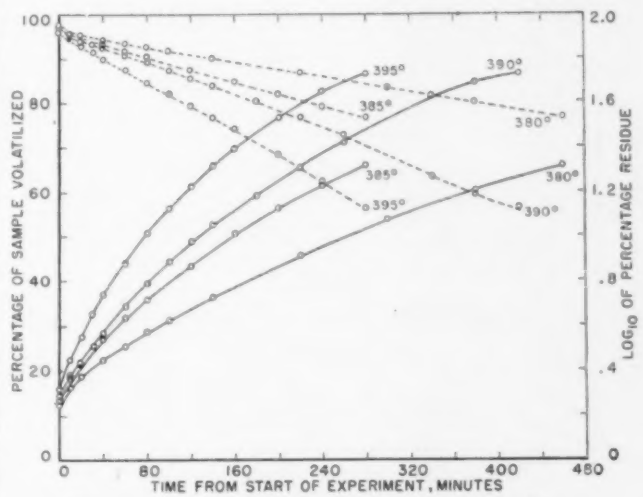

FIGURE 1. *Thermal degradation of polybutadiene.*

Solid lines represent percentage volatilization versus time and dashed lines represent logarithm of percentage residue versus time.

[1] Presented before the 132d Meeting of the American Chemical Society, New York, N. Y., September 7-12, 1957.

[2] Figures in brackets indicate the literature references at the end of this paper.

ing temperature. The fact that the logarithm of percentage residue versus time curves deviate only slightly from straight lines indicates that the reaction involved in the thermal degradation of polybutadiene approaches first order.

In figure 2 rate of volatilization is plotted versus amount volatilized. The apparent initial rates are obtained by extrapolating the straight parts of the rate curves to the ordinate. These rates, in percentage of sample per minute, are 0.21, 0.31, 0.42, and 0.63 for temperatures 380°, 385°, 390°, and 395° C, respectively. On plotting logarithm of the initial rates versus the inverse of absolute temperature, a straight line is obtained, whose slope indicates an activation energy of 62 kcal/mole.

Percentage volatilization of SBR versus time is shown plotted in figure 3 (solid lines). Here again there is considerable loss of weight during the heating up period. Plots of logarithm of percentage residue versus amount volatilized (dashed lines) deviate considerably from straight lines. The reaction involved in the thermal degradation of SBR appears to be more complicated than that for polybutadiene and the reaction is far from first order. Rate of volatilization versus amount volatilized is shown in figure 4. The rates, very high initially, drop rapidly with extent of volatilization. It is not possible to determine with any accuracy the activation energy from these rate curves.

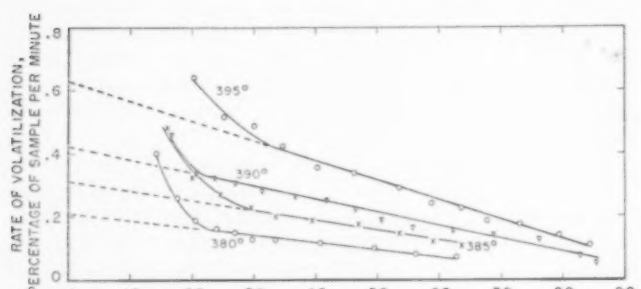

FIGURE 2. *Rates of volatilization of polybutadiene.*

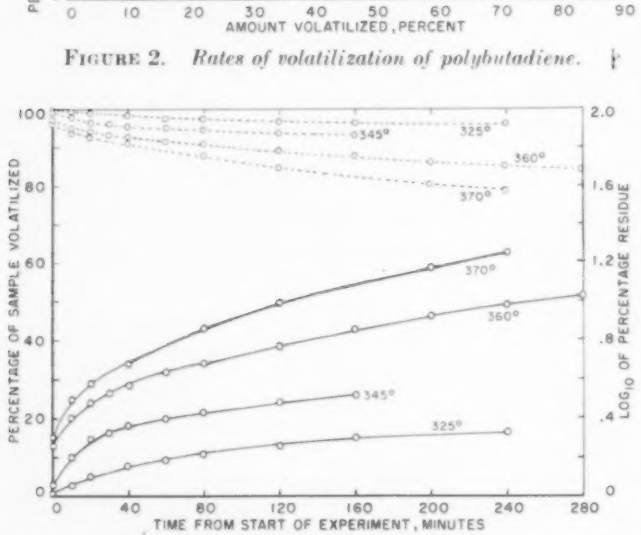

FIGURE 3. *Thermal degradation of SBR.*

Solid lines represent percentage volatilization versus time and dashed lines represent logarithm of percentage residue versus time.

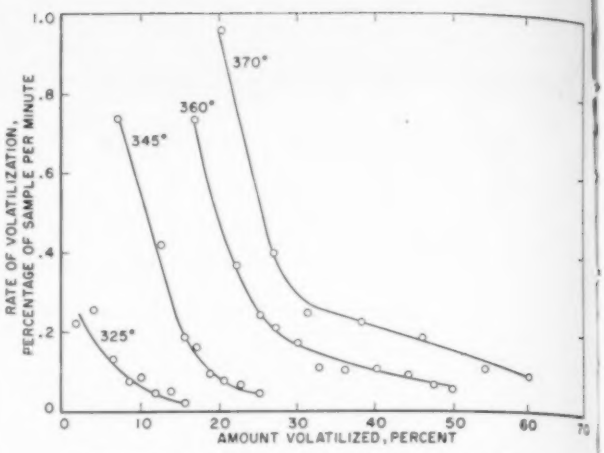

FIGURE 4. *Rates of volatilization of SBR.*

3. Thermal Degradation of Polyacrylonitrile and NBR

The polyacrylonitrile [3] of high purity and in the form of a fine white powder, had a number-average molecular weight of about 40,000. The NBR rubber was Goodrich Hycar 1042 consisting of about 30 percent of acrylonitrile and 70 percent of butadiene. The rubber was extracted for 24 hr with ethanol-toluene azeotrope in order to remove impurities. It was then kept in a vacuum at 60 to 70° C for 5 hr. The purified material analyzed 8.2 percent of nitrogen, which corresponds to 31 percent of acrylonitrile. Specimens of polyacrylonitrile and NBR were heated prior to pyrolysis, in a vacuum at 110° C to a constant weight.

Results of pyrolysis are shown in table 1. Fraction V_{-190} [4] represented less than 0.1 percent of the total volatilized and is not shown in this table. As in the case of many other polymers the ratio $V_{25}:V_{pyr}$ remained constant throughout the temperature range. On the average, this ratio is 12 :88 in the case of polyacrylonitrile, and 14 :86 in the case of NBR. In the latter case, in calculating the average ratio, results of experiment 1 were excluded, because volatilization was only 9 percent.

As seen from table 1, volatilization of polyacrylonitrile stabilizes at about 70 to 73 percent. This is in agreement with the work of Kern and Fernow [6], who found that dry distillation of this material was accompanied by carbonization of the residue. A possible explanation of this stabilization, as given by McCartney [7] and Houtz [8], is the formation, along the chain, of ring structures involving nitrogen from the CN groups. NBR, which contains only 31 percent of acrylonitrile, does not show any stabilization through the entire temperature range.

Fractions V_{pyr} from polyacrylonitrile and NBR had a tan waxlike appearance. They were not readily soluble in ordinary organic solvents, including

[3] The authors are indebted to C. A. Sperati of the Polychemicals Department, E. I. duPont de Nemours & Co., for supplying them with this polymer, which is used in the production of orlon fiber.

[4] For definition of fractions see footnote to table 1.

TABLE 1. *Pyrolysis of polyacrylonitrile and NBR*

Experiment number	Temperature	Volatilization	Volatile fractions [a] based on total volatilized	
			V_{pyr}	V_{25}
POLYACRYLONITRILE				
	°C	%	%	%
1	250	21.5	86.3	13.7
2	250	20.7	89.1	10.9
3	250	18.0	89.0	11.0
4	275	34.9	88.0	12.0
5	300	46.6	86.3	13.7
6	325	53.4	88.4	11.6
7	325	52.3	88.6	11.4
8	325	49.7	87.4	12.6
9	325	50.6	88.8	11.2
10	350	57.7	88.7	11.3
11	350	57.9	87.8	12.2
12	400	67.7	90.1	9.9
13	425	70.2	87.2	12.8
14	455	72.8	88.3	11.7
Average	----	----	88.1	11.9
NBR				
1	310	9.1	74.0	26.0
2	350	29.4	84.5	15.5
3	365	64.5	87.8	12.2
4	380	80.0	84.7	15.3
5	400	95.0	84.8	15.2
Avg (2 to 5 incl.)	----	----	85.5	14.5

[a] The following volatile fractions were collected: V_{pyr}, volatile at the temperature of pyrolysis, but not at 25° C; V_{25}, volatile at 25° C, but not at −190°. In the case of other polymers it was usually found necessary to separate this fraction into two parts to facilitate mass spectrometer analysis. Here it was found unnecessary to do so; V_{-190}, volatile at −190° C.

pyridine. Average molecular weight by the microcryoscopic method in diphenylamine was 330 ±9 for polyacrylonitrile and 401 ±3 for NBR.

Fraction V_{-190} from pyrolysis of polyacrylonitrile was analyzed in the mass spectrometer. This fraction consisted of hydrogen. The V_{-190} fraction from NBR was too small for analysis.

Fraction V_{25} from pyrolysis of polyacrylonitrile when first collected was a milky-white liquid. The color of the liquid changed after standing, first to tan and then to brown. Results of mass spectrometer analysis of this fraction are shown in table 2. V_{25} fractions that collected in experiments 1, 4, 5, 11, 13, and 14 were analyzed within 1 to 2 hours after they were collected. The time interval between collection and analysis was 1 day for experiments 2 and 7, and 1 week for experiments 3 and 8.

The main constituents in V_{25} are HCN, acrylonitrile, and vinylacetonitrile. The composition of V_{25} seems to depend on the time interval elapsing between pyrolysis and analysis. This suggests the possibility that some of the components, particularly HCN and acrylonitrile, react and become nonvolatile on standing and, as a result, the remaining volatile constituents become accentuated in the analysis. This could explain why Houtz [8] reported that pyrolysis at 400° C yielded only a trace of HCN. On the other hand, Hideo Nagao and coworkers [9] reported the evolution of a considerable amount of HCN when polyacrylonitrile was heated at temperatures from 200° to 350° C in an atmosphere of air or nitrogen. Burlant and Parsons [10] found ammonia as one of the decomposition products from pyrolysis of polyacrylonitrile. We could not find ammonia in the volatiles.

Results of mass spectrometer analysis of V_{25} from NBR are shown in table 3. Two of the analyses were made shortly after the fractions were collected and kept at the temperature of liquid N_2, a third one after an interval of 3 days at room temperature, and a fourth one after an interval of 8 days at the same temperature. All the analyses were similar and the average results are shown in table 3. The results

TABLE 3. *Mass-spectrometer analysis of V_{25} from pyrolysis of nitrile rubber*

Formula of component	Average of 4 analyses
	Mole %
C_2H_6	9.1
C_2H_8	4.7
C_3H_4	3.0
C_3H_6	2.9
C_4H_6	14.1
C_4H_8	8.3
C_4H_{10}	3.3
C_5H_6	2.5
C_5H_8	9.1
C_5H_{10}	4.8
C_5H_{12}	1.6
C_6H_6	4.3
C_6H_8	6.6
C_6H_{10}	5.4
C_6H_{12}	2.7
C_7 to C_{10} inclusive	17.6
Total	100.0

TABLE 2. *Mass-Spectrometer analysis of V_{25} from pyrolysis of polyacrylonitrile*

Component	Time interval between end of experiment and analysis									
	1 to 2 hours						1 day		1 week	
	Expt. 1 [a]	Expt. 4	Expt. 5	Expt. 11	Expt. 13	Expt. 14	Expt. 2	Expt. 7	Expt. 3	Expt. 8
	Mole %	*Mole %*	*Mole %*	*Mole %*	*Mole %*	*Mole %*	*Mole %*	*Mole %*	*Mole %*	*Mole %*
Hydrogen cyanide	34	22	16	68	66	63	------	28	------	------
Acrylonitrile	36	45	49	10	7	6	------	------	------	------
Vinylacetonitrile	30	30	32	13	13	12	88	63	86	59
Pyrrole	------	3	3	------	------	------	12	------	14	------
Acetonitrile	------	------	------	3	6	10	------	------	------	22
Butyronitrile	------	------	------	2	------	3	------	------	------	------
Propionitrile	------	------	------	4	8	6	------	9	------	19
Total	100	100	100	100	100	100	100	100	100	100

[a] Experiment numbers are the same as those given in table 1.

resemble those obtained previously for butadiene and SBR (formerly GR–S) [2]. It is rather surprising that none of the products characteristic of polyacrylonitrile pyrolysis showed up in these analyses, although two of the analyses were made shortly after the fractions were prepared and were kept in liquid N_2 until the time of analysis. It is likely that in the presence of unsaturated fragments resulting from pyrolysis of the butadiene in the copolymer, the hydrogen cyanide, acrylonitrile, and vinylacetonitrile, polymerize more rapidly than in their absence, and therefore do not show up in the analysis of the acrylonitrile-butadiene copolymer.

A comparison of thermal stabilities of the various polymers and copolymers discussed in this paper, and also of polystyrene, is shown in figure 5. The curves for polyacrylonitrile and NBR are based on data in table 1, and those for polystyrene, SBR, and polybutadiene were taken from figure 1 of reference [4]. The temperature, T_h°C, at which the sample loses half of its weight by vaporization in 35 min, can serve as a basis of comparison of thermal stability of polymers.

Results of rate studies in the tungsten spring balance are shown for polyacrylonitrile in figures 6 and 7. In figure 6, percentage of volatilization is plotted versus time from start of experiment. At lower temperatures, a considerable initiation period is observed. Beyond this period volatilization proceeds rapidly, but soon drops to a very small value, indicating stabilization of the residue. At higher temperatures the initiation period terminates during the 15-min heating-up period and the curves show stabilization of the polymer soon after the sample reaches the operating temperature. These facts can be observed more easily in figure 7, where rate of volatilization in percent of the original sample per minute is plotted against percentage volatilization. It is not possible to estimate with any degree of accuracy the initial rates or the activation energy based on any of the rates shown in figure 7.

Results of rate studies for NBR are shown plotted in figure 8, where percentage volatilization is plotted

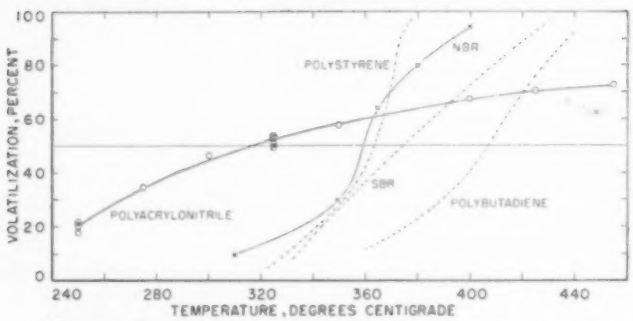

FIGURE 5. *Relative thermal stability of polymers and copolymers.*

Curves for polystyrene, SBR, and polybutadiene were taken from figure 4 of reference [4]. The T_A values are as follows: 407° C for polybutadiene, 374° C for SBR, 364° C for polystyrene, 360° C for NBR, and 316° C for polyacrylonitrile.

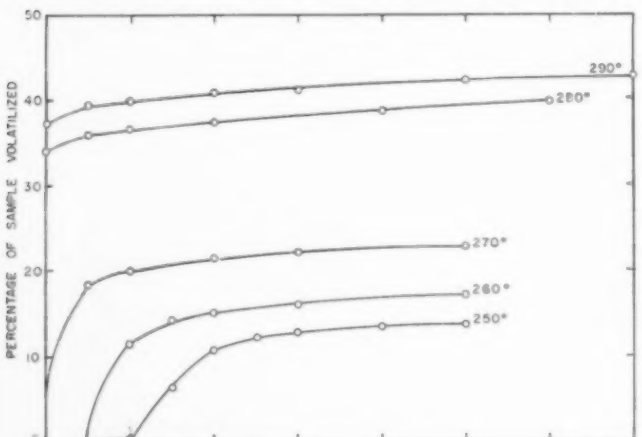

FIGURE 6. *Thermal degradation of polyacrylonitrile.*

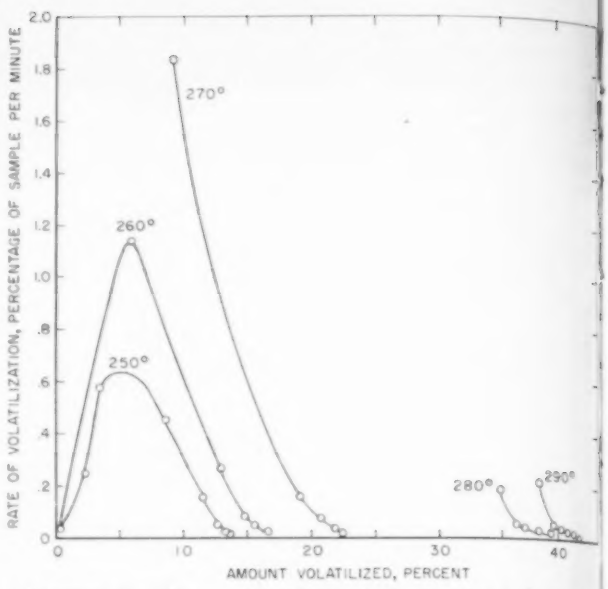

FIGURE 7. *Rates of volatilization of polyacrylonitrile.*

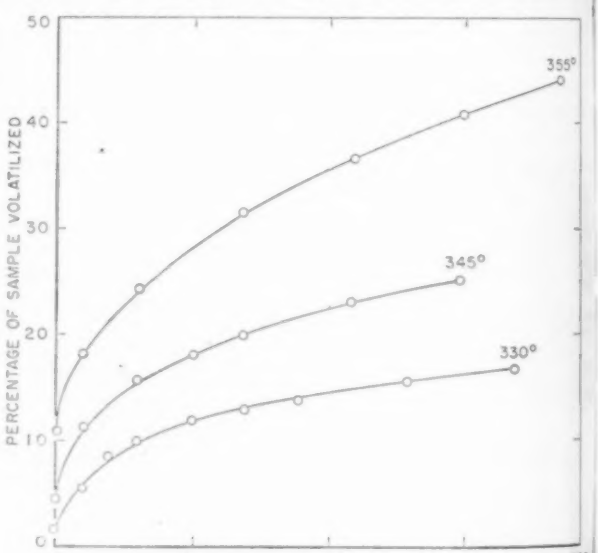

FIGURE 8. *Thermal degradation of NBR.*

versus time from start of experiment, and in figure 9, where rate of volatilization in percent of original sample per minute is plotted versus percentage volatilization. The two sets of curves resemble closely those for SBR shown above (figs. 3 and 4), and no definite conclusion as to initial rates and activation energy can be based on these curves.

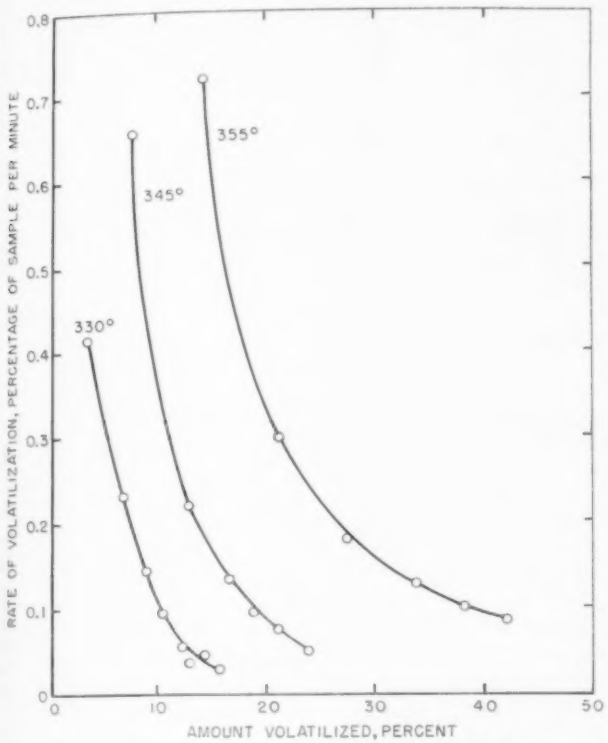

FIGURE 9. *Rates of volatilization of NBR.*

4. Discussion

The main constituents of the light volatile fraction V_{25} obtained in the pyrolysis of polyacrylonitrile, are hydrogen cyanide, acrylonitrile, and vinylacetonitrile. The hydrogen cyanide most likely forms by splitting-off the chain in the same manner as CH_3COOH in the pyrolysis of polyvinyl acetate [11], HCl in the pyrolysis of polyvinyl chloride [12], and HF in the pyrolysis of hydrofluoroethylene polymers [13].

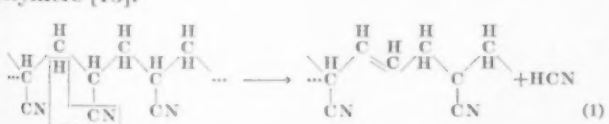

Formation of monomer can be visualized as follows. A random scission of a C—C bond in the chain results in two free radical ends.

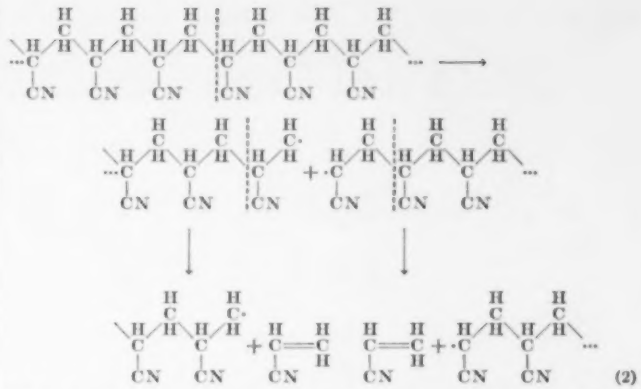

This is followed by an unzipping reaction yielding monomers, as shown in eq (2).

Formation of vinylacetonitrile could be explained if we assume a head-to-head arrangement at some positions in the chain, as shown in eq (3).

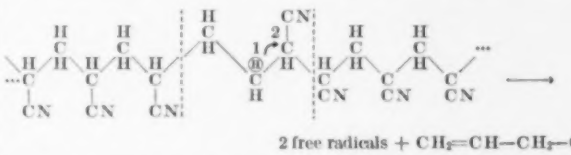

This formation involves 2 C—C scissions in the chain, followed by a hydrogen transfer from position 1 to position 2.

The pyrolysis curves for polyacrylonitrile (fig. 5) as well as the rate curves (figs. 6 and 7) show stabilization during pyrolysis. This is characteristic of polymers in which the loss of side groups from adjacent carbons of the chain results in conjugated double bonds in the chain, since these double bonds tend to enhance the thermal stability of the chain. Polyvinyl chloride [12] and polyvinylidene fluoride [13] may be cited as examples of a behavior similar to that of polyacrylonitrile.

5. References

[1] S. L. Madorsky and S. Straus, J. Research NBS **40,** 417 (1948) RP1886.

[2] S. L. Madorsky, S. Straus, D. Thompson, and L. Williamson, J. Research NBS **42,** 499 (1949) RP1989.

[3] S. L. Madorsky, J. Polymer Sci. **9,** 133 (1952); **11,** 491 (1953).

[4] S. Straus and S. L. Madorsky, J. Research NBS **50,** 165 (1953) RP2405.

[5] S. Straus and S. L. Madorsky, Ind. Eng. Chem. **48,** 1212 (1956).

[6] W. Kern and H. Fernow, J. prakt. Chem. **160,** 281 (1942); Rubber Chem. and Technol. **17,** 356 (1944).

[7] J. McCartney, Polymer degradation mechanisms, NBS Circ. **525,** 123 (1950).

[8] R. Houtz, Textile Research J. **20,** 786 (1950).

[9] Hideo Nagao, Moriya Uchida, and Teruo Yamaguchi, Kôgyô Kagaku Zasshi **59,** 698 (1958).

[10] W. J. Burlant and J. L. Parsons, J. Polymer Sci. **22,** 249 (1956).

[11] N. Grassie, Trans. Faraday Soc. **48,** 379 (1952); **49,** 835 (1953).

[12] R. R. Stromberg, S. Straus, and B. G. Achhammer (unpublished paper).

[13] S. L. Madorsky, V. E. Hart, and S. Straus, J. Research NBS **51,** 327 (1953) RP2461.

WASHINGTON, March 5, 1958.

Journal of Research of the National Bureau of Standards Vol. 61, No. 2, August 1958 Research Paper 2889

On the Motion of Two Cylinders in an Ideal Fluid*

Lloyd H. Carpenter

The complex potential of two cylinders moving in an infinite liquid is determined by the method of image doublets, and the solution is expressed as an infinite series in rectangular coordinates. Approximate solutions in finite form are given for various cases. A method for generalizing the solution for the case of more than two cylinders is indicated. Applications to the flow induced by a cylinder moving in the presence of plane boundaries are given and the stream lines are illustrated in certain cases.

1. Introduction

The problem of the motion of two cylinders in any manner with their axes always parallel was apparently first solved by Hicks.[1] The velocity potentials are found in general as definite integrals, which, when the cylinders move as a rigid body, are expressed in finite form as elliptic functions of bipolar coordinates. Greenhill [2] has expressed the solution as an infinite series in bipolar coordinates.

In a problem in wave motion the need arose for a solution of the potential flow for a cylinder moving parallel to a plane boundary. The problem is the same as that of two parallel cylinders of equal radii moving with equal velocities normal to the line of centers. Thus the flow is a special case of the classic results obtained by Hicks and Greenhill. However, it was necessary to have the potential function represented in rectangular coordinates to determine the additional term representing the wave motion. The bipolar coordinates used by Hicks and Greenhill are defined geometrically, and the transformation to rectangular coordinates does not admit a convenient representation. Therefore, the solution was obtained by the method of image doublets and is here generalized to the case of two cylinders moving in any manner with their axes always parallel. The present method may also be applied to the motion of more than two cylinders which was not done in the bipolar system with either Hicks' or Greenhill's analysis.

Only ideal fluids without vorticity are considered in this study.

2. Solution for Two Cylinders

Consider two parallel cylinders C and C' of radii b and b' momentarily at a distance f apart moving normal to their axes in a liquid at rest at infinity. Choosing the coordinate system as in figure 1, the cylinder velocities may be expressed as $Ue^{i\alpha}$ and $U'e^{i\alpha'}$, respectively.

The complex potential $w_0=\phi_0+i\psi_0$ due to C, in the absence of C', is that of a doublet whose axis is in the direction α

$$w_0=Ub^2\frac{e^{i\alpha}}{z}, \tag{1}$$

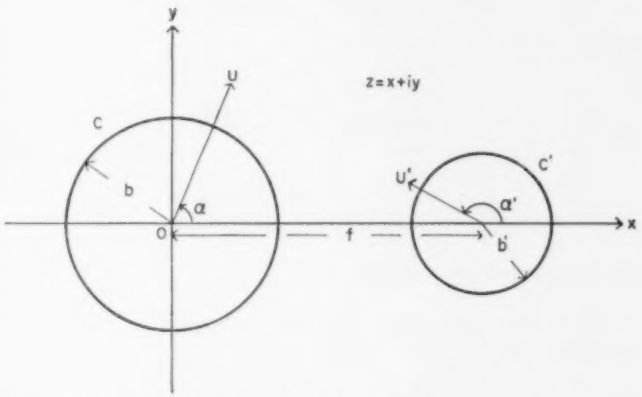

FIGURE 1. *Notation diagram for motion of two cylinders in an infinite liquid.*

where z is the complex coordinate position. The normal velocities introduced on C' by w_0 are cancelled by the image doublet whose axis is in the direction $\pi-\alpha$

$$w_1=-Ub^2\left(\frac{b'}{f}\right)^2\frac{e^{-i\alpha}}{z-(f-f_1)} \tag{2}$$

where

$$f_1=\frac{(b')^2}{f}. \tag{3}$$

The sum w_0+w_1 is the well known expression for the potential of a doublet in the presence of a cylinder (see Milne-Thomson [3]). Similarly, the normal velocities introduced on C by w_1 are cancelled by the second image doublet

$$w_2=Ub^2\left(\frac{b'}{f}\right)^2\left(\frac{b}{f-f_1}\right)^2\frac{e^{i\alpha}}{z-f_2} \tag{4}$$

where

$$f_2=\frac{b^2}{f-f_1}. \tag{5}$$

Continuing, an infinite sequence of image doublets of decreasing strength is obtained. The general expression for w_k is

*This problem was encountered in connection with a wave investigation sponsored by the Office of Naval Research, and the present account is published in order to make more convenient formulas available.

[1] W. M. Hicks, On the motion of two cylinders in a fluid, Quart. J. Pure and Appl. Math. **16**, 113 (1879).

[2] A. G. Greenhill, Functional images in Cartesians, Quart. J. Pure and Appl. Math. **18**, 231 (1882).

[3] L. M. Milne-Thomson, Theoretical Hydrodynamics, Article 8.82, p. 221 (MacMillan & Co., Ltd., London, 1938).

$$w_k=\left\{\begin{array}{l}\beta_k\dfrac{e^{i\alpha}}{z-f_k}\text{ for }k\text{ even}\\[2ex]\beta_k\dfrac{e^{-i\alpha}}{z-(f-f_k)}\text{ for }k\text{ odd}\end{array}\right\} \tag{6}$$

where $\beta_0=Ub^2$, $\beta_1=-Ub^2\left(\dfrac{b'}{f}\right)^2$,

$$\beta_k=\frac{(bb')^2}{(f-f_{k-2})^2(f-f_{k-1})^2}\beta_k-2 \tag{7}$$

and

$$f_k=\left\{\begin{array}{l}\dfrac{b^2}{f-f_{k-2}}\text{ for }k\text{ even}\\[2ex]\dfrac{(b')^2}{f-f_{k-1}}\text{ for }k\text{ odd}\end{array}\right\} \tag{7a}$$

it being understood $f_0=0$.

Similarly, starting with the potential of C' in the absence of C,

$$w_0'=U'(b')^2\frac{e^{i\alpha'}}{z-f'} \tag{8}$$

$$w_1'=-U'(b')^2\left(\frac{b}{f}\right)^2\frac{e^{-i\alpha'}}{z-f_1'} \tag{9}$$

and

$$w_k'=\left\{\begin{array}{l}\beta_k'\dfrac{e^{i\alpha'}}{z-(f-f_k')}\text{ for }k\text{ even}\\[2ex]\beta_k'\dfrac{e^{-i\alpha'}}{z-f_k'}\text{ for }k\text{ odd}\end{array}\right\} \tag{10}$$

where

$$\beta_0'=U'(b')^2,\beta_1'=-U'(b')^2\cdot\left(\frac{b}{f}\right)^2$$

$$\beta_k'=\frac{(bb')^2}{(f-f_{k-2}')^2(f-f_{k-1}')^2}\beta_{k-2}' \tag{11}$$

and

$$f_k'=\left\{\begin{array}{l}\dfrac{(b')^2}{f-f_{k-1}'}\text{ for }k\text{ even}\\[2ex]\dfrac{b^2}{f-f_{k-1}'}\text{ for }k\text{ odd}\end{array}\right\} \tag{11a}$$

and again $f_0'=0$.

Thus the complex potential $w=\phi+i\psi$ for the motion of two cylinders is

$$w=\sum_{k=0}^{\infty}(w_k+w_k') \tag{12}$$

where the w_k are obtained from eq (1) through (7) and the w_k' from eq (8) through (11).

3. Approximate Solutions

The series (12) converges rapidly for small values of bb'/f^2 so that for this case one or two terms of the series gives a close approximate solution

$$w\approx w_0+w_0'+w_1+w_1'\text{ for }\frac{bb'}{f^2}\text{ small.} \tag{13}$$

For larger values of bb'/f^2 a more accurate solution may be obtained by approximating the remaining terms. For this purpose let

$$\left.\begin{array}{l}\eta=\lim\limits_{k\to\infty}f_k\ (k\text{ odd})=\lim\limits_{k\to\infty}f_k'\ (k\text{ even})\\[1ex]\eta'=\lim\limits_{k\to\infty}f_k\ (k\text{ even})=\lim\limits_{k\to\infty}f_k'\ (k\text{ odd})\end{array}\right\} \tag{14}$$

The conditions

$$(f-\eta')\eta=b^2 \tag{15}$$

$$(f-\eta)\eta'=(b')^2 \tag{16}$$

and $\eta\leq b$, $\eta'\leq b'$ may be used to determine η and η'.

Now for k greater than some number n replace f_k by η' for k even, by η for k odd, and replace f_k' by η for k even, by η' for k odd giving

$$w_k\approx\frac{(bb')^2}{(f-\eta)^2(f-\eta')^2}w_{k-2}=\beta w_{k-2} \tag{17}$$

and

$$w_k'\approx\beta w_{k-2}' \tag{18}$$

for k sufficiently large. Thus the solution from (12) would be

$$w\approx\sum_{k=0}^{n}(w_k+w_k')+\{w_{n-1}+w_{n-1}'+w_n+w_n'\}\frac{\beta}{1-\beta} \tag{19}$$

because

$$\sum_{k=1}^{\infty}\beta^k=\frac{\beta}{1-\beta}, \tag{20}$$

An accurate solution for any value of bb'/f^2 can be obtained from eq (19) by an appropriate choice of n. It was found in the computations for the examples to follow that for $bb'/f^2=1/16$, $n=1$ gave an accurate result, and for the extreme case $bb'/f^2=1/4$ an accurate solution was obtained for $n=3$.

Again when bb'/f^2 is sufficiently small η and η' are negligible so that eq (19) reduces to

$$w\approx\{w_0+w_1+w_0'+w_1'\}\frac{1}{1-\left(\dfrac{bb'}{f^2}\right)^2} \tag{21}$$

where w_0, w_1, w_0', and w_1' are given by eq (1), (2), (8), and (9) after setting f_1 and f_1' equal to zero.

4. More Than Two Cylinders

When more than two cylinders are moving in an infinite liquid the method of solution is completely analogous to that given in section 2.

If n cylinders are moving in a liquid choose any one C_R as a reference and introduce an appropriate coordinate system. The complex potential of C_R in the absence of the other cylinders will be that of a doublet $w_{R,0}$. The image of $w_{R,0}$ is taken in each of the remaining $n-1$ cylinders in the same manner as before. Each of these $n-1$ image doublets will have an image in C_R and in each of the other cylinders as well. The process is continued in this manner with each doublet introducing $n-1$ image doublets at each step. The same process is applied starting with each of the $n-1$ remaining cylinders. Again the potential of the system will be the sum of the potentials of all the doublets. An application of this method will be given in section 6.

5. Cylinder Near a Plane Boundary

If $b^1=b$, $U'=U$, $\alpha'=\pi-\alpha$ the plane equidistant between the cylinder axes is a streamline and the solution represents the flow induced by a cylinder moving in the presence of a plane boundary. Figure 2 shows the streamlines for a cylinder moving toward a wall, $\alpha=0$.

The equations can be simplified when the cylinder moves parallel to the wall, $\alpha=\pi/2$, with its circumference touching the wall, $b/f=1/2$. In this case the complete solution is

$$w=iUb\sum_{k=0}^{\infty}\frac{1}{(k+1)^2}\left\{\frac{1}{\frac{z}{b}-k+1}+\frac{1}{\frac{z}{b}-k+1}\right\} \quad (22)$$

An approximate solution is obtained by taking n terms of the series and in the remaining terms replacing $k/(k+1)$ and $(k+2)/(k+1)$ by 1. Thus

$$w\approx iUb\sum_{k=0}^{n}\frac{1}{(k+1)^2}\left\{\frac{1}{\frac{z}{b}-k+1}+\frac{1}{\frac{z}{b}-k+1}\right\}$$

$$+iUb\frac{2}{\frac{z}{b}-1}\left\{\frac{\pi^2}{6}-\sum_{k=0}^{n}\frac{1}{(k+1)^2}\right\}. \quad (23)$$

The streamlines are shown in figure 3a. The computations were made with $n=3$. The streamlines for figure 3b were obtained by superposing a velocity $-U$ on the cylinder and the liquid.

The streamlines for liquid flowing around a cylinder parallel to a plane wall are shown in figure 4. Equation (19) was used with $n=1$, $\alpha=\pi/2$, $b/f=1/4$.

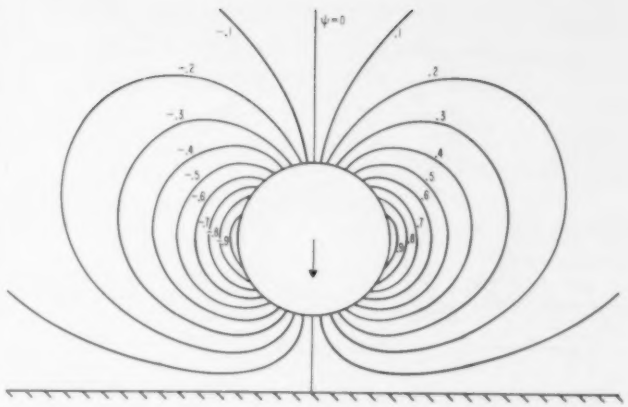

FIGURE 2. *Streamlines for cylinder moving toward a plane boundary.*

$U=1, b=1.$

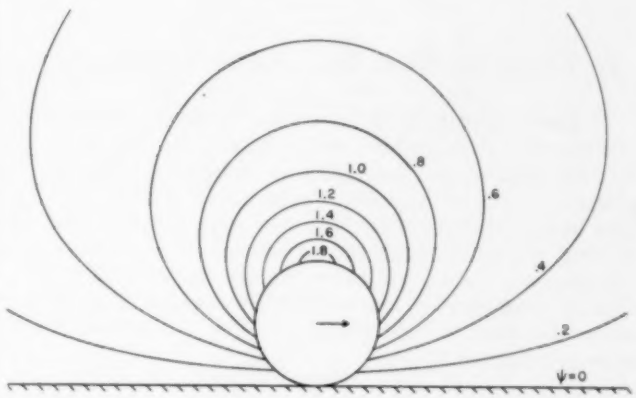

FIGURE 3a. *Streamlines for cylinder moving parallel to a plane boundary when the cylinder touches the boundary.*

$U=1, b=1.$

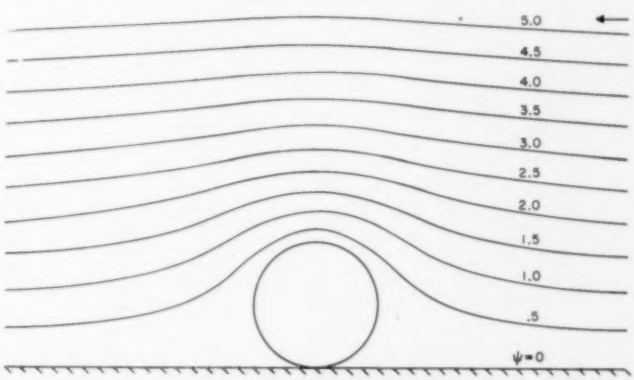

FIGURE 3b. *Streamlines for current flowing with general velocity U past a fixed cylinder against a plane boundary.*

Obtained from figure 3a by impressing a velocity $-U$ on the fluid and the cylinder. $U=1, b=1.$

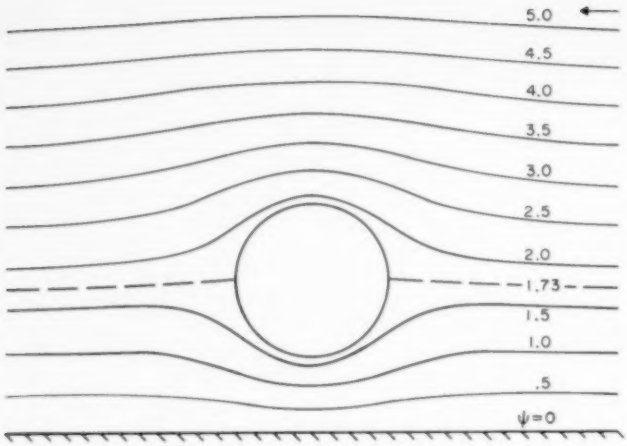

FIGURE 4. *Streamlines for current flowing with general velocity U past a fixed cylinder near a plane boundary.*

$U=1, b=1$.

6. Cylinder Near Two Plane Boundaries

If four cylinders of equal radii have symmetric positions and velocities with respect to two perpendicular planes as indicated in figure 5, then each plane is a streamline and the solution represents the flow induced by a cylinder moving in the presence of two perpendicular plane boundaries. Considering the case $f=4a$, $g=4a$, $\alpha=0$, an approximate solution is obtained by the method of section 4 stopping after the first set of images. The streamlines are shown in figure 6.

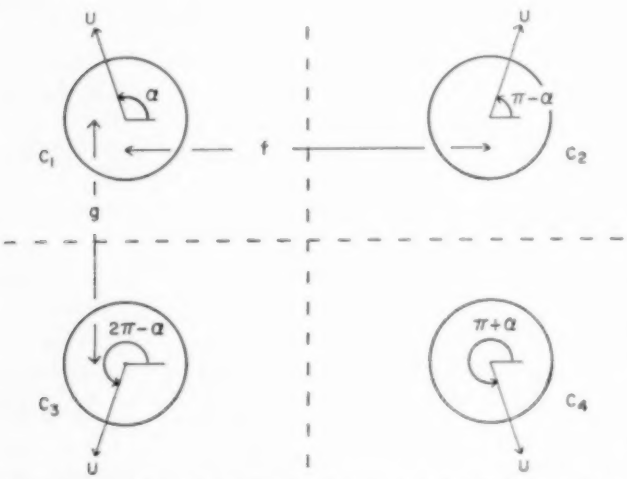

FIGURE 5. *Notation diagram for motion of a cylinder near two perpendicular plane boundaries.*

The dotted lines indicate the streamlines that can be considered as solid boundaries.

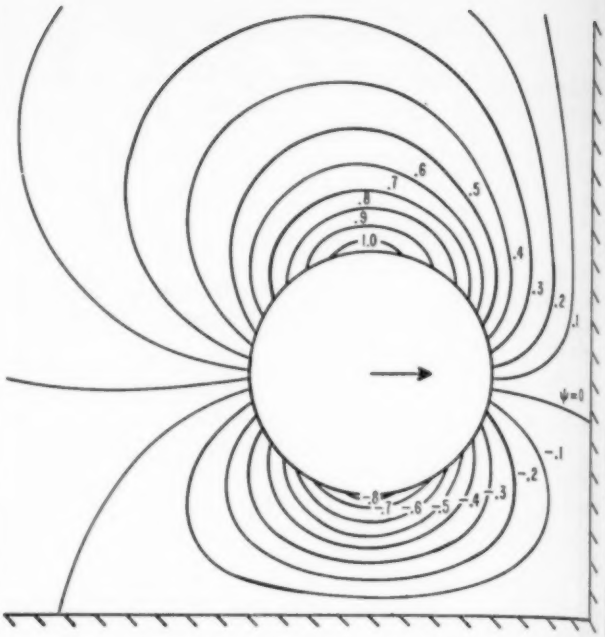

FIGURE 6. *Streamlines for a cylinder moving toward one of two perpendicular plane boundaries.*

$U=1, b=1$.

7. Cylinders Moving as a Rigid Body

If the velocity, $Ue^{i\alpha}$, is the same for each cylinder, they move as a rigid body. The previous solution for a cylinder moving parallel to a plane boundary is one example of this case. Another example is given in figure 7 where $b'=b=f/2$, $\alpha'=\alpha=0$. The solution simplifies to

$$w=Ub\sum_{k=0}^{\infty}\frac{(-1)^k}{(k+1)^2}\left\{\frac{1}{\frac{z}{b}-\frac{k}{k+1}}+\frac{1}{\frac{z}{b}-\frac{k+2}{k+1}}\right\}. \quad (24)$$

The approximate solution obtained by the method of section 5 is

$$w\approx Ub\sum_{k=0}^{n}\frac{(-1)^k}{(k+1)^2}\left\{\frac{1}{\frac{z}{b}-\frac{k}{k+1}}+\frac{1}{\frac{z}{b}-\frac{k+2}{k+1}}\right\}$$

$$+Ub\,\frac{2}{\frac{z}{b}-1}\left\{\frac{\pi^2}{12}-\sum_{k=0}^{n}\frac{(-1)^k}{(k+1)^2}\right\}. \quad (25)$$

The computations were made with $n=3$.

Another example is given in figures 8a and 8b where $b'=b=f/4$, $\alpha'=\alpha=0$. The solution was obtained using eq (19) with $n=1$.

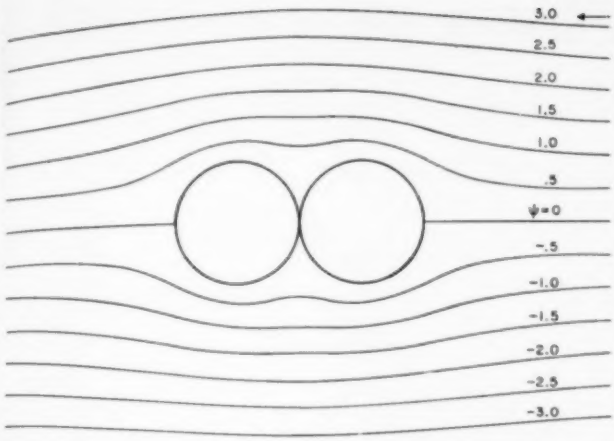

FIGURE 7. *Streamlines for current flowing with general velocity U past fixed cylinders.*

$U=1, b=1.$

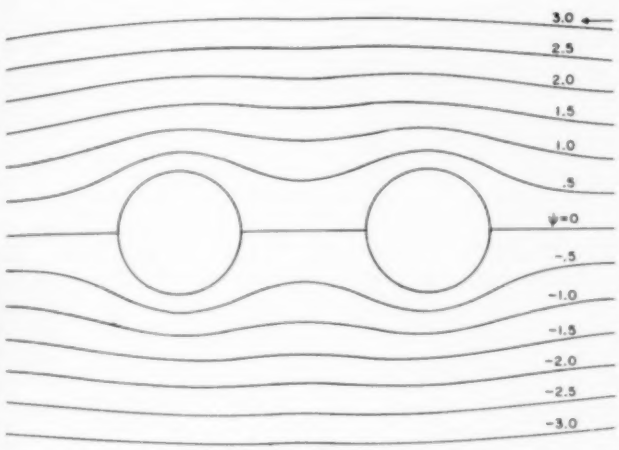

FIGURE 8a. *Streamlines for two cylinders moving as a rigid body.*

$U=1, b=1.$

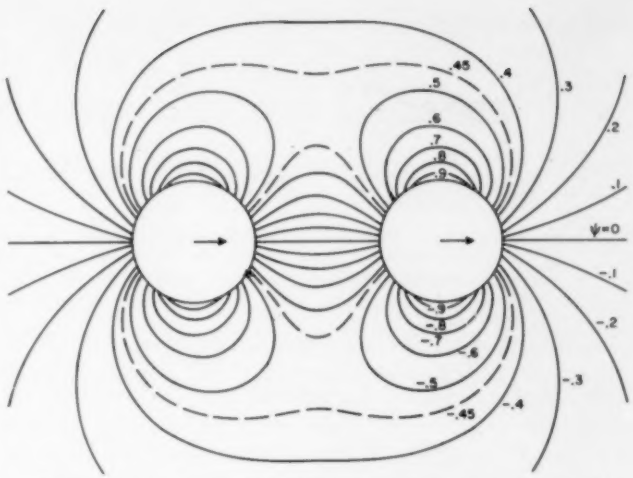

FIGURE 8b. *Streamlines for current flowing with general velocity U past fixed cylinders.*

$U=1, b=1.$

The author gratefully acknowledges the helpful suggestions of G. H. Keulegan and G. B. Schubauer.

WASHINGTON, March 11, 1958.

Journal of Research of the National Bureau of Standards Vol. 61, No. 2, August 1958 Research Paper 2890

Properties of Sodium Titanium Silicate Glasses[1]

Edgar H. Hamilton and Given W. Cleek

The glass-forming area of the Na_2O-TiO_2-SiO_2 system was surveyed. Glasses were made with refractive indices from 1.5184 to 1.8005, nu values from 51.5 to 23.2, and densities from 2.42 to 3.00. The glasses have higher dispersions and have considerably lower densities than the PbO glasses with comparable refractive indices.

1. Introduction

In order to give the optical designer greater freedom in his choice of glasses for use in optical devices there is a need for glasses that cover a considerable range of refractive indices, and for each index value, a range of dispersions. Most commercially available optical glasses having high refractive indices and high dispersions contain PbO in varying amounts. In general the refractive index and the dispersion increase with increasing PbO content. However, in PbO glasses there is a limiting value of dispersion for a given value of refractive index.

It has long been known that small additions of TiO_2 to a glass causes a relatively large increase in refractive index and dispersion. One of the early references to the use of TiO_2 in glass is that of Harcourt about 1870. He is reported to have produced "two 'nearly flawless' 3-inch disks of titanium glass and two of borate glass" [1].[2] The well-known work of Schott and Winkleman [2], in association with Abbe, the optical designer, was the first systematic attempt to determine the effect of chemical composition on the physical properties of glass. The immediate object of their work was the development of glasses having desirable optical properties. TiO_2 was one of the 28 oxides for which they studied the effects of composition on the physical properties of glass.

Colbert [3] has compared the effect of TiO_2 and PbO on the refractive indices of glasses. He added TiO_2 to a base glass of the composition $Na_2O,3SiO_2$ and PbO to a base glass of the same composition and found that in each series the refractive indices increased sharply.

Three series of glasses in the ternary system, Na_2O-TiO_2-SiO_2 were reported by Turnbull and Lawrence [4]. However, they did not survey the glass-forming area in the system. More recently Varguine [5] has reported on the glass-forming area of the Na_2O-TiO_2-SiO_2 system, but he gives data on only one series of glasses in the ternary system.

Thus, although studies have been made of glasses containing TiO_2, it was deemed desirable to make a systematic survey of the entire glass-forming region of the Na_2O-TiO_2-SiO_2 system, because it appeared that compositions in this ternary system could be used for the development of optical glasses having high refractive indices and high dispersions. Some of the properties of the glasses made in this survey are reported. The phase equilibrium diagram of the ternary system has not been determined, but information on the binary sides of the ternary system is available from previous work [6, 7, 8].

2. Experimental Procedure

The glasses were made in 500-g melts from batch materials of sufficient purity to satisfy the requirements for optical glass. The melts were made in platinum crucibles and stirred with a platinum–10 percent-rhodium stirrer. The melts were cast in the form of blocks approximately 3 by 3 by ¾ in. The details of the melting procedure are given in previous publications [9, 10]. The sag point [11] of each glass was used to establish an annealing temperature from which the glasses were cooled at 2½° C per hr to 350° C.

The liquidus temperature of each glass was determined by a temperature gradient method [12].

Refractive indices were determined on polished samples of the glasses in the form of 60° prisms for the C, D, F, and G′ lines by the NBS Optical Instrument Section.

The densities of the glasses were determined by the method described by Glaze, Young, and Finn [13].

The glasses were not analyzed. The compositions in table 1 are all calculated from batch.

3. Results

3.1. Glass-Forming Area of the Na_2O–TiO_2–SiO_2 System

The compositions of the melts are given in table 1 and are plotted in the triangular diagram of figure 1. Binary sodium silicate melts were made containing from 15 to 40 mole percent of Na_2O. The glass containing 15 mole percent of Na_2O devitrified during annealing and the other binary glasses developed a hazy appearance. The haziness of the annealed glasses increased with increasing SiO_2 content. Due to their hygroscopic nature none of the binary glasses could be polished in a water medium. This was also true of glasses containing 5 mole percent of TiO_2 and 25 or more mole percent of Na_2O. All the other ternary glasses containing 35 or more mole percent of Na_2O could be polished in a water medium but did not maintain a polished surface for more than a few weeks time.

[1] The work described in this report was sponsored by the Bureau of Ordnance, Department of the Navy.

[2] Figures in brackets indicate the literature references at the end of this paper.

TABLE 1. *Ternary Na_2O-TiO_2-SiO_2 compositions*

Melt	Na_2O	TiO_2	SiO_2	n_D	ν	ρ	Liquidus temperature	Primary phase [1]	Remarks
	Mole %	*Mole %*	*Mole %*				°C		
E1971	15	------	85	------	------	2.335	------	A	Devitrified in anneal.
E1972	20	------	80	------	------	2.387	1105	A	Hygroscopic—could not polish.
E1973	25	------	75	------	------	2.469	789	------	Do.
E1974	30	------	70	------	------	2.433	------	------	Do.
E1977	33.3	------	66.7	------	------	2.480	874	------	Do.
E1975	35	------	65	------	------	2.499	------	------	Do.
E1976	40	------	60	------	------	2.526	------	------	Do.
E1994	15	5	80	1.5184	51.5	2.429	>1220	A	Seedy.
E1995	20	5	75	1.5272	50.4	2.480	994	A	Do.
E1996	25	5	70	1.5318	49.7	2.512	------	B	Seedy, hygroscopic.
E1967	30	5	65	------	------	2.533	798	B	Hygroscopic—could not polish.
E1968	35	5	60	------	------	2.567	------	------	Do.
E1969	40	5	55	------	------	2.590	------	------	Do.
E1970	45	5	50	------	------	2.607	------	------	Devitrified in anneal.
E1922	10	10	80	1.5481	43.5	2.439	>1260	A	Seedy—prism gave poor imagery.
E1999	12.5	10	77.5	1.5532	43.8	2.490	------	------	
E1960	15	10	75	1.5574	43.8	2.517	ca. 1200	A	
E2002	17.5	10	72.5	1.5618	43.7	2.546	1075	A	
E1961	20	10	70	1.5635	43.7	2.561	920	A	Striae.
E2003	22.5	10	67.5	1.5655	43.6	2.581	800	D	
E1907	25	10	65	1.5666	43.5	2.595	850	D	Hygroscopic.
E2000	27.5	10	62.5	1.5668	43.4	2.607	802	D	Do.
E1962	30	10	60	1.5672	43.2	2.615	806	B	Hygroscopic, striated.
E2001	32.5	10	57.5	1.5675	43.1	2.625	------	------	Hygroscopic.
E1908	35	10	55	1.5688	42.6	2.635	840	C	Do.
E1963	40	10	50	------	------	2.649	------	------	Hygroscopic—could not polish.
E1807	45	10	45	------	------	------	------	------	Hygroscopic—surface devitrification.
E1795	50	10	40	------	------	------	------	------	Devitrified in mold.
E1794	60	10	30	------	------	------	------	------	Do.
E1959	12.5	12.5	75	1.5732	40.4	2.524	ca. 1300	A	
E1925	10	15	75	1.5868	36.4	2.520	>1260	A	Striated.
E1987	12.5	15	72.5	1.5936	37.3	2.565	------	------	Do.
E1926	15	15	70	1.5982	37.8	2.601	1099	A	Do
E1988	17.5	15	67.5	1.6015	37.9	2.625	1024	A	
E1927	20	15	65	1.6019	38.2	2.641	845	D	
E2057	22.5	15	62.5	1.6015	38.4	2.655	------	------	
E1928	25	15	60	1.6016	38.5	2.668	883	D	
E2005	27.5	15	57.5	1.6015	38.6	2.678	765	D	
E1929	30	15	55	1.6006	38.6	2.684	840	E	Hygroscopic.
E1930	35	15	50	1.6007	38.2	2.696	905	E	Do.
E1931	40	15	45	1.6020	37.1	2.706	925	C	Do.
E1932	45	15	40	------	------	------	1005	C	Hygroscopic—devitrified.
E1978	16.7	16.7	66.7	1.6147	36.1	2.645	1016	A	Striated.
E1914	23	17	60	1.6185	36.4	2.692	------	------	
E1938	10	20	70	1.6257	31.4	2.570	------	------	Index prism gave poor imagery.
E1989	12.5	20	67.5	1.6338	32.2	2.633	------	------	
E1980	15	20	65	1.6412	32.7	2.678	1090	------	
E1990	17.5	20	62.5	1.6427	33.1	2.703	999	------	Striated.
E1936	20	20	60	1.6424	33.5	2.712	928	------	
E2007	22.5	20	57.5	1.6416	33.8	2.732	850	D	
E1909	25	20	55	1.6402	34.1	2.740	890	E	
E1986	30	20	50	1.6362	34.5	2.749	912	E	
E2009	32.5	20	47.5	1.6335	34.7	2.752	------	------	Hygroscopic.
E1910	35	20	45	1.6348	34.2	2.746	938	E	Do.
E1934	40	20	40	1.6358	33.3	2.750	906	E	Do.
E1809	45	20	35	------	------	------	------	------	Devitrified in mold.
E1923	10	25	65	------	------	------	>1275	------	Contained devitrification.
E1942	15	25	60	1.6817	29.0	2.744	1185	------	
E1991	17.5	25	57.5	1.6842	29.3	2.771	1110	F_2	
E1943	20	25	55	1.6837	29.7	2.789	1034	F_2	
E2010	22.5	25	52.5	1.6817	30.1	2.800	990	F_1	
E1889	25	25	50	1.6783	30.6	2.806	921	F_1	
E2011	27.5	25	47.5	1.6755	30.8	2.811	------	------	
E1890	30	25	45	1.6739	30.9	2.815	922	E	
E1891	35	25	40	1.6709	30.8	2.817	955	E	Hygroscopic.
E1924	10	30	60	------	------	------	------	------	Devitrified.
E1944	15	30	55	1.7249	26.0	2.813	>1280	------	
E1992	17.5	30	52.5	1.7267	26.4	2.839	1198	F_2	
E1945	20	30	50	1.7255	26.7	2.855	1106	F_1	
E2012	22.5	30	47.5	1.7228	27.1	2.866	1042	F_1	
E1946	25	30	45	1.7184	27.6	2.869	985	F_1	
E2013	27.5	30	42.5	1.7145	27.9	2.873	------	------	
E1947	30	30	40	1.7109	28.1	2.871	920	E	
E2014	32.5	30	37.5	1.7072	28.3	2.871	------	------	
E1948	35	30	35	1.7061	28.2	2.869	959	E	Hygroscopic.
E1804	40	30	30	------	------	------	908	E	Devitrified in mold
E2019	33.3	33.3	33.3	1.7304	26.7	2.914	970	E	
E1952	20	35	45	------	------	------	1178	------	Devitrified in mold.
E2025	22.5	35	42.5	1.7643	24.7	2.922	------	------	
E1983	25	35	40	1.7595	25.1	2.934	1038	F_1	
E2015	27.5	35	37.5	1.7530	25.5	2.934	------	------	
E1982	30	35	35	1.7496	25.7	2.932	960	F_1	
E2016	32.5	35	32.5	1.7437	26.0	2.920	------	------	
E1949	35	35	30	1.7413	26.0	2.926	952	E	Striated-hygroscopic.

See footnote at end of table.

TABLE 1. *Ternary* Na_2O-TiO_2-SiO_2 *compositions*—Continued

Melt	Na_2O	TiO_2	SiO_2	n_D	ν	ρ	Lquidus temperature	Primary phase [1]	Remarks
	Mole %	*Mole %*	*Mole %*				°C		
E1953	20	40	40	----------	----------	----------	----------	F_1	Devitrified in mold.
E2027	22.5	40	37.5	----------	----------	2.984	----------	----------	
E1954	25	40	35	1.8005	23.2	2.995	1060	F_1	Devitrified streaks in glass.
E1955	30	40	30	1.7874	23.9	2.988	1012	F_1	Stones.
E1956	35	40	25	----------	----------	----------	980	F_1	Devitrified in mold.
E1958	25	45	30	----------	----------	----------	1102	F_1	Devitrified in mold.
E1957	30	45	25	----------	----------	----------	1040	F_1	Do.
E1883	25	50	25	----------	----------	----------	----------	----------	Devitrified in mold.

[1] Primary phases: A = SiO_2; B = $Na_2Si_2O_5$; C = Na_2SiO_3; D = Unknown; E = Na_2O-TiO_2-SiO_2; F_1 = Unknown; F_2 = Unknown.

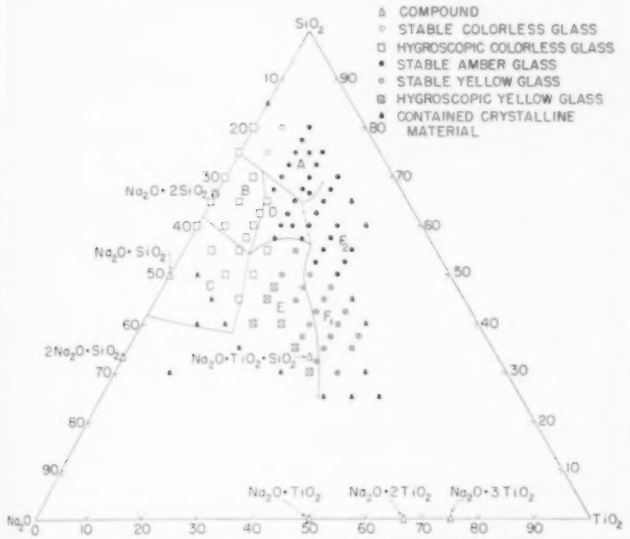

FIGURE 1. *Glass-forming area of the* Na_2O-TiO_2-SiO_2 *system*

Primary fields are: A, SiO_2; B, Na_2O·$2SiO_2$; C, Na_2O·SiO_2; E, Na_2O·TiO_2·SiO_2; D, F_1 and F_2, unidentified.

All of the ternary glasses containing 5 mole percent and some containing 10 and 15 percent of TiO_2 were practically colorless except when viewed edgewise. The remainder of the ternary glasses were either amber or yellow in color. As the Na_2O/SiO_2 ratio is increased, the amount of color in the glasses decreases rapidly, so that glasses are obtained whose color compares favorably with PbO glasses having comparable optical properties. The composition ranges of the hygroscopic, amber, and yellow glasses are indicated in figure 1.

3.2. Liquidus Temperatures

The liquidus temperatures of many of the glasses are given in table 1 and plotted in figure 2. The letters under the curves indicate the primary phases at the liquidus. The letters, A, B, C, and E stand for SiO_2, Na_2O·$2SiO_2$, Na_2O·SiO_2, and Na_2O·TiO_2·SiO_2, respectively. The compositions of the primary phases designated D, F_1, and F_2 were not determined. The approximate composition ranges of the primary fields are indicated, insofar as they are known, in figure 1. A region designated F_2 is located adjacent to the D and F_1 primary fields. The approximate boundaries of this field, if it is a primary field, are not known. In the F_2 field adjacent to the D field

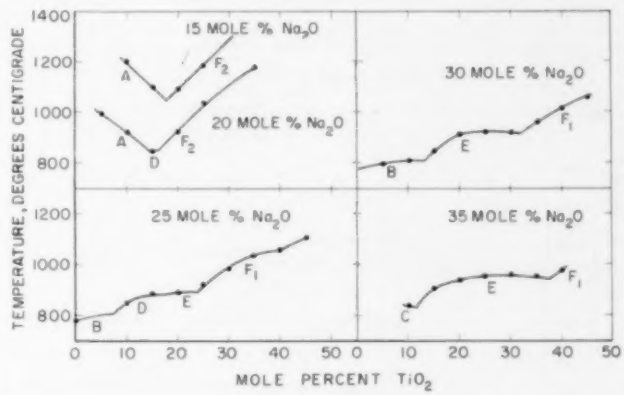

FIGURE 2. *Liquidus temperatures of glasses in five series of* Na_2O-TiO_2-SiO_2 *glasses.*

Primary phases present at the liquidus are: A, SiO_2; B, Na_2O·$2SiO_2$; C, Na_2O·SiO_2; E, Na_2O·TiO_2·SiO_2; D, F_1 and F_2 were not identified.

the crystals appearing at the liquidus and from 20 to 50 degrees below the liquidus, are too small to permit the determination of their properties by microscopic means. At lower temperatures phase D is observed, but it is believed that the submicroscopic crystals are not phase D. Adjacent to the phase F_1 field crystals with the same appearance and properties with the exception of refractive indices as phase F_1, were observed.

The properties of the crystals from phases D, E, and F_1 are:

Phase D. Composition unknown. Thick rods with high birefringence, n_{max} about 1.70 and n_{min} about 1.60.

Phase E. Composition believed to be Na_2O·TiO_2·SiO_2. Rod-shaped crystals with low birefringence, parallel extinction, negative elongation. n_{max} about 1.77 and n_{min} about 1.73.

Phase F_1. Composition unknown. Needle-shaped crystals with moderate birefringence, parallel extinction, positive elongation, n_{max} about 2.00, and n_{min} below 2.00.

3.3. Refractive Indices and Dispersions

Glasses were obtained with refractive indices from 1.5184 to 1.8005 and nu values [3] from 51.5 to 23.2.

[3] Nu value, ν, is defined as:

$$\nu = \frac{n_D - 1}{n_F - n_C}.$$

The refractive indices of the glasses are plotted in figure 3. The lines connect glasses containing equal moles of TiO_2. No simple relation is readily evident between refractive indices and increase in Na_2O content of the glasses.

The nu values of the glasses are plotted in figure 4. As in the case of the refractive index curves of figure 3, the nu value curves change slope and direction as the TiO_2 content of the glasses is increased.

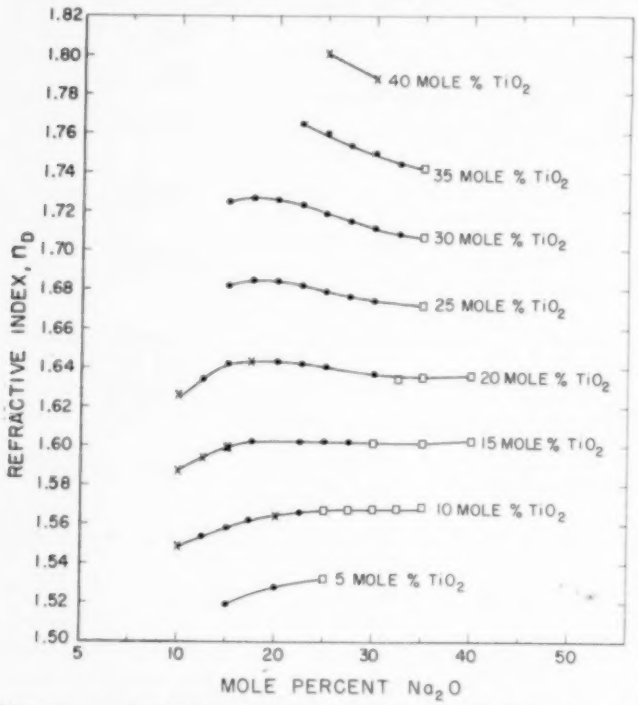

FIGURE 3. *Refractive indices of the* Na_2O-TiO_2-SiO_2 *glasses.*
Glasses which contained striae are identified by × and hygroscopic glasses by □.

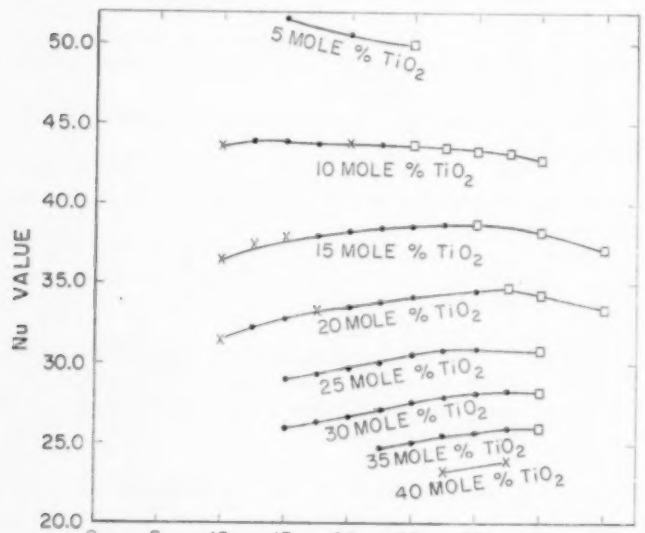

FIGURE 4. *Nu values of the* Na_2O-TiO_2-SiO_2 *glasses.*
Glasses which contained striae are identified by × and hygroscopic glasses by □.

In figure 5, the optical properties of typical optical flint glasses [14] and some of the Na_2O-TiO_2-SiO_2 glasses are compared. All of the curves for the experimental glasses seem to parallel each other. The glasses containing 25 and 30 mole percent of Na_2O all plot on the same line. Typical optical flint glasses with refractive indices above 1.605 have lower dispersions (higher nu values) than the Na_2O-TiO_2-SiO_2 glasses with corresponding refractive indices.

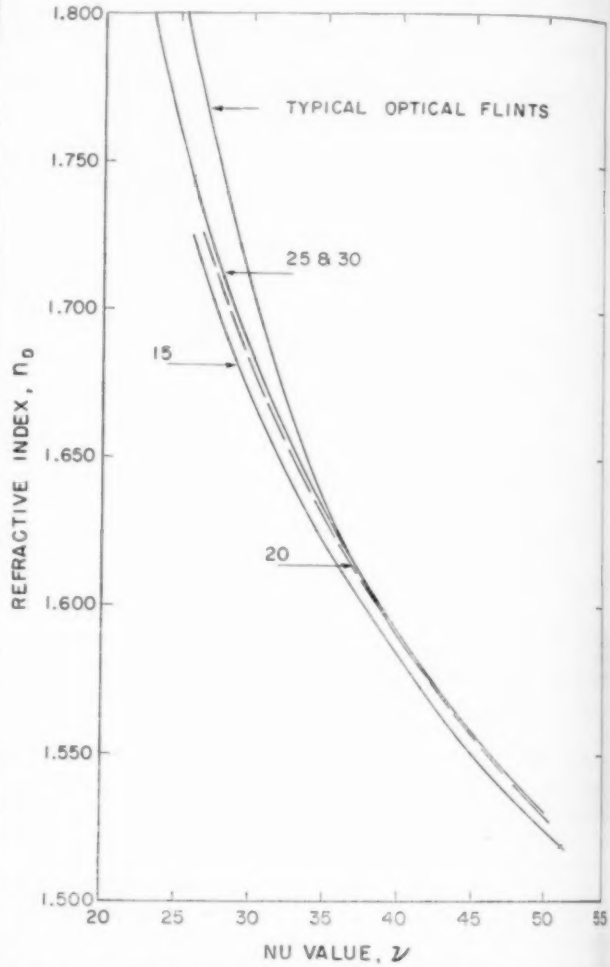

FIGURE 5. *Refractive indices versus nu values of* Na_2O-TiO_2-SiO_2 *and typical optical flint glasses.*
The numbers 15, 20, 25, and 30 indicate the mole percent of Na_2O in the Na_2O-TiO_2-SiO_2 glasses plotted on the respective curves.

3.4. Densities

The densities of the glasses containing TiO_2 are considerably lower than for PbO glasses with the same indices of refraction. The density of the TiO_2 glasses range from 2.42 to 3.00 while the density of the PbO glasses cover the range of 3.0 to 5.0. For this reason the less dense TiO_2 glasses may be of interest in applications where weight is a factor of prime importance.

The densities of the glasses are plotted in figure 6. There is a definite increase in density from series to series as TiO_2 is increased. As Na_2O is increased in

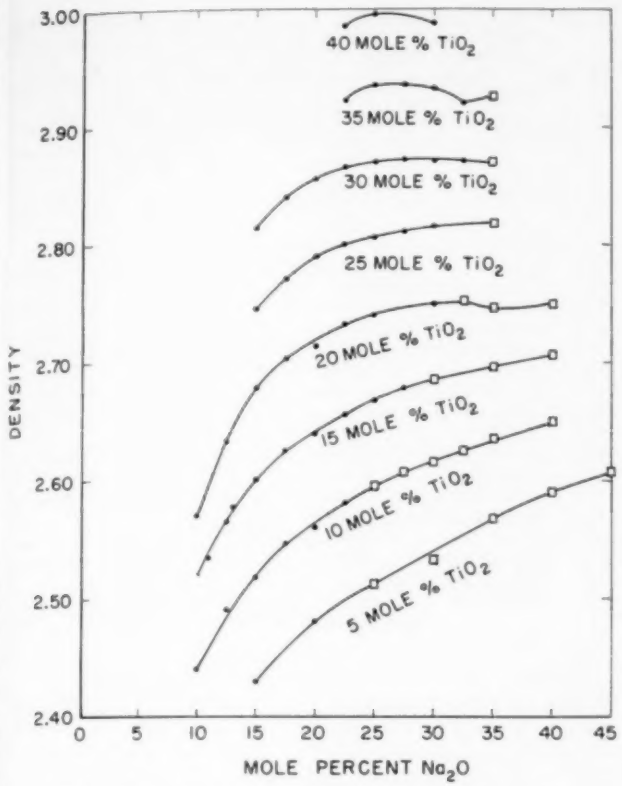

FIGURE 6. *Densities of* Na_2O-TiO_2-SiO_2 *glasses.*
Hygroscopic glasses are indicated by □.

each series of constant TiO_2 content, the density of the glasses containing less than 30 mole percent of TiO_2 increase. However, the amount of change in density per unit change in composition is not constant. An exception to this observation is the hygroscopic glasses containing 20 mole percent of TiO_2, but the values of density of these glasses may be affected by absorbed moisture.

3.5. Spectral Transmittances

The spectral transmittances of the glasses containing 25 mole percent of TiO_2 are plotted in figure 7. The ultraviolet absorption edge shifts toward the visible with increase in SiO_2 content. The sharpness of the absorption edge decreases with increase in color. In figure 8 the spectral transmittances of the glasses containing 25 mole percent of Na_2O are plotted. The absorption edge shifts to longer wavelengths with increase in TiO_2 content of the glasses. In the case of two glasses with visible yellow color the absorption edge not only shifts with increase in TiO_2, but it is not as sharp as for the colorless glasses. This is also evident in figure 9 where the sharpness of the absorption edge decreases with increase in color of the glass. The glasses are listed in figures 7, 8, and 9 in the order of increasing visible color.[4]

[4] It is recognized that some of the glass color may be due to the presence of impurities such as iron or platinum. The iron contents of the batch materials, calculated as Fe_2O_3 are: sand, 0.006 percent; soda ash, 0.001 percent; and TiO_2, 0.001 to 0.01 percent. The amount of platinum would depend on the corrosiveness of the individual melts on the platinum crucible, and no data is available. The heat treatment of the glasses is another factor which could affect the color.

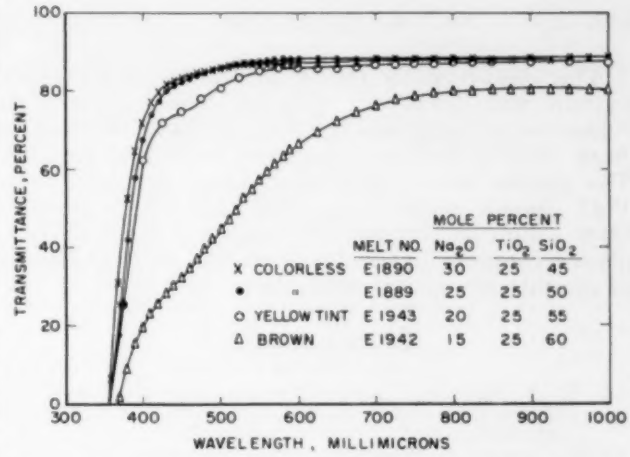
TRANSMITTANCE, PERCENT
WAVELENGTH, MILLIMICRONS
MOLE PERCENT
MELT NO. Na2O TiO2 SiO2
X COLORLESS E1890 30 25 45
• " E1889 25 25 50
O YELLOW TINT E1943 20 25 55
Δ BROWN E1942 15 25 60

FIGURE 7. *Spectral transmittances of some* Na_2O-TiO_2-SiO_2 *glasses containing 25 mole percent of* TiO_2.

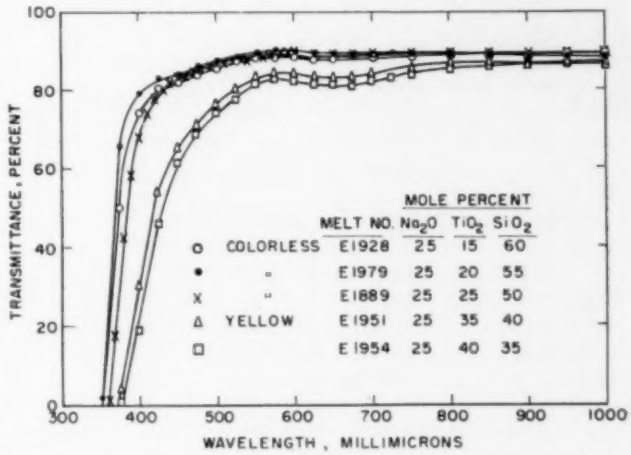
TRANSMITTANCE, PERCENT
WAVELENGTH, MILLIMICRONS
MOLE PERCENT
MELT NO. Na2O TiO2 SiO2
O COLORLESS E1928 25 15 60
• " E1979 25 20 55
X " E1889 25 25 50
Δ YELLOW E1951 25 35 40
□ E1954 25 40 35

FIGURE 8. *Spectral transmittances of some* Na_2O-TiO_2-SiO_2 *glasses containing 25 mole percent of* Na_2O.

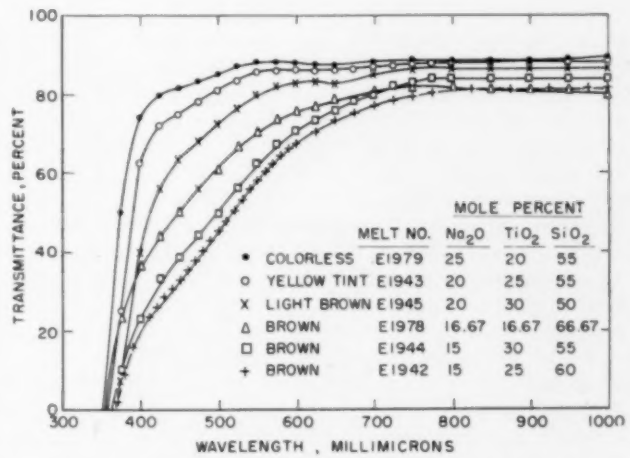
TRANSMITTANCE, PERCENT
WAVELENGTH, MILLIMICRONS
MOLE PERCENT
MELT NO. Na2O TiO2 SiO2
• COLORLESS E1979 25 20 55
O YELLOW TINT E1943 20 25 55
X LIGHT BROWN E1945 20 30 50
Δ BROWN E1978 16.67 16.67 66.67
□ BROWN E1944 15 30 55
+ BROWN E1942 15 25 60

FIGURE 9. *Spectral transmittances of some* Na_2O-TiO_2-SiO_2 *glasses with increasing color.*

4. Summary

The glass-forming region of the Na_2O-TiO_2-SiO_2 system was surveyed. Glasses were made with refractive indices from 1.5184 to 1.8005, nu values from 51.5 to 23.2, and densities from 2.42 to 3.00. The glasses have considerably lower densities than PbO glasses with comparable optical properties. Over a limited composition range the color of TiO_2 glasses compares favorably with that of PbO glasses of comparable optical properties.

5. References

[1] W. V. Harcourt, Researches on glass, read by Prof. Stokes in Sec. A, British Association (1871), Nature **4** 351 (1871).

[2] H. Hovestadt, Jena glass, translated by J. D. and A. Everett (London, 1902).

[3] W. Colbert, Comparison of effect of TiO_2 and PbO on refractive index of glasses, J. Am. Ceram. Soc. **29,** 45 (1946).

[4] R. C. Turnbull and W. G. Lawrence, The role of titania in silica glasses, J. Am. Ceram. Soc. **35** 48 (1952).

[5] V. V. Varguine, Le bioxide de titane dans le verre Diagramme d'equilibre et proprietes des verres au titane, Travaux du IV[e] Congres International du verre, p. 41 (Paris, 1956).

[6] F. C. Kracek, The system sodium oxide-silica, J. Phys. Chem. **34,** 1583 (1930).

[7] E. W. Washburn and E. N. Bunting, Note on phase equilibra in the system Na_2O-TiO_2, BS J. Research **12,** 239 (1934) RP648.

[8] E. N. Bunting, Phase equilibria in the systems TiO_2, TiO_2-SiO_2 and TiO_2-Al_2O_3, BS J. Research **11,** 719 (1933) RP619. R. W. Ricker and F. A. Hummel, Reactions in the system TiO_2-SiO_2, revision of the phase diagram, J. Am. Ceram. Soc. **34,** 271 (1951). R. C. De Vries, Rustum Roy and E. F. Osborne, The system TiO_2-SiO_2, Trans. Brit. Ceram. Soc. **53,** 525 (1954).

[9] Given W. Cleek and Edgar H. Hamilton, Properties of barium titanium silicate glasses, J. Research NBS **57,** 317 (1956) RP2720.

[10] Edgar H. Hamilton, G. W. Cleek, and O. H. Grauer, Some properties of glasses in the barium oxide-boric oxide-silica system, J. Am. Ceram. Soc., **41,** 209 (1958).

[11] Sam Spinner, Given W. Cleek, and Edgar H. Hamilton, Determination and use of the sag point as a reference point in the heating of glasses, J. Research NBS **59,** 227 (1957) RP2791.

[12] Oscar H. Grauer and Edgar H. Hamilton, An improved apparatus for the determination of liquidus temperature and rates of crystal growth in glass, J. Research NBS **44,** 495 (1950) RP2096.

[13] F. W. Glaze, J. C. Young, and A. N. Finn, The density of some soda-lime-silica glasses as a function of composition, BS J. Research **9,** 799 (1932) RP507.

[14] Francis W. Glaze and Clarence H. Hahner, Optical glass at the National Bureau of Standards, NBS Cir. 469 (1948).

WASHINGTON, April 14, 1958.

Journal of Research of the National Bureau of Standards Vol. 61, No. 2, August 1958 Research Paper 2891

Wavelengths From Thorium-Halide Lamps

William F. Meggers and Robert W. Stanley*

The present system of international secondary standards of wavelength for spectroscopic measurements is based on interferometric determinations of wavelengths emitted at atmospheric pressure by an electric arc between iron electrodes. Because of the poor quality and uneven distribution of these iron standards they are not suitable for accurate measurement of wavelengths in the spectra of heavier elements, most of which are more complex and consist of much sharper lines than the standards. Quartz-tube lamps containing a small quantity of a thorium halide, when excited by microwaves, emit thousands of uniformly sharp and evenly distributed lines whose wavelengths, or positions in a spectrum, can be determined with about one-tenth the error of locating iron-arc lines. Preliminary values of 222 vacuum wavelengths emitted by a thorium-iodide lamp have been measured relative to 5462.2705 and 4047.7144 A emitted by a similar lamp containing mercury-198. Fabry-Perot interferometers with plate separations of 25, 40, or 50 millimeters were used with a stigmatic grating spectrograph in making these measurements. The thorium wavelengths range from 3288.7356 to 6991.5839 A in vacuum and from 3287.7885 to 6989.6562 A in standard air. The accuracy in relative value of 27 classified thorium lines is tested by means of the combination principle, which indicates that the average error is less than 1 part in 20 million.

1. Introduction

During the past half-century the wavelengths of hundreds of radiations from the iron arc at atmospheric pressure have been measured with interferometers to serve as international standards of wavelength for spectroscopic measurements. The history and results of this activity were summarized in *Wavelengths From Iron-Halide Lamps* [1][1], in which it was shown that the accuracy of measurement could be increased by a factor of 2 or 3 if the iron lines were emitted by simple lamps containing a trace of iron halide excited, at low pressure and moderate temperature, by microwaves. But the iron arc in air is still the main source of internationally adopted standard wavelengths.

The actual application of the adopted iron standards to wavelength measurements in various spectra is handicapped by two serious defects in the iron-arc spectrum. First, because of the high temperature (6,300° K) of the iron arc and the relatively small atomic number ($Z=26$) and mass ($A=56$) of the iron atom its spectral lines are excessively broadened on account of Doppler-Fizeau effect. Moreover, an electric arc between iron electrodes at atmospheric pressure produces lines of various kinds; strongly self-reversed lines involving low energy levels, diffuse lines involving high energy levels, and unstable lines of variable wavelength due to "pole effect." Second, the distribution of strong or similar lines in the arc spectrum of iron is such that no uniform spacing of wavelength standards is possible, and unduly large gaps between usable standards are unavoidable in certain spectral regions. Consequently many spectroscopists have expressed dissatisfaction with the international standards of wavelength emitted by the iron arc. Thus, Harrison [2] states that the wavelength precision of measurements in the MIT Wavelength Tables has been limited primarily by "the insufficiency of adequate wavelength standards in some spectral regions, particularly of standard lines of suitable intensities." Likewise, Bovey [3] in giving a preliminary list of 6-figure wavelengths of plutonium excited in a furnace complains that "A serious difficulty for accurate measurement has been the width of the iron-arc lines, many of which are several times wider than the emission lines from a furnace." Also Fred and Tomkins [4] in describing the first two spectra of americium to 7 figures, announce that "Most of the uncertainty in the wavelengths is due to the poor quality of the standards, since the agreement in the hfs intervals shows that the line positions can be measured to another decimal place."

Logically the iron-arc standards should have been used only for measuring atmospheric arc and spark spectra of metals lighter than iron, because, other things equal, the heavier atoms emit sharper lines which cannot be measured accurately relative to standards that are broader and badly spaced. When the arc spectrum of cerium ($Z=58$, $A=140$) is photographed beside that of the standard iron arc it is readily seen that all cerium lines are narrower than iron lines, and a comparison with thorium ($Z=90$, $A=232$) or with uranium ($Z=92$, $A=238$) is even more embarrassing for iron. This was observed by Harrison [5], who remarked that "In the extensive series of wavelength measurements made with the automatic comparator, which resulted in the publication of the *Massachusetts Institute of Technology Wavelength Tables*, the most serious limitation on precision was found to arise from the lack of satisfactory standard lines. Measurements on lines in such complex spectra as cerium and thorium, for example, showed much better internal consistency than did those on the iron standards themselves." To assist in remedying this situation, Harrison [5] cleverly contrived a complicated machine for the rapid direct determination of wavelengths from Fabry-Perot interferometer patterns. He called this machine the WINMAC

* Present address, Purdue University, Lafayette, Ind.

[1] Figures in brackets indicate the literature references at the end of this paper.

(Wavelength interferometric measurement and computation), and in 1950 he reported [6] that "the WINMAC is now being readied for what is hoped will be an extensive series of wavelength determinations of intermediate wavelength standards in cerium, thorium, and other elements." Unfortunately this hope did not materialize. However, this is not seriously regretted now because in the meantime great improvements over the traditional arcs and sparks at atmospheric pressure have been made in spectroscopic light sources.

The most simple, convenient, efficient, and economical type of spectroscopic light source is an evacuated tube of fused quartz enclosing a trace of gas, metal vapor, or volatile metallic compound excited by microwaves generated by vacuum-tube oscillators or by magnetrons. The prototype was the low pressure, water-cooled Hg^{198} lamp described by Meggers and Westfall [7], who also discovered that "clean-up" in such discharges varied inversely with frequency. In most laboratories magnetrons producing 2,450 Mc, or more, soon replaced vacuum-tube oscillators producing 100 to 300 Mc for the excitation of these lamps. The preparation of similar lamps with other volatile metals was described by Zelikoff, Wyckoff, Aschenbrand, and Loomis [8], while Corliss, Bozman, and Westfall [9] demonstrated that such lamps can be made to emit the spectra of all metals that form volatile compounds. A precise procedure for the preparation of electrodeless discharge tubes containing very pure rare earths and highly radioactive elements has been described by Tomkins and Fred [10]. Compared with conventional arcs and sparks, these lamps require a minimum amount of sample, which is enclosed and conserved. Also, they operate at relatively low temperature and pressure, and consequently emit spectral lines of greatly reduced width usually free of self-reversal. When operated with continuous wave power and moderate gas or vapor pressure, these lamps strongly favor the spectra of neutral atoms, but pulsed discharges and/or reduced pressures enhance the second and third spectra. Lamps viewed end-on when excited by a 100-watt magnetron emit spectra comparable in intensity to a 10-ampere 220-volt d-c arc, but with line widths much less than half as great. Bright, sharp lines are especially needed for the resolution of complex Zeeman patterns, or for the measurement of isotopic-spectroscopic effects. The development of these electrodeless lamps has thus greatly increased the range and precision of spectroscopic observations.

Now the accurate description and quantum interpretation of the spectra of rare-earth types of atoms and ions is still in a very unsatisfactory state, because of their extreme complexity and because pure samples have not been available in the past. The latter difficulty has recently been overcome either by efficient separation or by artificial preparation, but extreme complexity of the spectra remains as an obstacle to successful analysis. It is primarily for this reason that wavelengths must be measured with greater accuracy, and for this purpose reference standards of greater precision and better distribution than those from an iron arc are absolutely necessary. Fortunately the simple electrodeless lamps referred to provide the means for obtaining a greatly improved system of standard wavelengths [11]. Lamps containing a trace of a thorium halide excited by microwaves emit approximately 20,000 lines of uniformly sharp character and even distribution between 2000 and 12000 A. Since these lines are characteristic of heavy atoms and ions of even mass ($Z=90$, $A=232$) they have relatively small Doppler-Fizeau widths, and are entirely free from hyperfine structure or isotope shifts. By imaging a thorium-halide lamp inside a similar one containing Hg^{198} (or vice versa) both sources can be caused simultaneously to illuminate a Fabry-Perot interferometer and stigmatic spectrograph. From the interference patterns the wavelengths of thorium lines can then be determined to 8 figures relative to the previously determined values of the mercury lines. The purpose of this paper is to present preliminary results of such wavelength measurements for 222 radiations from thorium, covering slightly more than one octave of spectrum.

2. Light Sources

The thorium source used in this investigation was an electrodeless discharge tube containing a few milligrams of thorium iodide and pure helium gas at a pressure of 5 mm of Hg or less. The tube was prepared by C. H. Corliss in a manner previously described [9]. The tube blank is made of Vycor glass; it has a bore of approximately 5 mm and a length of 11.3 cm. The discharge was excited at a frequency of 2,450 Mc obtained from a commercial diathermy generator.

The thorium tube used throughout the investigation was chosen from among several that were made at the same time. After a warmup period of 30 to 60 sec, the tube would glow very brightly for approximately 3 min. At the end of this time the thorium spectrum would weaken, and the discharge would be confined to a narrow filament near the center of the tube, indicating that the pressure in the tube had increased. The period of high intensity mentioned above was accompanied by a gradual movement of the thorium iodide deposit from the top to the bottom of the tube. As soon as the thorium spectrum began to weaken, the discharge tube was removed from its holder, cooled in water, and replaced in an inverted position with the thorium iodide deposit again at the top of the tube. For many of the photographs, this 3-min running time was sufficient. For longer exposures it was necessary to cool and invert the tube several times. This change could be made within 30 sec.

The primary standard on which the thorium measurements were based was a NBS-Meggers Hg^{198} lamp [7], that contained 1 mg of Hg^{198} and argon at a pressure of approximately 3 mm of Hg. The mercury tube was excited by a second diathermy generator at the same frequency of 2,450 Mc. The Hg^{198} source was cooled by an air stream from a small blower.

3. Experimental Method

The optical arrangement was the same as that used by the authors in the previous investigation of iron wavelengths from an electrodeless tube [1]. For this reason, only a brief description will be given here. The Fabry-Perot interferometer consisted of aluminized quartz plates separated by 3 sets of invar pins either 25, 40, or 50 mm in length. Good interference fringes were also obtained with plate separation of 67.5 mm, but lack of time did not permit the exploitation of the higher orders of interference.

The evacuated ($<10^{-4}$ mm Hg) interferometer was mounted externally in parallel light. Both thorium and Hg^{198} lamps were placed on the optical axis but at right angles to it and parallel to the spectrograph slit, so that both sources were observed side-on. The Hg^{198} lamp was farther from the slit so that it could be imaged inside the thorium tube. From this point on, light from both lamps traveled the same path through condensing lens, interferometer, projection lens, and thence through the slit and spectrograph. The quartz-fluorite achromatic projection lens had the proper focal length (50 cm or 100 cm) to form six or more circular fringes on the spectrograph slit, which was 25 mm long and either 0.15 or 0.30 mm wide. Accuracy of measurement was thus favored by the large scale of the interference patterns and by a slit width that made the fringes approximate rectangles.

Dispersion in the horizontal direction was produced by a 15,000-line-per-inch concave grating in the Wadsworth mounting. The curvature of the plate holder was decreased so as to favor the horizontal focus and thus produce sharp images of the Fabry-Perot fringes from both lamps, simultaneously over as large a range as possible. This instrument was used to photograph diametral sections of interference patterns for waves between 4400 and 7000 A, with a slit width of 0.30 mm and a reciprocal dispersion of 5 A/mm in the first-order grating spectrum. Because of the higher density of lines in the ultraviolet spectrum of thorium, the region from 3275 to 4500 A was photographed in the second-order grating spectrum with a reciprocal dispersion of 2.45 A/mm and slit width of 0.15 mm. Under these conditions most of the measured interference patterns were free from overlaps of neighboring lines, but if many more thorium wavelengths are to be measured larger grating dispersion or smaller slit width will be necessary. In each wavelength range several spectrograms were made with different exposure times, and with slight mechanical-pressure changes in the interferometer spacing to alter the interference configurations or fractional orders for all spectral lines.

The interferometer plates were the same ones used previously for measurements of iron and mercury wavelengths [1, 12, 13]. The last series of measurements [13] suggested that the dispersion of phase change in the aluminum films was very small between 3300 and 6000 A, so no corrections on account of phase change were applied to these thorium wavelengths. No significant differences were found between results from the 25-, 40-, and 50-mm etalons.

All mercury lines that appeared with sufficient intensity were measured along with the thorium lines. The green (5462.2705 A) and violet (4047.7144 A) lines of Hg^{198} were chosen as standards respectively for the long- and short-wave interference spectrograms described above. The values of other Hg^{198} lines measured on these spectrograms agreed quite well with unpublished wavelengths [13], the greatest difference being 0.0002 A. This supports our assumption that any possible corrections to these thorium preliminary wavelengths on account of dispersion of phase-change in the interferometer films are negligible.

The interferograms were measured at the National Bureau of Standards with the interference comparator designed by K. Burns [14], and at Purdue University with a comparator made by Carl Leiss. In order to measure as many thorium wavelengths as possible within a given time, it was found desirable to measure just 5 diameters of each interference pattern. As mentioned before [7], by measuring the diameters of 5 interference rings, the least-squares evaluation of the fractional order at the center may be made with a minimum of arithmetical computation because some of the steps are easily performed mentally. Even with this conservation of time and labor the thorium wavelengths presented in this paper required the bisection of more than 12,000 interference fringes and calculations for more than 1,200 individual patterns.

Another way to reduce the time and labor involved in interferometric comparisons of wavelengths is to begin with the largest orders of interference consistent with finding the correct integral order for each line. If grating measurements of wavelength are to be refined and replaced by interferometric values, the initial orders of interference should not be so great that errors in the grating values lead to wrong integral orders. For example, if a thorium wavelength near 5000 A is to be measured relative to 5462.2705 A of Hg^{198}, the whole order of the thorium wavelength with a 25-mm etalon will be about 100,000, and the error in the grating value must be less than ± 0.02 A if it is to yield the correct integral order. We assumed that the available grating values of thorium wavelengths justified beginning the interferometric observations with a 25-mm etalon and then testing these values with a 40-mm etalon. If the integral orders of interference are in error because of too large errors in the grating values, the 25- and 40-mm etalon values will differ radically, but if the integral orders are correct, the results will agree within a very small possible error of observation. This bold procedure saved much time and labor by eliminating interferometric observations with all smaller etalons which do not contribute anything to the accuracy attainable with the larger etalons.

Two independent sets of grating values of thorium wavelengths were available, one in the *MIT Wavelength Tables* [2] representing wavelengths emitted by a thorium arc, and the second representing unpublished wavelengths from thorium halide lamps measured by R. Zalubas in the National Bureau of

TABLE 1. *Thorium wavelengths: grating and interferometer values*

	λ_{air}	λ_{vac}	λ_{vac} (25 mm)	Change in order	λ_{vac} (40 mm)
MIT	4165. 813	4166. 987	4166. 9750	----	4166. 9832
NBS	4165. 782	4166. 956	4166. 9403	+1	4166. 9403
MIT	3869. 639	3870. 736	3870. 7308	----	3870. 7416
NBS	3869. 665	3870. 762	3870. 7606	−1	3870. 7604
MIT	3854. 547	3855. 640	3855. 6333	----	3855. 6222
NBS	3854. 512	3855. 605	3855. 6036	+1	3855. 6035
MIT	3421. 189	3422. 170	3422. 1673	----	3422. 1618
NBS	3421. 215	3422. 196	3422. 1908	−1	3422. 1910

Standards. Both sets were referred to the adopted secondary standards of wavelength obtained from the iron arc at atmospheric pressure. We gave preference to the MIT grating values because these were objectively measured and calculated by automatic machines [2], and therefore entirely free from human errors. This was a mistake; the only errors in integral orders of 25-mm etalons occurred because of errors larger than 0.02 A in the MIT grating values as shown in table 1. The first line shows in succession the MIT wavelength in air, its value in vacuum [15], and discordant results from 25-mm etalons and from 40-mm etalons. The second line gives similar data for NBS grating wavelengths, but the results from 25- and 40-mm etalons are in perfect agreement because the integral orders were corrected as indicated by the NBS grating values. The interferometric values for these four lines show that the MIT grating values have errors of +0.047, −0.025, +0.036, and −0.021 A, respectively, whereas the NBS errors are +0.016, +0.001, +0.001, and +0.005 A. No explanation of the large and erratic errors in the MIT grating values is offered, but this experience should be a warning that some 7-figure MIT wavelengths may not be trustworthy beyond 5 figures.

4. Results

The thorium wavelengths obtained as a result of this investigation are presented in table 2. Since the interferometer was evacuated and the separation of the interferometer plates was always expressed in terms of vacuum wavelengths of Hg^{198} standards, all the measured wavelengths of thorium are valid only in vacuum. Column 1 displays only that part of the vacuum wavelength that can be expressed in whole angstroms, the fraction that must be added to this is given in columns 2, 3, and 4, depending on whether it was measured respectively with 25-, 40-, or 50-mm etalons. A figure in parentheses following each fraction shows the number of individual determinations. Column 5 contains the average preliminary vacuum wavelength resulting from all the observations. In column 6 the vacuum wavelenghts of column 5 are changed to values in standard air with the aid of Edlén's conversion table [15]. Column 7 quotes unpublished estimated relative intensities of thorium lines as given by Zalubas, and column 8 indicates the particular spectrum to which each wavelength belongs.

It is a common characteristic of all complex spectra that neutral atoms dominate the visible, and singly-ionized atoms predominate in the ultraviolet. In these preliminary measurements of thorium wavelengths with Fabry-Perot etalons no difference in character could be observed between the Th I and Th II lines, and there is no reason to suspect that one category is more accurately measured than the other. Unfortunately none of the thorium wavelengths has been measured a sufficient number of times with any given etalon to compute a meaningful probable error or standard deviation. A considerable number of the wavelengths from a given etalon are limited to a single observation and a comparison of these with the over-all averages may give an impression of the uncertainty in individual observations.

Because of the lack of sufficient observational material to calculate probable errors of the thorium wavelengths, an attempt was made to test their relative values by means of the combination principle. Although the Th II spectrum has been extensively analyzed [16] no recurring wavenumber differences were found between Th II lines in table 2. Somewhat better fortune was encountered with Th I lines. Even though the published analysis of Th I is extremely fragmentary [17] it is now being extended by Zalubas [18] who has reported that 27 of our interferometric values of Th I lines test the constancy of 4 wavenumber differences, viz., 2869.261, 3687.990, 5563.143, and 6362.396 K (=cm^{-1}) between low-energy levels established for neutral thorium atoms. These are presented in table 3 as 14 pairs of vacuum wavelengths in A, and their reciprocals, or vacuum wavenumbers in K. The mean deviation of the 14 differences from their arithmetical averages is 0.001_2 K, that is 1 part in about 20 million. The pairs numbered 2 and 3 account for two-thirds of the summed deviations; if these are ignored the remaining 12 exhibit an average departure of only 0.0005 K, or 1 part in about 40 million, but this may be discounted as accidental.

The 222 wavelengths (3288.7356 to 6991.5839 A) of thorium radiations in table 2 are presented as a preliminary set of improved standard wavelengths for the measurement of highly-dispersed complex spectra. The average interval between these stand-

TABLE 2. *Wavelengths in thorium spectra*

1	2	3	4	5	6	7	8
Whole angstrom	Fractional angstrom			Vacuum	Air	Relative intensity	Spectrum
	25 mm(obs.)	40 mm(obs.)	50 mm(obs.)				
6991	5840 (2)	5839 (3)	5839 (1)	6991. 5839	6989. 6562	900	I
6945	5265 (3)	5266 (3)	5263 (1)	6945. 5265	6943. 6112	600	I
6913	1334 (3)	1338 (3)	1333 (1)	6913. 1336	6911. 2264	400	I
6836	8110 (4)	8114 (2)	8108 (1)	6836. 8110	6834. 9249	75	I
6830	9196 (2)	9205 (1)	9201 (1)	6830. 9200	6829. 0355	150	I
6758	3179 (3)	3178 (2)	3176 (1)	6758. 3178	6756. 4528	250	I
6729	3153 (2)	3161 (1)	3162 (1)	6729. 3157	6727. 4585	200	I
6680	--------	5511 (1)	5522 (1)	6680. 5516	6678. 7076	30	I
6664	1088 (4)	1089 (3)	1094 (1)	6664. 1090	6662. 2694	250	I
6660	--------	5161 (1)	5161 (1)	6660. 5161	6658. 6774	50	I
6595	7610 (4)	7610 (3)	7608 (1)	6595. 7610	6593. 9397	200	I
6593	--------	3059 (1)	3051 (1)	6593. 3055	6591. 4849	100	I
6590	3595 (4)	3600 (2)	3596 (1)	6590. 3596	6588. 5398	200	I
6585	7248 (4)	7254 (3)	7251 (1)	6585. 7251	6583. 9065	200	I
6555	9715 (2)	9710 (4)	9707 (1)	6555. 9711	6554. 1605	100	I
6533	1468 (5)	1465 (4)	1466 (1)	6533. 1467	6531. 3423	400	I
6492	5317 (2)	5312 (4)	5313 (1)	6492. 5313	6490. 7378	120	I
6459	0675 (4)	0678 (3)	0680 (1)	6459. 0677	6457. 2834	500	I
6415	--------	3881 (3)	3876 (1)	6415. 3880	6413. 6152	200	I
6413	6717 (4)	6721 (4)	6719 (1)	6413. 6719	6411. 8996	250	I
6378	6939 (3)	6940 (4)	6933 (1)	6378. 6939	6376. 9310	350	I
6344	6134 (4)	6143 (4)	6135 (1)	6344. 6138	6342. 8600	300	I
6329	0286 (2)	0285 (4)	0270 (1)	6329. 0284	6327. 2788	180	I
6263	1499 (4)	1493 (4)	1504 (1)	6263. 1496	6261. 4177	180	I
6259	1546 (3)	1546 (3)	1548 (1)	6259. 1546	6257. 4237	100	I
6226	2497 (2)	2494 (4)	2494 (1)	6226. 2495	6224. 5275	100	I
6208	9379 (5)	9380 (4)	9378 (1)	6208. 9379	6207. 2205	160	I
6193	--------	6188 (1)	6186 (1)	6193. 6187	6191. 9054	100	I
6184	3324 (4)	3331 (4)	3326 (1)	6184. 3327	6182. 6219	400	I
6153	6954 (5)	6962 (3)	6959 (1)	6153. 6958	6151. 9932	120	I
6104	2838 (2)	2837 (2)	2849 (1)	6104. 2839	6102. 5946	90	I
6089	7161 (2)	7159 (2)	7160 (1)	6089. 7160	6088. 0306	125	I
6087	0592 (5)	0596 (2)	0586 (1)	6087. 0592	6085. 3745	100	I
6050	7258 (2)	7259 (2)	7259 (1)	6050. 7259	6049. 0510	100	I
6039	3696 (5)	3700 (4)	3696 (1)	6039. 3697	6037. 6978	140	I
6022	7042 (1)	7038 (2)	--------	6022. 7040	6021. 0362	140	I
6008	7362 (4)	7361 (4)	7364 (1)	6008. 7362	6007. 0725	180	I
5976	7202 (2)	7208 (4)	7213 (1)	5976. 7207	5975. 0656	250	I
5975	3202 (5)	3196 (4)	3193 (1)	5975. 3199	5973. 6651	250	I
5940	4710 (4)	4708 (4)	4708 (1)	5940. 4709	5938. 8255	140	I
5887	3325 (1)	3331 (1)	3329 (1)	5887. 3329	5885. 7017	120	I
5854	3043 (4)	3033 (2)	3053 (1)	5854. 3040	5852. 6817	200	I
5805	7508 (5)	7507 (4)	7509 (1)	5805. 7508	5804. 1414	300	I
5792	2686 (5)	2686 (3)	2683 (1)	5792. 2686	5790. 6629	------	Hg^{198}
5791	2494 (3)	2495 (2)	2492 (1)	5791. 2494	5789. 6439	200	I
5771	1983 (5)	1983 (4)	1980 (1)	5771. 1983	5769. 5982	------	Hg^{198}
5762	1484 (4)	1489 (4)	1489 (1)	5762. 1487	5760. 5510	600	I
5726	9766 (1)	9771 (3)	--------	5726. 9770	5725. 3887	250	I
5708	6864 (4)	6870 (4)	6872 (1)	5708. 6867	5707. 1033	200	II
5659	--------	4963 (1)	4958 (1)	5659. 4960	5657. 9258	100	I
5641	3109 (3)	3122 (3)	3120 (1)	5641. 3115	5639. 7461	250	II
5616	8789 (2)	8790 (4)	--------	5616. 8790	5615. 3202	350	I
5588	5775 (5)	5780 (5)	5781 (1)	5588. 5778	5587. 0265	500	I
5580	9073 (3)	9080 (4)	9080 (1)	5580. 9077	5579. 3585	300	I
5574	9014 (4)	9015 (4)	9010 (1)	5574. 9014	5573. 3538	350	I
5559	8862 (3)	8862 (4)	8859 (1)	5559. 8862	5558. 3426	400	I
5549	7171 (4)	7169 (3)	7172 (1)	5549. 7170	5548. 1761	300	I
5540	8001 (5)	8000 (5)	7999 (1)	5540. 8000	5539. 2615	400	I
5511	5243 (4)	5247 (4)	5238 (1)	5511. 5244	5509 9937	300	I
5500	7828 (5)	7831 (5)	7831 (1)	5500. 7830	5499. 2552	250	I

TABLE 2. *Wavelengths in thorium spectra*—Continued

1	2	3	4	5	6	7	8	
Whole angstrom	Fractional angstrom			Vacuum	Air	Relative intensity	Spectrum	
	25 mm(obs.)	40 mm(obs.)	50 mm(obs.)					
5462	2705 (5)	2705 (5)	2705 (1)	5462. 2705	5460. 7530	------	Hg 198	
5453	7338 (1)	7343 (2)	--------	5453. 7341	5452. 2188	250	I	
5432	6213 (4)	6211 (2)	6216 (1)	5432. 6212	5431. 1116	300	I	
5427	1859 (2)	1865 (3)	--------	5427. 1863	5425. 6781	250		II
5418	9915 (5)	9916 (5)	9916 (1)	5418. 9916	5417. 4856	200	I	
5409	1568 (4)	1570 (3)	1573 (1)	5409. 1569	5407. 6535	200	I	
5388	1093 (1)	1083 (1)	1087 (1)	5388. 1087	5386. 6109	300	I	
5345	0672 (3)	0678 (3)	0681 (1)	5345. 0676	5343. 5813	500	I	
5328	4573 (3)	4575 (3)	4572 (1)	5328. 4574	5326. 9755	400	I	
5278	9691 (2)	9687 (2)	--------	5278. 9689	5277. 5002	400		II
5259	8245 (3)	8245 (3)	--------	5259. 8245	5258. 3609	300	I	
5232	6158 (3)	6160 (3)	--------	5232. 6159	5231. 1596	900	I	
5178	4028 (3)	4023 (3)	--------	5178. 4025	5176. 9606	400	I	
5160	0408 (3)	0413 (3)	--------	5160. 0411	5158. 6041	700	I	
5155	6781 (1)	6789 (3)	--------	5155. 6787	5154. 2429	400	I	
5116	4694 (2)	4700 (2)	--------	5116. 4697	5115. 0443	250	I	
5069	3865 (2)	3870 (2)	--------	5069. 3868	5067. 9739	900	I	
5051	2039 (2)	2039 (2)	--------	5051. 2039	5049. 7959	400		II
5030	0581 (2)	0594 (2)	--------	5030. 0588	5028. 6564	400		II
5018	6537 (3)	6542 (2)	--------	5018. 6539	5017. 2545	500		II
5003	4922 (3)	4922 (2)	--------	5003. 4922	5002. 0968	400	I	
4941	0205 (4)	0204 (2)	--------	4941. 0205	4939. 6417	350	I	
4921	1894 (3)	1886 (2)	--------	4921. 1890	4919. 8155	600		II
4896	3214 (4)	3216 (2)	--------	4896. 3215	4894. 9546	350	I	
4880	0950 (2)	0965 (1)	--------	4880. 096	4878. 733	200	I	
4866	8360 (2)	8360 (1)	--------	4866. 8360	4865. 4769	350	I	
4864	5306 (3)	5309 (1)	--------	4864. 5307	4863. 1722	1000		II
4842	1949 (2)	1953 (2)	--------	4842. 1951	4840. 8426	400	I	
4809	4775 (3)	4770 (2)	--------	4809. 4773	4808. 1334	350	I	
4790	7254 (3)	7259 (2)	--------	4790. 7256	4789. 3867	300	I	
4767	9328 (2)	9334 (1)	--------	4767. 9330	4766. 6001	200	I	
4753	7427 (2)	7432 (2)	--------	4753. 7430	4752. 4139	500		II
4705	3059 (3)	3060 (2)	--------	4705. 3060	4703. 9897	500	I	
4687	5062 (2)	5055 (1)	--------	4687. 5060	4686. 1944	1200	I	
4674	9691 (2)	9689 (2)	--------	4674. 9690	4673. 6608	600	I	
4669	4787 (3)	4789 (2)	--------	4669. 4788	4668. 1720	700	I	
4664	5076 (1)	5076 (2)	--------	4664. 5076	4663. 2021	200	I	
4633	0584 (3)	0583 (2)	--------	4633. 0583	4631. 7611	1100	I	
4596	7072 (3)	7085 (1)	--------	4596. 7074	4595. 4198	600	I	
4589	7122 (2)	7124 (1)	--------	4589. 7123	4588. 4266	400	I	
4572	2522 (2)	2533 (1)	--------	4572. 2526	4570. 9715	500	I	
4557	0912 (2)	0890 (1)	--------	4557. 090	4555. 813	500	I	
4536	5251 (2)	5266 (1)	--------	4536. 526	4535. 254	300	I	
4511	7906 (3)	7910 (2)	--------	4511. 7908	4510. 5257	800		II
4494	5941 (3)	5942 (2)	--------	4494. 5941	4493. 3335	1200	I	
4483	4270 (3)	4269 (2)	--------	4483. 4270	4482. 1694	300	I	
4466	5936 (3)	5940 (3)	--------	4466. 5938	4465. 3406	300		II
4459	2531 (5)	2530 (3)	--------	4459. 2531	4458. 0018	600	I	
4446	5562 (2)	5561 (2)	--------	4446. 5561	4445. 3082	300	I	
4434	2074 (4)	2076 (2)	--------	4434. 2075	4432. 9628	600		II
4410	1211 (5)	1210 (3)	--------	4410. 1211	4408. 8828	600	I	
4404	1635 (5)	1641 (3)	--------	4404. 1637	4402. 9270	400	I	
4402	8179 (1)	8183 (1)	--------	4402. 8181	4401. 5817	400	I	
4392	3440 (7)	3440 (2)	--------	4392. 3440	4391. 1104	3000		II
4383	0917 (5)	0915 (2)	--------	4383. 0916	4381. 8604	900	I	

TABLE 2. *Wavelengths in thorium spectra*—Continued

1	2	3	4	5	6	7	8
Whole angstrom	Fractional angstrom			Vacuum	Air	Relative intensity	Spectrum
	25 mm(obs.)	40 mm(obs.)	50 mm(obs.)				
4379	4069 (5)	4072 (2)	----------	4379. 4070	4378. 1768	500	I
4375	3535 (2)	3538 (1)	----------	4375. 3536	4374. 1244	600	I
4367	1572 (5)	1575 (2)	----------	4367. 1573	4365. 9303	600	I
4359	5624 (4)	5624 (3)	----------	4359. 5624	4358. 3374	------	Hg^{198}
4343	4765 (4)	4760 (2)	----------	4343. 4763	4342. 2555	300	I
4332	0620 (3)	0617 (1)					
4319	6302 (1)	6307 (1)	----------	4332. 0619	4330. 8441	300	I
4316	4681 (3)	4681 (2)	----------	4319. 6305	4318. 4160	700	I
4308	3878 (3)	3878 (2)	----------	4316. 4681	4315. 2544	400	I
4301	0490 (3)	0486 (1)	----------	4308. 3878	4307. 1763	700	I
				4301. 0489	4299. 8393	600	I
4293	0176 (3)	0178 (2)					
4278	5178 (3)	5181 (2)	----------	4293. 0177	4291. 8102	400	I
4274	5599 (3)	5603 (2)	----------	4278. 5179	4277. 3142	1200	II
4258	6946 (3)	6941 (2)	----------	4274. 5600	4273. 3574	1000	II
4236	6563 (3)	6560 (1)	----------	4258. 6944	4257. 4959	700	I
				4236. 6562	4235. 4635	600	I
4231	6183 (3)	6180 (1)					
4216	0152 (2)	0161 (1)	----------	4231. 6182	4230. 4268	600	I
4210	0766 (3)	0762 (2)	----------	4216. 0156	4214. 8283	200	I
4194	1981 (3)	1980 (2)	----------	4210. 0764	4208. 8907	3000	II
4179	2375 (3)	2374 (2)	----------	4194. 1980	4193. 0165	900	I
				4179. 2374	4178. 0598	3000	II
4166	9403 (3)	9403 (2)					
4159	7078 (3)	7074 (2)	----------	4166. 9403	4165. 7659	1000	I
4151	1566 (3)	1570 (2)	----------	4159. 7076	4158. 5351	800	I
4133	9191 (3)	9191 (1)	----------	4151. 1568	4149. 9865	800	II
4128	5761 (3)	5759 (2)	----------	4133. 9191	4132. 7534	600	II
				4128. 5760	4127. 4117	1400	I
4116	9199 (3)	9201 (2)					
4109	5788 (3)	5791 (1)	----------	4116. 9200	4115. 7587	800	I
4101	4985 (3)	4984 (2)	----------	4109. 5789	4108. 4195	800	II
4095	9025 (3)	9031 (2)	----------	4101. 4984	4100. 3412	1100	I
4087	6743 (2)	6739 (2)	----------	4095. 9028	4094. 7470	1600	II
				4087. 6741	4086. 5205	1600	II
4068	5993 (3)	5992 (2)					
4060	3990 (3)	3991 (2)	----------	4068. 5993	4067. 4507	400	I
4047	7144 (3)	7144 (2)	----------	4060. 3990	4059. 2525	1000	I
4044	5366 (3)	5371 (2)	----------	4047. 7144	4046. 5712	------	Hg^{198}
4037	1880 (3)	1878 (2)	----------	4044. 5368	4043. 3945	800	I
				4037. 1879	4036. 0475	1800	I
4020	2649 (4)	2649 (2)					
4013	6295 (3)	6292 (2)	----------	4020. 2649	4019. 1289	4000	II
4009	3433 (3)	3438 (2)	----------	4013. 6293	4012. 4950	2000	I
3995	6786 (3)	6787 (2)	----------	4009. 3435	4008. 2104	1600	I
3981	2147 (3)	2153 (2)	----------	3995. 6786	3994. 5490	1200	I
				3981. 2150	3980. 0892	1100	I
3968	5145 (3)	5142 (2)					
3950	0814 (2)	0810 (1)	----------	3968. 5144	3967. 3919	2000	I
3934	0243 (3)	0243 (1)	----------	3950. 0813	3948. 9636	1000	I
3924	9103 (3)	9106 (1)	----------	3934. 0243	3932. 9108	1400	I
3906	2992 (2)	2926 (1)	----------	3924. 9104	3923. 7993	400	I
				3906. 2924	3905. 1861	1500	II
3870	7606 (2)	7604 (2)					
3864	5008 (3)	5011 (2)	----------	3870. 7605	3869. 6635	600	I
3855	6036 (3)	6035 (2)	----------	3864. 5009	3863. 4055	1200	II
3843	0497 (3)	0499 (2)	----------	3855. 6036	3854. 5105	1200	II
3840	7829 (3)	7837 (2)	----------	3843. 0498	3841. 9600	1200	II
				3840. 7833	3839. 6941	2500	I
3829	4707 (3)	4709 (2)					
3819	7691 (1)	7692 (1)	----------	3829. 4708	3828. 3845	3200	I
3814	1497 (3)	1497 (2)	----------	3819. 7692	3818. 6855	500	I
3804	1545 (3)	1550 (2)	----------	3814. 1497	3813. 0674	1200	II
3786	6748 (1)	6749 (1)	----------	3804. 1547	3803. 0750	4000	I
				3786. 6749	3785. 5997	1000	II

TABLE 2. *Wavelengths in thorium spectra*—Continued

1	2	3	4	5	6	7	8
Whole angstrom	Fractional angstrom			Vacuum	Air	Relative intensity	Spectrum
	25 mm(obs.)	40 mm(obs.)	50 mm(obs.)				
3782	0398 (1)	0405 (1)	.....	3782. 0402	3780. 9663	350	I
3772	4418 (3)	4418 (2)	.....	3772. 4418	3771. 3703	1500	I
3764	0037 (3)	0027 (2)	.....	3764. 0032	3762. 9345	1200	I
3753	6349 (3)	6353 (2)	.....	3753. 6351	3752. 5685	3500	II
3743	9871 (3)	9873 (2)	.....	3743. 9872	3742. 9231	1100	I
3728	9626 (3)	9622 (1)	.....	3728. 9624	3727. 9022	800	I
3720	4924 (3)	4926 (1)	.....	3720. 4925	3719. 4345	3000	I
3712	3595 (2)	3597 (2)	.....	3712. 3596	3711. 3037	600	II
3702	0310 (3)	0313 (2)	.....	3702. 0312	3700. 9780	300	I
3693	6171 (3)	6171 (2)	.....	3693. 6171	3692. 5661	1200	I
3683	5343 (3)	5347 (2)	.....	3683. 5345	3682. 4861	1000	I
3671	0137 (1)	0141 (1)	.....	3671. 0139	3669. 9687	750	I
3669	1842 (3)	1844 (2)	.....	3669. 1843	3668. 1396	1000	I
3657	7352 (3)	7354 (2)	.....	3657. 7353	3656. 6936	1000	I
3651	1962 (2)	1971 (1)	.....	3651. 1967	3650. 1566	.....	Hg^{198}
3643	2866 (3)	2867 (2)	.....	3643. 2867	3642. 2487	2200	I
3633	8656 (3)	8654 (2)	.....	3633. 8655	3632. 8299	1000	I
3623	8282 (3)	8280 (2)	.....	3623. 8281	3622. 7951	800	I
3616	1633 (1)	1634 (1)	.....	3616. 1634	3615. 1324	2000	II
3613	4575 (3)	4573 (2)	.....	3613. 4574	3612. 4271	1400	I
3599	1459 (3)	1464 (2)	.....	3599. 1462	3598. 1196	2000	I
3593	8040 (3)	8042 (2)	.....	3593. 8041	3592. 7788	2000	I
3585	1985 (2)	1981 (2)	.....	3585. 1983	3584. 1753	800	I
3577	5786 (3)	5782 (2)	.....	3577. 5784	3576. 5573	1000	II
3568	2818 (3)	2825 (2)	.....	3568. 2822	3567. 2635	1200	I
3560	4658 (1)	4657 (1)	.....	3560. 4657	3559. 4490	2500	II
3552	4161 (3)	4158 (2)	.....	3552. 4159	3551. 4013	1000	I
3545	0306 (3)	0300 (2)	.....	3545. 0303	3544. 0176	1500	I
3540	5980 (3)	5983 (2)	.....	3540. 5982	3539. 5867	4000	II
3519	4094 (3)	4095 (2)	.....	3519. 4094	3518. 4033	1000	I
3512	1610 (3)	1613 (2)	.....	3512. 1612	3511. 1570	1000	I
3504	7880 (1)	7870 (1)	.....	3504. 7875	3503. 7852	500	I
3499	6215 (3)	6216 (2)	.....	3499. 6216	3498. 6206	900	I
3494	5174 (2)	5174 (1)	.....	3494. 5174	3493. 5177	2000	II
3480	1680 (3)	1688 (1)	.....	3480. 1683	3479. 1723	800	II
3469	2126 (3)	2125 (2)	.....	3469. 2125	3468. 2193	2000	II
3463	8419 (2)	8417 (2)	.....	3463. 8418	3462. 8500	2000	II
3452	6910 (3)	6908 (2)	.....	3452. 6909	3451. 7019	900	I
3443	5652 (3)	5651 (2)	.....	3443. 5651	3442. 5785	800	I
3434	9827 (3)	9831 (2)	.....	3434. 9829	3433. 9985	3000	II
3422	1908 (3)	1910 (2)	.....	3422. 1909	3421. 2097	2500	I
3413	9918 (3)	9918 (2)	.....	3413. 9918	3413. 0127	1800	I
3406	5346 (3)	5348 (2)	.....	3406. 5347	3405. 5575	1400	I
3397	7021 (3)	7022 (2)	.....	3397. 7022	3396. 7273	1400	I
3393	0083 (1)	0087 (1)	.....	3393. 0085	3392. 0348	6000	II
3386	5033 (3)	5030 (2)	.....	3386. 5032	3385. 5312	800	II
3381	8300 (3)	8305 (2)	.....	3381. 8303	3380. 8595	900	I
3375	9438 (3)	9446 (2)	.....	3375. 9439	3374. 9746	1600	I
3359	5663 (3)	5668 (3)	.....	3359. 5666	3358. 6014	2000	II
3352	1910 (3)	1913 (2)	.....	3352. 1911	3351. 2278	2500	II
3338	8296 (3)	8297 (2)	.....	3338. 8296	3337. 8697	2000	II
3331	4347 (2)	4343 (1)	.....	3331. 4345	3330. 4765	1800	I
3326	0765 (3)	0768 (2)	.....	3326. 0767	3325. 1201	3000	II
3325	7088 (3)	7088 (2)	.....	3325. 7088	3324. 7523	2000	II
3310	3174 (3)	3180 (2)	.....	3310. 3176	3309. 3650	800	I
3305	1894 (3)	.....	.....	3305. 1894	3304. 2381	3000	I
3293	4685 (3)	4686 (1)	.....	3293. 4685	3292. 5202	3000	II
3288	7355 (3)	7357 (2)	.....	3288. 7356	3287. 7885	1600	II

TABLE 3. *Test of* Th I *wavelengths*

Line pair	Wavelength	Wavenumber	Wavenumber difference
	A	*K*	*K*
1	4494.5941	22248.950	2869.260
	5160.0411	19379.690	
2	4375.3536	22855.296	2869.255
	5003.4922	19986.041	
3	3840.7833	26036.356	2869.267
	4316.4681	23167.089	
4	3643.2867	27447.744	2869.261
	4068.5993	24578.483	
5	3599.1462	27784.367	2869.261
	4013.6293	24915.106	
6	3331.4345	30017.099	2869.261
	3683.5345	27147.838	
7	3310.3176	30208.582	2869.261
	3657.7353	27339.321	
8	4896.3215	20423.495	3687.989
	5975.3199	16735.506	
9	3829.4708	26113.269	3687.989
	4459.2531	22425.280	
10	3305.1894	30255.452	3687.993
	3764.0032	26567.459	
11	4896.3215	20423.495	5563.143
	6729.3157	14860.352	
12	4258.6944	23481.375	5563.143
	5580.9077	17918.232	
13	4104.4984	24381.333	6362.396
	5549.7170	18018.937	
14	4037.1879	24769.716	6362.396
	5432.6212	18407.320	

ards is 10 A from 3300 to 4300 A, 17 A from 4300 to 5300 A, 23 A from 5300 to 6300 A, and 30 A from 6300 to 7000 A. This distribution according to wavelength corresponds closely to an average spacing of standards at intervals of 72 K on a wavenumber scale throughout the range 14300 to 30400 K. Since spectra are always measured in wavelength units, but interpreted in wavenumber units (proportional to energy) this is suggested as the ideal distribution of secondary standards of wavelength. It is emphasized again that the values in table 2 are only a preliminary list which should be refined by comparing still higher orders of interference, and perhaps measuring still more wavelengths to decrease the intervals between standards.

The present list of 222 thorium wavelengths in table 2 may serve for immediate direct measurement of complex spectra from 3300 to 7000 A, and by photographing these standards in a grating's second-order spectrum and doubling the values, they may serve also for the measurement of spectra from 6600 to 14000 A photographed in the grating's first order.

Finally, the most important next step is to extend the measurement of wavelengths from thorium-halide lamps to shorter waves, that is from 3300 to 2000 A or less. When this is done the iron arc at atmospheric pressure may be abandoned as a source of standard wavelengths (except for rough measurements) but still retained as an aid in recognizing the thorium standards. Because of the highly complex character of thorium spectra, and the lack of striking groups of lines or useful maps, it will be convenient (and perhaps necessary) to juxtapose the simpler and more familiar spectrum of the iron arc for purposes of orientation.

R. W. Stanley acknowledges the support received from a grant of the National Science Foundation.

References

[1] R. W. Stanley and W. F. Meggers, J. Research NBS **58,** 41 (1957) RP2733.
[2] G. R. Harrison, MIT Wavelength Tables, xv (John Wiley & Sons, New York, N. Y., 1939).
[3] L. Bovey, Spectrochimica Acta **10,** 383 (1958).
[4] M. Fred and F. S. Tomkins, J. Opt. Soc. Am. **47,** 1076 (1957).
[5] G. R. Harrison, J. Opt. Soc. Am. **36,** 644 (1946).
[6] G. R. Harrison, J. Opt. Soc. Am. **40,** 132 (1950).
[7] W. F. Meggers and F. O. Westfall, J. Research NBS **44,** 447 (1950) RP2091.
[8] M. Zelikoff, P. H. Wyckoff, L. M. Aschenbrand, and R. S. Loomis, J. Opt. Soc. Am. **42,** 818 (1952).
[9] C. H. Corliss, W. R. Bozman, and F. O. Westfall, J. Opt. Soc. Am. **43,** 398 (1953).
[10] F. S. Tompkins and M. Fred, J. Opt. Soc. Am. **47,** 1087 (1957).
[11] W. F. Meggers, Anal. Chem. **28,** 616 (1956); Trans. Int. Astron. Union **9,** 226 (1957).
[12] W. F. Meggers and K. G. Kessler, J. Opt. Soc. Am. **40,** 737 (1950).
[13] K. G. Kessler and W. F. Meggers, J. Opt. Soc. Am. **45,** 902 (1955); and unpublished data.
[14] W. F. Meggers and C. J. Humphreys, J. Research NBS **18,** 543 (1937) RP992.
[15] B. Edlén, J. Opt. Soc. Am. **43,** 339 (1953).
[16] J. R. McNally, Jr., G. R. Harrison, and H. B. Park, J. Opt. Soc. Am. **32,** 334 (1942); ibid. **35,** 390 (1945).
[17] Ph. Schuurmans, Physica **12,** 589 (1946) (Dissertation, Univ. Amsterdam, 1946).
[18] R. Zalubas (unpublished data, 1957–1958).

WASHINGTON, April 22, 1958.

Journal of Research of the National Bureau of Standards Vol. 61, No. 2, August 1958 Research Paper 2892

An Electrical-Analog Method for Transient Heat-Flow Analysis

A. F. Robertson and Daniel Gross

An electronic instrument is described which permits solution of transient heat-flow problems by use of direct analogy to electrical networks. The instrument is of the so-called "fast-time" type, simulating the transient involved in times of the order of 10^{-6} that of the thermal prototype. A photoformer type of input-signal generation is used and this, together with a variable-frequency master oscillator, permits flexibility of input-signal waveform and time scale.

Some applications of the instrument to the field of fire research are described. The discussion of errors includes consideration of those resulting from the lumping of circuit elements.

1. Introduction

Laboratories in which studies are performed on the fire-resistance behavior of building structural components have been frequently asked to predict or estimate the fire performance of structures that have not been tested. In some cases data are available upon which useful estimates may be based. In most cases, however, the quality of the resulting estimates is largely dependent on the experience and feeling the estimator has for the problem. In an effort to assist in placing such estimates on a more exact basis, an electronic device for performing the necessary computations was designed and constructed at the Bureau.

Fire-resistance tests are performed on portions of buildings for the purpose of determining the suitability of the construction in withstanding the effects of fire. While mechanical behavior may frequently limit the usefulness of the structure in this respect, it often happens that thermal transmission is the critical factor in determining its ability to resist fire. The procedure used during such tests [1][1] requires application to the furnace-enclosed structure of a time-varying temperature function corresponding to the standard fire exposure. The procedure also permits heat losses to occur from the unexposed portion of the specimen by both radiation and convection. These conditions make it impractical to use analytical methods for solution of the heat-transfer equation.

Because of this it seemed desirable to use some high-speed approximation methods for computing the thermal behavior of structures exposed to fire. Both digital and conventional analog computers were considered and used with a certain degree of success for approximate solutions of such problems. However, it seemed likely that use of the direct analogy between thermal and electrical circuits might permit greater flexibility in the solution of problems and simplify the "coding".

The device constructed is somewhat similar to the one developed by Lawson & McGuire [2]. This makes use of the analogy between electrical and thermal circuits directly without the need for a large assembly of electronic mathematical-operator units which, in conventional computers, are assembled in appropriate fashion to solve the mathematically expressed relationship describing the heat-transfer problem. This direct use of the analogy permits building a basic signal-generating and measuring unit which is much more compact than the usual analog computer. The theory, construction problems, operation, and limitations of this device are briefly described.

[1] Figures in brackets indicate the literature references at the end of this paper.

2. Analogies

In many engineering investigations of the physical behavior of mechanical, electrical, fluid dynamic, thermal, and optical systems, the complexity of analytical or approximate numerical solutions of the mathematical formulation of the problem may become very difficult and excessively time consuming. In the past this has often resulted in the use of intuitive design procedures. In such cases an approximate prototype of the system involved was constructed and experimental studies made of its performance. In many instances it was difficult to vary the design parameters without extensive rebuilding of the prototype. Because of this, scientists and engineers concerned with the design of such systems have, with increasing frequency, made use of analogies. Thus an electrical system may be analogous to a mechanical, thermal, or other system provided there is a likeness between the two systems. Usually such a likeness is not one of appearance or form but a resemblance of physical behavior. Thus, if it can be shown that the mathematical descriptions of the behavior of two different systems are similar, then it is usually possible to use one system as a means for studying the behavior of the other. The ease with which electrical circuits can be assembled and their behavior studied have made them particularly useful as analogs.

Analogs have long been used by men, maps perhaps represent one of the earliest useful forms. Kirchhoff [3] in 1845 utilized the analogy between current flow in a plate and flux distribution between charged parallel-line conductors in a uniform medium to determine the capacitance between certain configurations of such conductors. Since then, hundreds of publications have appeared on the subject of analog

470483—58——4

techniques. Higgins [4] has compiled a very extensive bibliography of electroanalogic methods in which appear references to almost a thousand original papers. Soroka's paper [5] provides one of the better introductions to the great versatility of analog techniques in the solution of engineering problems. His later book [6] provides a detailed exposition of many possible analog methods and techniques.

Beuken [7] presented one of the early descriptions of the use of electrical circuits for analysis of transient heat-flow phenomena. Paschkis [8] has constructed and made extensive use of a similar but larger device. Both of these instruments are of the so-called "long-time" type. This implies that the thermal transients are studied by means of electrical circuits requiring transient periods of several minutes or more duration. This permits the use of potentiometric-type instruments for data-recording purposes. The major drawback to the use of such systems is the requirement for use of rather large capacitors.

Lawson and McGuire [2] describe a device of the "fast-time" type. Here the electrical transient is completed in a few milliseconds and the problem repetitively solved, measurements being made by means of cathode-ray presentation of the data. This latter device was intended primarily for solution of problems quite similar to those considered here. In their paper they present a rather comprehensive exposition of the basis of the electrical-thermal transient analogy, together with a discussion of means of application to one-dimensional space problems and some discussion of the possible errors involved in the use of lumped circuit elements. Because of the extensive discussions in the literature of the various types of analog systems possible it would serve little purpose to repeat the descriptions here. A brief indication will, however, be made of the theoretical basis for use of electrical models for solution of transient heat-flow problems. This should not be taken to imply that heat-flow problems are the only type for which the instrument to be described may be used. It consists essentially of a voltage versus time signal-generation unit, means for application of the generated signal repetitively to an electrical network, and provision for measuring the transient voltages which are developed within the model. Thus, any electrical network that can be used as an analogy of another type of system may be used with this instrument.

By definition the rate of heat flow $\partial Q/\partial t$ in the direction of a one-dimensional thermal gradient is given as the product of the conductivity k, the area A across which heat flow is taking place, and the temperature gradient $\partial\theta/\partial x$ or,

$$\partial Q/\partial t = -kA\partial\theta/\partial x, \tag{1}$$

the negative sign indicating that flow takes place in the direction of a negative temperature gradient.

The difference in the heat-flow rates into and out of a small elemental section along the path of heat flow, or the heat-flow gradient, is equal to the product of the volumetric heat capacity ρs, rate of temperature rise $\partial\theta/\partial t$, and area over which heat is flowing. Thus

$$\frac{\partial}{\partial x}\frac{\partial Q}{\partial t} = -A\rho s\frac{\partial\theta}{\partial t}. \tag{2}$$

Combining these two equations we obtain,

$$\frac{\partial\theta}{\partial t} = \frac{k}{\rho s}\frac{\partial^2\theta}{\partial x^2}. \tag{3}$$

This is the one-dimensional form of the well-known Fourier equation of heat conduction.

In a similar manner we may develop the equations for a series-resistance, shunt-capacitance electrical transmission line for the particular case in which the capacitance is assumed proportional to the volume of the line.[2] From the definition of electrical units and Kirchoff's laws,

$$i = -\frac{a}{r}\frac{\partial v}{\partial x}, \tag{4}$$

where i is the current, r the resistivity of the line material, a the cross-sectional area and $\partial v/\partial x$ the voltage gradient. The current gradient in the direction of flow becomes,

$$\frac{\partial i}{\partial x} = -ca\frac{\partial v}{\partial t}, \tag{5}$$

where c is the capacitance per unit volume and $\partial v/\partial t$ is the rate of voltage rise. Equations (4) and (5) may be combined to form,

$$\frac{\partial v}{\partial t} = \frac{1}{rc}\frac{\partial^2 v}{\partial x^2}. \tag{6}$$

Equations (3) and (6) are obviously similar and thus justify the use of the electrical system as an analog to the thermal system. In a similar way, eq (1) and (4) and (2) and (5) may be considered as analogous. Table 1 has been prepared to list the properties of the two systems in analogous form, assuming equivalence of the cross-sectional areas of the thermal and electrical circuits.

Because of difficulties of constructing within small dimensions, electrical models of such transmission lines in which the capacitance is distributed along its length, it is common practice to approximate this by a lumped system network. Three such networks, incorporating a series of either **T, L,** or **Π** sections, such as those bounded by dotted brackets are shown in figure 1. It may be seen that although the three lines consist of different arrangements of resistance and capacitance elements, the lines are identical except for portions of the first and last sections. The resistors, R, of these lines then correspond to the total resistance of the thermal circuit divided by the number of sections, N, used in the electrical model. In a similar way the capacitors correspond to the sectional heat capacity of

[2] This differs from the geometrical considerations commonly used in determining capacitance. Such treatment is used, however, to permit development of the equations shown and to thus maintain true similitude of the thermal-electrical analogy.

TABLE 1. *Analogous elements of thermal and electrical systems*

Thermal			Electrical		
Property	Symbol	Unit	Property	Symbol	Unit
Temperature	θ	° C	Voltage	v	volt
Time	t_t	second	Time	t_e	second
Heat-flow rate	$\partial Q/\partial t_t$	watt	Current	i	microampere
Heat capacity	ρs	joule/cm ^{3} ° C	Capacitance	c	microfarad/cm ^{3}
Conductivity	k	watt/cm ° C	Conductivity	$1/r$	1/megohm cm
Length	x_t	cm	Length	x_e	cm
Temperature gradient	$\partial\theta/\partial x_t$	° C/cm	Voltage gradient	$\partial v/\partial x_e$	volt/cm
Rate of temperature rise	$\partial\theta/\partial t_t$	° C/second	Rate of voltage rise	$\partial\theta/\partial t_e$	volt/second

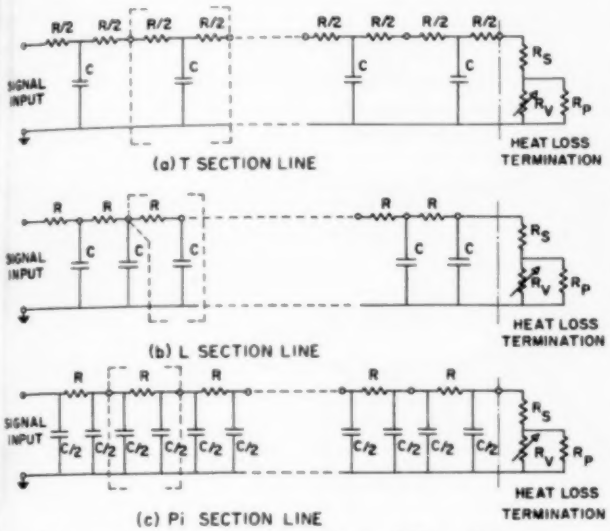

FIGURE 1. *Comparison of* **T**, **L**, *and* **Pi** *section lines.*

the thermal model, $\rho s x/N$. The termination, R_f, comprising a varistor, or positive voltage coefficient resistor R_v, together with series and parallel resistors, R_s and R_p, if necessary, is used to simulate the convective and radiative heat losses from the cool end of the thermal structure. The detailed technique for using such elements was described by Lawson and McGuire [2].

Again considering the similarity between eq (3) and (6) together with the analogous properties shown in table 1, it is common practice to substitute electrical for thermal properties directly and to solve the electrical problem, but to think of the solution as a thermal one. In performing this conversion it will be found convenient to use scaling factors. Thus rather than substituting directly electrical capacitance for heat capacity we have,

$$c=\frac{\rho s}{n} \quad \text{or} \quad n=\frac{\rho s}{c},$$

similarly for resistivity

$$r=\frac{1}{mk} \quad \text{or} \quad m=\frac{1}{kr},$$

and for time

$$t_e=\frac{t_t}{mn\phi} \qquad \phi=\frac{t_t}{mnt_e},$$

where n, m, and ϕ are the capacity, resistivity, and time-scaling factors, respectively. Factors such as these may be used both to obtain control over the size of the electrical components used as well as to provide a legitimate manner for conversion from thermal to electrical units as implied by these equations. This latter objective may, however, also be obtained by the assumption of such conversion ratios without their explicit mention. Table 2 shows the modifications of the analogous thermal and electrical elements when capacity, resistivity, and time-scaling factors are employed. The relationships developed maintain the identity of eq (4) and (5).

TABLE 2. *Modification of analogy relationships by application of scaling factors*

Property	Thermal system	Electrical system	
		Direct analogy ($m=n=\phi=1$)	Modified analogy ($m=1/kr$, $n=\rho s/c$, $\phi=t_t/mnt_e$)
Resistivity	$1/k$	r	mr
Capacity	ρs	c	nc
Time	t_t	t_e	$mn\phi t_e$
Length	x_t	x_e	$\sqrt{\phi}\,x_e$
Temperature	θ	v	v
Heat flow	$\partial Q/\partial t_t$	i	$i/m\sqrt{\phi}$
Heat-loss resistance	$1/h$	R_f	$m\phi R_f$

As an example of the manner in which an electrical model may be constructed it will be assumed that we wish to represent a concrete floor slab which is 10.16 cm (4 in.) thick. We will assume that the model is to have 20 sections of the **L** type. This problem is shown in figure 2.

For a resistivity scaling factor of m we have for the resistance,

$$\frac{x}{kN}=\frac{mrx}{N}=mR, \quad \text{or} \quad R=\frac{x}{Nmk}.$$

Inserting numerical values and using a consistent set of dimensions for both electrical and thermal systems,

$$R=\frac{x}{Nmk}=\frac{10.16}{(20)\,(0.0156)\,(m)}=\frac{32.6}{m}.$$

If $m=652$, each network resistor is 0.050 meg, a convenient value.

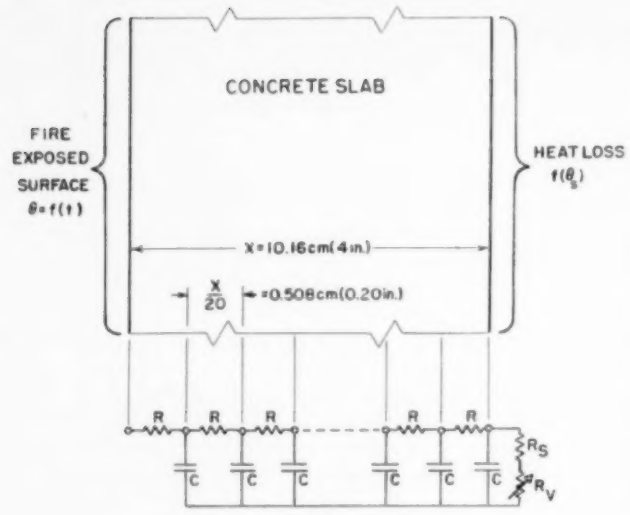

FIGURE 2. *Method of development of electrical model for a fire-exposed concrete slab.*

Thermal properties: k=0.0156 w/cm ° C (0.90 Btu/hr ft ° F); ρ=2.24 g/cm (140 lb/ft³); s=0.837 joule/g ° C (0.2 Btu/lb ° F). Electrical values: R=50K R_s=400 K; R_v=varistor; C=449 $\mu\mu$f.

In a similar fashion, for a capacity scaling factor of n we have,

$$\frac{\rho s x}{N}=\frac{ncx}{N}=nC \quad \text{or } C=\frac{\rho s x}{Nn}.$$

Again inserting numerical values,

$$C=\frac{\rho s x}{Nn}=\frac{(2.24)(0.837)(10.16)}{(20)(n)}=\frac{0.953}{n}.$$

If n=2120, each network capacitor is 0.000449 μf.

Finally, for ϕ=1,

$$t_t=mnt_e=(652)\ (2120)t_e=1.38\times10^6 t_e.$$

Thus, in using the scale ratios proposed, the thermal time scale has been compressed by a factor of about 10^6. To provide for a thermal period of 8 hr, we represent this by $8\times10=80$ divisions of 6 min each. Each division therefore corresponds to $6\times60/1.38\times10^6=261$ μsec, and the master oscillator is adjusted to operate at a frequency of 3.83 kc. The appropriate varistor assembly is connected at the end of the network corresponding to the upper surface of the floor slab to represent radiative and convective heat losses.

If, as is often likely, it is found that capacitors or resistors of the particular sizes suggested are not readily available the value of m and/or n may be changed and the frequency similarly adjusted. The ease with which this may be done is one of the desirable features of this particular instrument. It not only greatly facilitates construction of models but, as shown in table 2, permits the use of a given model to simulate a whole range of structure sizes simply by independent change of the time scale, i. e. a change in ϕ. When this is done it is important to remember that all dimensions of the thermal system are changed. Thus in the analog of a multicomponent thermal body a change of time scale will result in the simulation of a new thermal system in which all dimensions in the direction of heat flow are scaled in the same ratio. If special terminations have been used to simulate heat-loss conditions for such a system, care must be taken to adjust these separately according to the scaling relationships shown in table 2.

3. General Description of Instrument

The instrument constructed was of the "fast-time" type in which a particular problem is solved repetitively at a speed much higher than that used for the thermal prototype. The ratio of the speed of the electrical operation to the speed of the thermal process was of the order of 10^6. This requires cathode-ray presentation for read-out of the repetitively solved problem. In order to reduce the cost and time involved in its construction, commercial electronic instruments were used wherever it seemed practical.[3]

A block diagram of the device is shown in figure 3. This has been divided into three interrelated functional units: (a) The signal generator; (b) the electrical model; and (c) the measuring circuits. The three power supplies are not shown.

The signal generator unit selected was of the photoformer type [9, 10]. This type was chosen because of the great flexibility of waveforms possible with such a system and the ease with which they could be interchanged. A cathode-ray tube is arranged with an opaque mask covering a portion of its face. A phototube with appropriate amplifier is arranged to view the face of the cathode-ray tube. The amplified output of the phototube is applied to the vertical deflection plates of the cathode-ray tube in such a way that when the spot is "seen" by the phototube it is deflected downwards and forced to be partially hidden by the mask. The application of a relaxation-type timing sweep to the horizontal plates of the cathode-ray tube results in the spot following the mask outline on the cathode-ray tube screen. Since for given operating conditions the position of the spot on the screen bears a fixed relationship to the voltage applied to the deflection plates, a voltage-time signal may be taken from them which is controlled by the shape of the mask.

In practice, a commercial oscilloscope was used in conjunction with a photomultiplier tube as the generator. A special impedance converter was built to modify the balanced high-impedance signal applied to the deflection plates into a low-impedance single-ended output signal suitable for application to the model.

The electrical model was custom-made for each thermal situation being simulated. Figure 4 shows a photograph of one of the models used. It consists

[3] The special components and instruments used in the assembly are listed in the appendix of this paper.

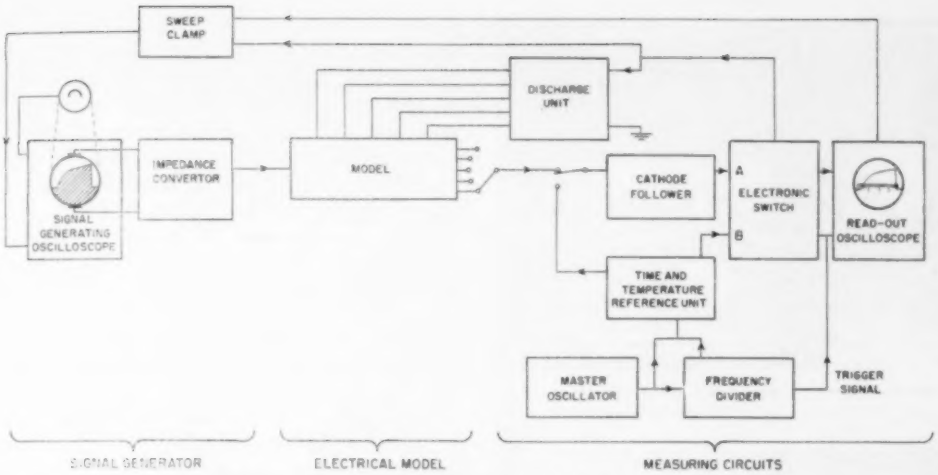

FIGURE 3. *Block diagram of the instrument.*

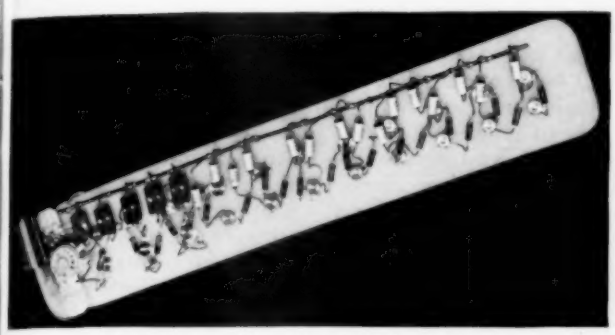

FIGURE 4. *View of an electrical model.*

of a series of resistors representing the thermal resistance of the prototype and a group of capacitors shunting these resistors to ground and representing the heat capacity of the thermal system. The assembled model assumes the form of a plug-in unit, provisions being made for twenty discharge points.

The measuring unit comprised a number of circuits which may be briefly described as follows:

1. The master oscillator is a variable-frequency square-wave generator used as a time-reference source.

2. The frequency-divider circuit generates the decade-time markers and submultiples of these for synchronizing signals.

3. The temperature and time-reference unit is a mixing device which assembles the calibrated time scale with a variable d-c voltage for making "temperature" measurements.

4. The discharge unit is a special circuit used for discharging the capacitors used in the model. This discharge process is accomplished every alternate sweep of the viewing oscilloscope during the period of presentation of the time and temperature reference signal.

5. The cathode follower is a special high input-impedance circuit which permits making voltage measurements on the model without serious electrical loading of it.

6. The electronic switch provides a means for alternate presentation of the signal from the model and that from the time and temperature reference unit.

7. The read-out oscilloscope provides a means for study of the electrical behavior of the model and permits direct measurement of voltage corresponding to temperature changes within the model. This oscilloscope is used to generate the time-sweep signal for the signal generator. Trigger operation is used and the sweep signal applied to the signal generator is clamped on alternate cycles in such a way that a signal is generated only when required for application to the model.

Figure 5 shows the assembled device. The power supplies have been mounted below the desk while the remainder of the equipment is assembled in two relay racks. The electrical model is seen near the mid-height of the right-hand rack.

4. Special Electronic Circuits

Figure 6 presents the complete circuit diagram for the specially constructed portions of the unit. Also shown diagrammatically are the commercially available electronic units which formed a part of the complete device. The high- and low-voltage power supplies were of the regulated type and are not indicated in this diagram. The special considerations which were involved in the selection of the instruments and circuits follow.

4.1. Signal-Generating Oscilloscope

The particular oscilloscope used was of the low-accelerating voltage, single-anode, electrostatic-deflecting type. It was chosen to permit achievement of high linearity between mask size and output signal. It was fitted with a tube having a short persistence type P–15 phosphor. The short phosphorescent decay time, down 90 percent in 2.8 μsec, of this phosphor was found necessary to permit close following of transient mask shapes. The

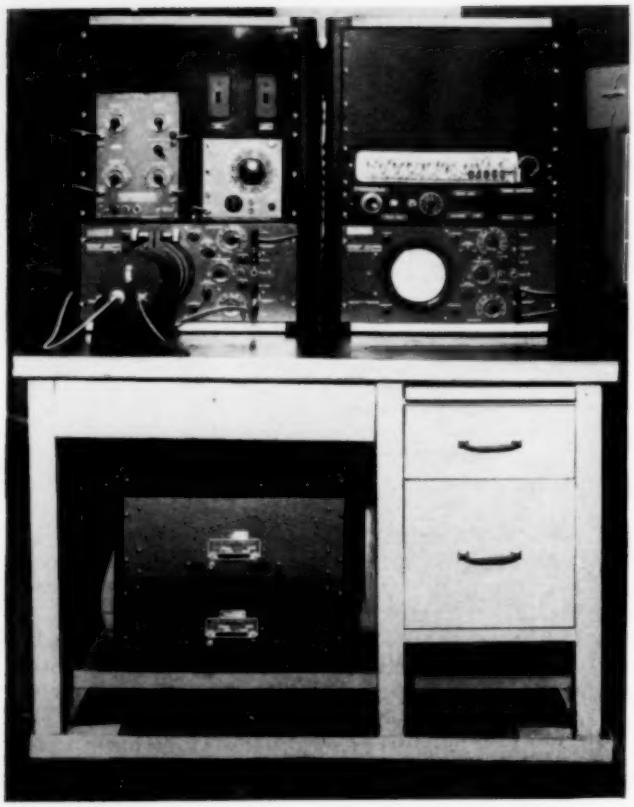

FIGURE 5. *Transient heat-flow analyzer.*

photomultiplier tube associated with the oscilloscope was selected to have a spectral sensitivity which permitted efficient use with the cathode-ray tube phosphor. The high-output sensitivity of this tube was also a factor involved in its selection. A darkened hood was of course used to shield the photomultiplier from room illumination. In using this photoformer circuit it was found that the delay time of the oscilloscope direct-coupled amplifiers caused considerable hunting. This had the effect of superimposing a small a-c signal in excess of 80 kc on the signal being generated. The presence of this high-frequency signal was not considered objectional for normal use in solving problems since it was completely filtered out by the first section of the network to which it was applied. It could be greatly reduced in amplitude by shunting the photomultiplier output by a 150 $\mu\mu$f capacitor. A more proper way of eliminating this hunting would involve design of a special amplifier having short time delay and possibly incorporation of negative feedback. In using a signal generator of this type it is essential that the spot remain on the tube screen during periods when signals are not being generated. To permit this type of operation, the generating oscilloscope was modified by insertion of clamp circuits on the horizontal deflection circuit to prevent the spot from leaving the right-hand edge of the screen. The circuit used is shown in figure 7. It does not abruptly limit spot deflection at one position but has the effect of greatly reducing the deflection sensitivity when the spot approaches the edge of the screen. This type of operation was achieved easily and

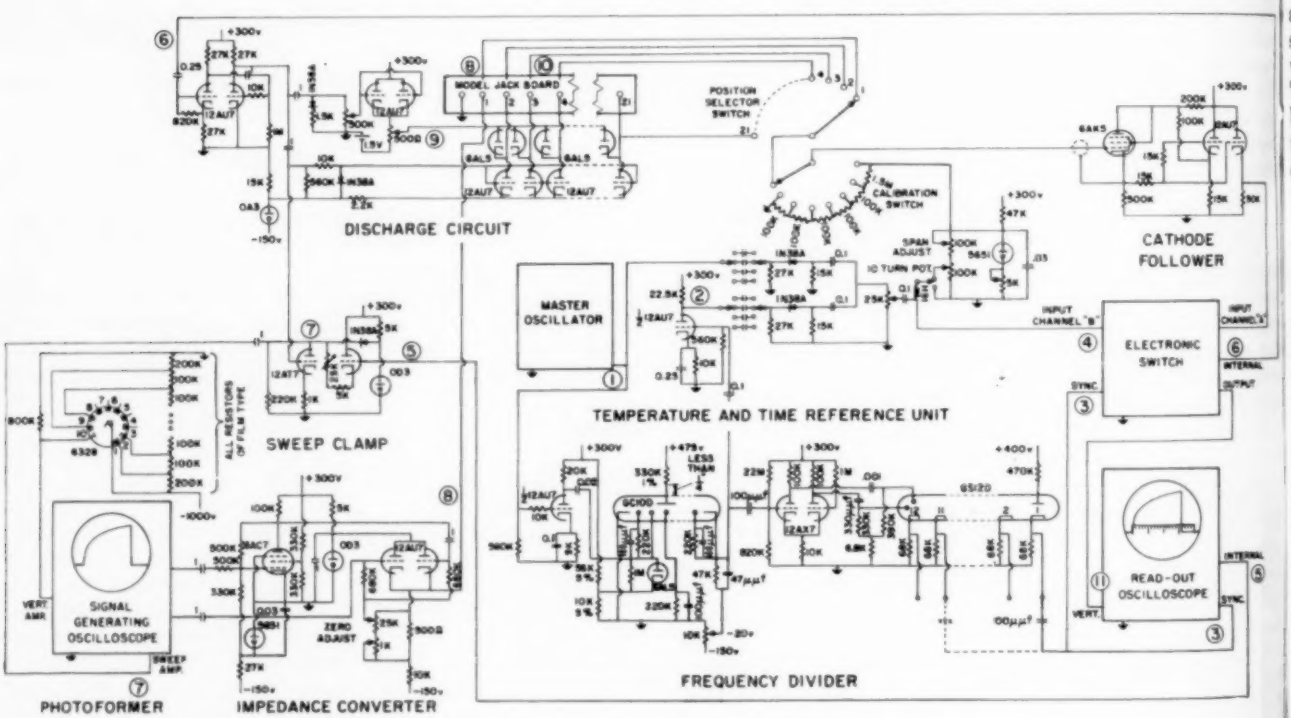

FIGURE 6. *Circuit diagram of analyzer.*

Capacitance values are in microfarads unless otherwise indicated in micromicrofarads ($\mu\mu$f).

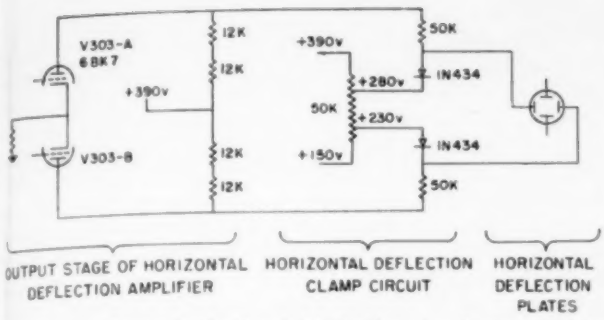

FIGURE 7. *Clamp for horizontal deflection circuit of generating oscilloscope.*

seemed desirable to assist in preventing "burning" of the phosphor of the cathode-ray tube screen. The oscilloscope used was provided with a beam-blanking circuit for removal of the return trace image. This feature was undesirable in the unit as used for signal generation and the instrument controls were accordingly set to remove this circuit from operation.

4.2. Impedance Converter

This circuit was designed to combine the balanced but out-of-phase voltages applied to the vertical deflecting plates of the generating oscilloscope into a single-phase output signal with ground as a reference level. Capacity coupling was used, although direct coupling if practical would have provided for more rapid and easy adjustment of the output level with respect to ground. The pentode is used here as a unity-gain phase inverter and the twin triode as an averaging circuit. This was acceptable as a substitute for a true addition circuit because of the very similar size of the two signals being averaged. The output impedance of the converter as measured by the shunt resistance required for 50-percent attenuation of signal was found to be about 250 ohms.

4.3. Sweep Clamp

The horizontal timing sweep used for forming the input signal was obtained from an internal connection to the sweep-generating circuit of the viewing oscilloscope. The sweep clamp provided a means for rejecting every alternate sweep cycle and thus only generating an input signal when it was necessary to apply one to the model.

4.4. Cathode Follower

This circuit is used as a high-impedance probe feeding a wide-band impedance converter. The circuit while probably not original with us has the unique feature of permitting high-impedance operation with large input signals. The potential divider between plate and cathode of the first stage of the twin triode serves as a variable plate-supply source for the 6AK5 used as cathode-follower input stage. In this manner large voltage signals can be followed while at the same time limiting the potential drop across the input tube. The input impedance as measured by the decay of voltage on a capacitor was found to be at least 8,000 meg. Frequency response was highly linear up to 25 kc. The output of this circuit is mixed with the time and calibration signal by the electronic switch.

4.5. Master Oscillator

The time-reference standard for the unit comprises a variable-frequency square-wave oscillator. The output of this unit was fed to both the temperature and time-reference unit, and the frequency divider. The former comprised differentiating, rectifying, and mixing circuits.

4.6. Frequency Divider

This circuit made use of "Dekatron" glow-counter tubes of both scale of 10 and scale of 12 types in series. The former permitted accentuation of each tenth timing mark while the latter permitted generation of a synchronizing signal as a submultiple of the scale of 10 count. The output from each of the 12 cathodes of this tube were separately available so that considerable flexibility was possible in generating a time signal appropriate to the input signal being used. The output from this scale of 12 count was used to synchronize the time sweep of the viewing oscilloscope and the switching frequency of the electronic switch. An internal connection was made to the electronic switch to provide a square-wave output in synchronism with the trigger input signal. This output was used to operate both the sweep clamp and the discharge circuit.

4.7. Discharge Circuit

This unit comprises three circuits: (a) A twin triode amplifier and phase inverter, the output of which is split into two signals to drive; (b) the discharge triodes for each individual section of the model; and (c) the clamp-diode reference-level generator. This last circuit was necessary to permit balancing out the potential drop across the clamp diodes and thus to permit discharge of the network model to the ground-reference level. In the original unit, 20 discharge triodes consisting of 10 twin triodes, were used permitting complete discharge of a 20-section electrical model. The discharge circuit was assembled as a unit in a relay-rack section, 3 in. high. A total of 3 discharge circuit assemblies could be installed in the relay rack illustrated in figure 5. This corresponds to a model requiring 60 discharge points.

4.8. Read-Out or Viewing Oscilloscope

The same type of oscilloscope was used for observation of behavior of the model as was used for the signal generator. This was done largely because of the facilities it provided for driven-sweep operation from an external trigger signal. This together with the requirement of a highly linear time-sweep source for the signal generator are the only essential requirements of the unit. High linearity of the vertical

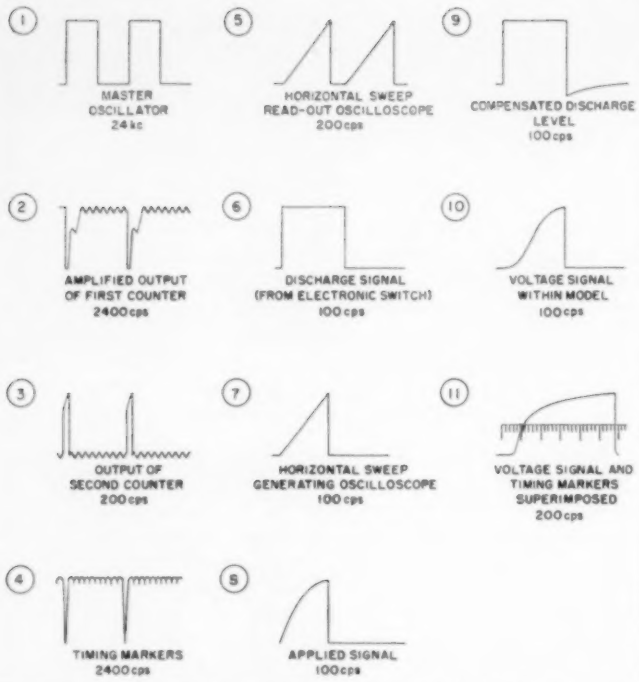

FIGURE 8. *Waveforms experienced in normal circuit operation with master oscillator frequency of 24 kc.*

Numbers shown correspond to small encircled numbers in circuit diagram.

deflection amplifiers is not essential because of the method used in comparing two different input signals.

Figure 8 presents the waveforms observed with the use of an oscilloscope with 2-meg input impedance. The points on the circuit at which measurements were made with respect to ground are indicated in figure 6 by small encircled numbers. These waveforms have been presented for the case in which the standard time versus temperature curve was being used as the input signal and the master oscillator was set for 24-kc operation.

5. Performance and Limitations

The performance of the device and the limitations on its use will be described in terms of the errors involved and a comparison between the results obtained by means of analog measurements and those obtained analytically and experimentally. To date, our main interest has been with one-dimensional problems, but the extension to 2 and even 3 dimensions presents practical rather than theoretical difficulties.

5.1. Errors

The errors involved in the solution of transient heat-flow problems by means of the electrical analogy described may be divided into (1) errors due to "lumping," also known as truncation errors, and (2) errors due to experimental sources. Since an iterative process is not involved, the errors due to rounding off introduced in numerical computations are absent.

a. Errors Due to Lumping

These are errors introduced when a line consisting of distributed parameters is represented by one composed of a finite number of sections or lumps. The error is a function of the boundary and initial conditions, the number of lumps, the type of lumping element used (i. e., whether **T, L,** or **Pi**), and the ratio of the time at which measurements are taken to the resistance-capacitance product of the electrical model (the Fourier number). Error analyses are so far available for only a very few types of problems. Lawson and McGuire [2] have shown that for a semi-infinite slab, the surface temperature of which was instantaneously raised to and maintained at a constant level, the temperatures for **T, L,** and **Pi** section networks are identical after the first section. Klein, Touloukian, and Eaton [11] have analyzed the distribution of errors in a finite bar (represented by different numbers of **T**-sections) one end of which is instantaneously raised to a temperature that is maintained constant thereafter while the other end is maintained at a constant reference temperature. They found that departure of the lumped system from the distributed system at the center of the bar was reduced (after high positive departures during the very early part of the transient) from a maximum of −6 percent with a 5-section model to a maximum of −2 percent with an 11-section model. Greater departures were found toward the leading section in a lumped system so that this point may yield unreliable information for the earliest part of the transient. Clarke [12] has analyzed the error in a finite bar represented by different numbers of **L** sections, one end of which is supplied with a constant heat flux, the other end being perfectly insulated. He found that departure of the lumped system from the distributed system at the insulated end of the bar was always positive and decreased with the time at which measurements are made. Friedmann [13] has estimated an upper bound for the global or maximum error between the exact solution of the heat-conduction equation examined by Klein et al. and the exact solution of its lumped parameter analog.

The numerical solution for the distribution of lumping errors in the problem of a finite bar with perfectly insulated sides, one end of which is instantaneously raised to a temperature that is maintained constant thereafter while the other end remains perfectly insulated, seems to have been overlooked by workers in this field. The solution for the lumped system of **T**-sections was found in Jaeger [14], while the exact thermal solution was given by Carslaw and Jaeger [15]. Some of the results of the analytical calculations are shown in a series of curves in figures 9 and 10. The comparison between the errors at the center in each of the lumped circuits as shown in figure 9 indicates the improvement in the results as more sections are used to represent the distributed system. For a given lumped circuit of 10 sections, error curves for three points (corresponding to the lengths 0.05, 0.25, and 0.75) are shown in figure 10. The errors are greatest at the first section and attenuate rapidly for points further removed from the

source. A similar series of curves were derived from the data of Klein et al. for an 11-section system and are shown in figure 11. The similarity in the error distribution for the cases of short- and open-circuit terminations suggests that changes in the circuit termination do not result in appreciable changes in the distribution of errors within a lumped line.

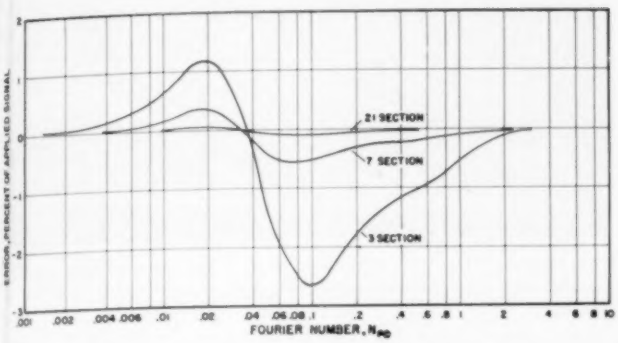

FIGURE 9. *Lumping error at the center of a system represented by 3, 7, and 21* **T** *sections.*

Open-circuit termination.

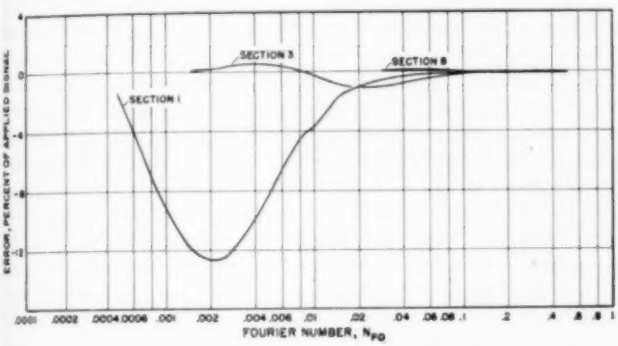

FIGURE 10. *Lumping error at sections 1, 3, and 8 in a system represented by 10* **T** *sections.*

Open-circuit termination.

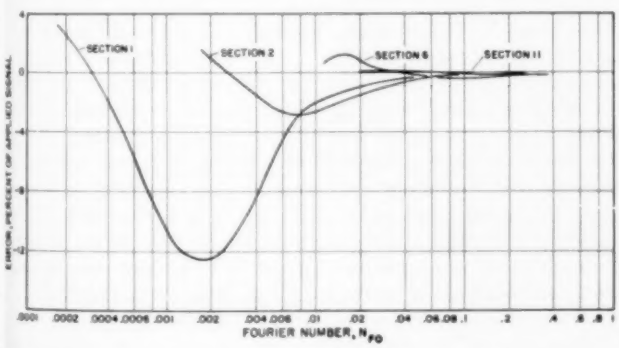

FIGURE 11. *Lumping error at sections 1, 2, 6, and 11 in a system represented by 11* **T** *sections.*

Short-circuit termination. Data from reference [11].

b. Errors Due to Experimental Sources

These include (a) consistent errors due to the measuring-circuit impedance and response, or due to leakage and stray currents arising from the network capacitors or the mounting system; and (b) random errors in measuring capacitance, resistance, voltage, time, etc. Paschkis and Heisler [16] have shown that for the case where leakage is significant, the error due to network capacitor or mounting system leakage decreases as the number of sections of the network decreases. The versatility of the time scale employed here permits operation with network resistors below the megohm range and capacitors below the microfarad range for all materials under study, thereby minimizing stray currents due to the network elements. The parallel impedance introduced by the discharge-circuit elements and the measuring circuit is of the order of several thousand megohms. The extent to which the photoformer can generate a square-wave pulse at the operating frequencies is limited to about 1 percent of the time period available for measurements. The over-all sweep and signal-generation linearity of the device as measured with a linear-rise input function was found to be within the sweep-linearity specification of the oscilloscope alone, namely, "any 10-percent increment is within 10 percent of any other 10-percent increment . . .". It is estimated that for the one-dimensional case errors due to all experimental sources (which limit the accuracy of the method) are within 2 percent of full-scale. This is entirely apart from the much larger uncertainty associated with the values of the thermal properties of materials.

5.2. Comparison With Analytic Solution

Figure 12 is a comparison between the analog and analytic solutions for temperature curves within a

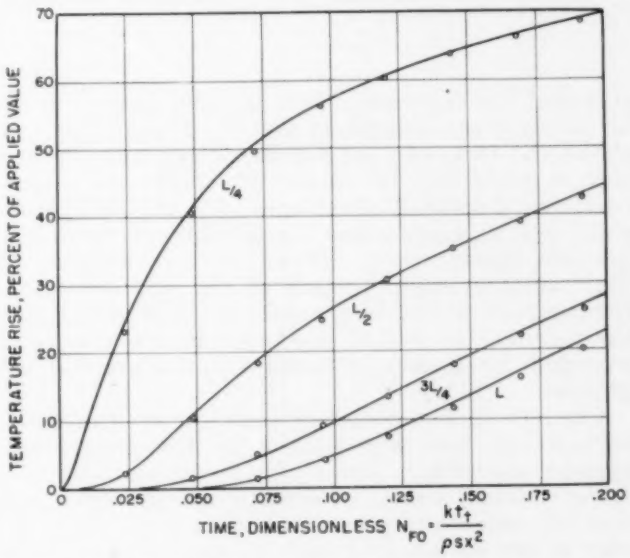

FIGURE 12. *Comparison between analog and analytic solutions for a one-dimensional problem.*

——, Analytic solution; ○, analog solution.

finite bar with perfectly insulated sides, one end of which is instantaneously raised to a temperature that is maintained constant thereafter while the other end remains perfectly insulated. From the preceding discussion on errors and since we are using a 20-section network representation, it is evident that the difference between the analog and analytic solutions are principally due to experimental sources. The maximum error is seen to be within the estimated 2 percent of the applied signal.

5.3. Comparison With Experimental Results

Figure 13 is a comparison between the analog and experimental results on a horizontal 4-in. concrete slab the lower surface of which was subjected to the standard fire exposure. This problem was set up as an illustrative example in section 2 and figure 14 shows the form of read-out oscilloscope display for such a problem. In normal use only two curves would be displayed simultaneously; the calibration scale, and a temperature versus time curve for the position under study. However, for purposes of illustrating a larger portion of the solution, time-temperature curves for a number of locations within the specimen as well as the two surfaces have been recorded by means of multiple photographic exposures.

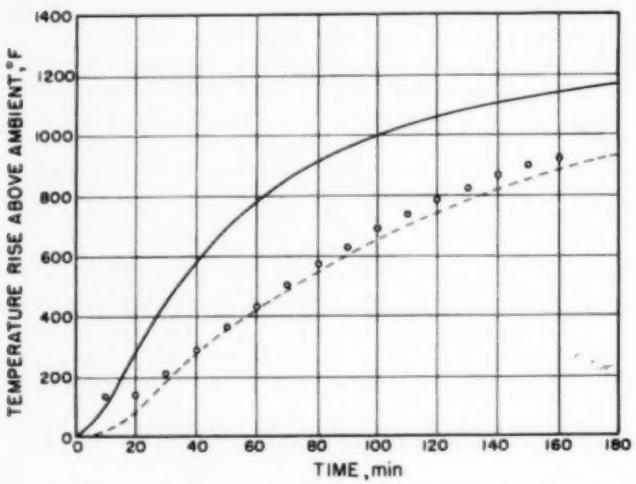

FIGURE 13. *Temperature rise at center-plane of a 4-in. concrete slab subjected to standard fire exposure.*

——, Analog solution $s=0.837$ joule/g ° C - - - -, analog solution $s=2.09$ joules/g ° C; ○, experimental results.

Convective and radiative heat loss on the upper surface has been represented by the appropriate varistor assembly. The analog result was obtained using constant values of density, specific heat, and thermal conductivity as noted in figure 2. The device is not set up to handle temperature or time-varying properties although these variations over the temperature range considered may be appreciable. Since the values themselves are subject to considerable uncertainty, their variation with temperature may be considered only a refinement. However, the effect of variable properties may be quickly investigated by duplicate tests at several different but constant values of the property in question. Or, alternately, by designing a line such that the thermal constants represented at each section vary as the mean temperature likely to be obtained at those points. The broken line in figure 13 represents the temperature curve for a specfic heat of 2.09 joules/g ° C (0.5 Btu/lb ° F) and illustrates how the device may be used to estimate thermal properties when direct thermal property measurement is impractical. The extent of the physical changes taking place during fire exposure and the role that moisture plays are a few of the uncertain variables which may cause considerable difference between experimental and analog results.

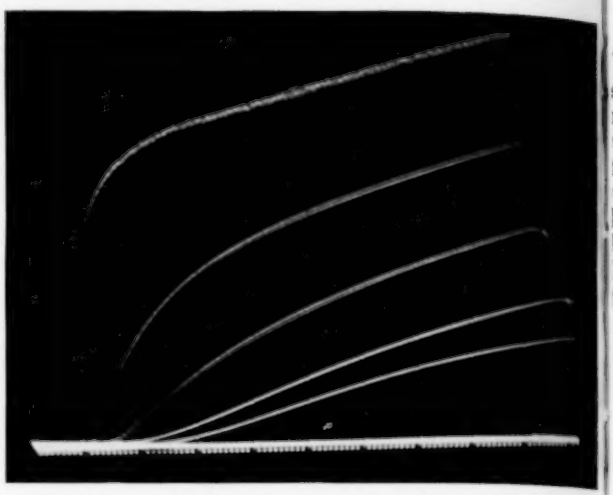

FIGURE 14. *Multiple-exposure photograph of read-out oscilloscope display for transient one-dimensional heat flow in a homogeneous slab.*

Large time-scale markers correspond to 1-hr time periods.

6. Conclusions

An electronic instrument has been constructed which permits the solution of transient heat-flow problems by means of analogous resistance-capacitance electrical networks. On the basis of the work completed, the reliability of the instrument as well as its flexibility with regard to input-signal waveform and time scale have been demonstrated. For an assumed one-dimensional problem in which thermal properties were independent of temperature and high accuracy was achieved in the construction of the electrical model, the errors were found to be within 2 percent of the applied signal. The instrument has been applied to a variety of problems in the field of fire research where a rapid estimation of the thermal endurance of structures of given thermal properties may be obtained. Although not yet attempted, the method may be extended to two- and three-dimensional transient heat-flow problems.

The authors acknowledge the assistance of Dwight Y. Sumida for performing the computations necessary for the error analysis, of James S. Evans, Jr., now with Hughes Aircraft Company, for design of the cathode-follower circuit, and of William H. Bailey for aid in assembling the device and for the preparation of the illustrations. They also appreciate the kind permission granted by Mr. E. O. P. Klein and by Professors Y. S. Touloukian and J. R. Eaton of Purdue University to print the results shown in figure 11.

7. References

[1] American Society for Testing Materials, Standard methods of fire tests of building construction and materials, ASTM Designation E110–55.

[2] D. I. Lawson and J. H. McGuire, The solution of transient heat flow problems by analogous electrical networks, Inst. Mech. Engr. Proc. [A] **167,** 275 (1952).

[3] G. Kirchhoff, Flow of an electric current through a plane, particularly through a circular disc (in German) Ann. Phys. Chem. **64,** 499 (1845); **67,** (1846).

[4] T. J. Higgins, Electroanalogic methods, Appl. Mechanics Rev., p. 1 (Jan. 1956); p. 49 (Feb. 1956); and p. 49 (Feb. 1957).

[5] W. W. Soroka, Experimental aids in engineering design analysis, Mech. Eng. **71,** 831 (Oct. 1940).

[6] W. W. Soroka, Analog methods in computation and simulation (McGraw-Hill Book Co., Inc., New York, N. Y., 1954).

[7] L. Beuken, Construction of an electrical analogy apparatus for the analysis of non-stationary heat flow, Econ. Tech. Tijdschr. **19,** No. 3, 43 (June 1939).

[8] V. Paschkis and H. D. Baker, A method for determining unsteady state heat transfer by means of an electrical analogue, ASME Trans. **64,** 105 (Feb. 1942).

[9] D. M. MacKay, A high-speed electronic function generator, Letter to the Editor, Nature **159,** 406 (March 22, 1947).

[10] D. J. Mynall, Electronic analog computing, Electronic Eng. **19,** 259 (1947).

[11] E. O. P. Klein, Y. S. Touloukian, and J. R. Eaton, Purdue University (personal communication).

[12] L. N. Clarke, The effect of the number of sections on the accuracy of a particular RC electrical analogue, Australian J. Appl. Sci. **3,** No. 2, 119 (June 1952).

[13] N. E. Friedmann, Truncation error in a semi-discrete analogy of the heat equation, J. Math. Phys. **35,** No. 3, 299 (Oct. 1956).

[14] J. C. Jaeger, Introduction to the Laplace transformation, p. 52 (Council for Scientific and Industrial Research, Melbourne, Australia, Jan. 1946).

[15] H. S. Carslaw and J. C. Jaeger, Conduction of heat in solids, p. 83 (Oxford University Press, 1947).

[16] V. Paschkis and M. P. Heisler, The accuracy of measurement in lumped R–C cable circuits as used in the study of transient heat flow, Trans. AIEE **63,** 165 (1944).

8. Appendix. Instrument and Components List

The special components and instruments used in the assembly are listed below. It is quite possible that other equally satisfactory components could have been used.

Generating oscilloscope. DuMont type 340–R, cathode ray tube type 5AQP–15, short-persistence phosphor.

Viewing oscilloscope. DuMont type 340–R, cathode ray tube type 5AQP–1.

Oscillator. Rutherford Electronics Co., model G1 pulse and square wave oscillator. Frequency range 1 to 100,000 pulses per second.

Electronic switch. DuMont type 330, arranged for triggered operation.

Multiplier phototube. RCA–6328, 9-stage type with S–4 response.

Photomultiplier power supply. C. J. Applegate model 123A, 1,000 v "Uniplug".

Counter tubes. Distributed by Atomic Instrument Co. One type GC10D single decade (scale of 10) and one type GS12D (scale of 12) "Dekatron" cold cathode glow transfer counter tubes.

Direct-current voltage supplies. Low-voltage regulated supply, −150 v, 125 ma. High-voltage regulated supply, +300 v, 300 ma.

WASHINGTON, April 29, 1958.

Journal of Research of the National Bureau of Standards Vol. 61, No. 2, August 1958 Research Paper 2893

Effect of Crystal Field and Spin-Orbit Coupling on Magnetic Susceptibility of Systems with f^2 Electron Configuration*

Charles M. Herzfeld and Daniel B. Levine

The effects of a crystal field of octahedral symmetry and of spin-orbit coupling on an ion with f^2 electron configuration are considered. Only fourth-degree terms in the crystal-field potential are taken into account. The eigenvalues and eigenvectors of the resulting 33×33 secular determinant are determined numerically on the 704 electronic computer at the National Bureau of Standards for eight values of D/ζ, where D is a crystal-field parameter, and ζ the spin-orbit coupling constant of the ion. Perturbations by an external magnetic field are computed using second-order perturbation theory. All eigenvalues are tabulated for $D/\zeta=-10^{-4}$, -2×10^{-4}, -5×10^{-4}, -10^{-3}, -2×10^{-3}, -5×10^{-3}, -10^{-2}, -10^{-1}. They can be adapted directly to any finite nonzero positive value of ζ and, by interpolation, for values of D/ζ not tabulated. The magnetic susceptibility of a powder is calculated and displayed as a function of temperature and D/ζ, for $\zeta=\infty$, 10^3 cm^{-1}, and 5×10^2 cm^{-1}. The relation of the results of the calculations to measurements on compounds of U^{+4} is discussed.

1. Introduction

The magnetic and optical properties of ionic and atomic species in solids are affected considerably by their neighbors in the lattice. Crystal-field theory [1][1] furnishes a simple but reliable technique for taking such effects into account. In this paper are discussed the combined effects of the crystal field and the ionic spin-orbit coupling on the magnetic susceptibility of ions with an f^2 electron configuration. Examples of such systems are the Nd^{+3} ($4f^2$) and U^{+4} ($5f^2$) salts; in the discussion the results are applied to some of the latter. Penney and Schlapp [2] have studied the properties of ions with f^2 configuration in a crystal field of cubic symmetry, with the assumption that the energy of spin-orbit coupling is very large (effectively infinite) compared to the crystal-field effect. They considered terms of fourth degree in the potential expansion, but neglected terms of sixth degree. Recently Hutchison and Candela [3] have treated the problem taking the sixth-degree terms in the potential into account, but they also assumed the effect of the ionic spin-orbit coupling to be large compared to the crystal-field splittings. The calculation reported in this paper makes no special assumption about the relative size of the crystal-field effect and the spin-orbit coupling, but neglects the sixth-degree terms in the potential expansion.

The Hamiltonian of an ion embedded in a crystal lattice, in the presence of an external magnetic field, may be written schematically in the form

$$\mathrm{H}=\mathrm{H}_0+\zeta\, L\cdot S+\mathrm{H}_c+\mu\cdot H. \qquad (1)$$

Here H_0 is the sum of three types of terms: The kinetic energy of the electrons of the ion, the potential energy of the electrons in the field of the nucleus, and the energy of mutual repulsion of the electrons. The term proportional to ζ gives (approximately) the spin-orbit interaction of the electrons. H_c summarizes the perturbations of the electrons arising from the neighbors of the ion in the lattice, and $\mu\cdot H$ is the energy of the ion with magnetic moment μ in an external magnetic field H. The eigenvalues of H are required for the calculation of the magnetic susceptibility.

2. Eigenvalues of the Hamiltonian

The form of the crystal-field energy H_c depends on the symmetry of the site of the ion. If this symmetry is cubic, H_c can be written in the form [1]

$$\mathrm{H}_c=C+A\Sigma_i(x_i^4+y_i^4+z_i^4-(3/5)\,r_i^4)+\text{higher terms}. \qquad (2)$$

Here C is a constant which can be disregarded for this calculation, x_i, y_i, and z_i are the coordinates of the ith electron (the nucleus of the ion is at the origin), $r_i=(x_i^2+y_i^2+z_i^2)^{1/2}$, and A gives the magnitude and sign of the classical potential energy. Two cases of cubic symmetry are of interest: 1. The ion is at the center of a regular octahedron, with negative charges located at the vertices. 2. The ion is at the center of a cube, with negative charges located at the vertices. In this calculation only the octahedral case is considered, where $A=(35e\epsilon)/(4r_0^5)$, with e the electronic charge, ϵ the charge at a given vertex, and r_0 the distance from center to vertex.

The ground state of a free ion with f^2 electron configuration is $^3H_4$, but since the effect of spin-orbit coupling is to be taken into account explicitly, the crystal-field calculation must involve all 33 states of the ^3H Russell-Saunders level: $^3H_4$, $^3H_5$, and $^3H_6$. The most convenient representation is SLM_SM_L, with $S=1$ and $L=5$. The matrix for $\mathrm{H}_c+\zeta L\cdot S$ is written out explicitly in this representation, using matrix elements calculated from the formulas of

*This research was supported by the U. S. Air Force through the Air Force Office of Scientific Research of the Air Research and Development Command, under contract No. CSO and A 680-56-21. Reproduction in whole or in part is permitted for any purpose of the United States Government.

[1] Figures in brackets indicate the literature references at the end of this paper.

Schlapp and Penney [4]. This matrix depends on two unknown parameters: ζ, which gives the magnitude of the spin-orbit coupling, and D, the magnitude of the crystal-field perturbation. D is proportional to A of eq (2), and to $\langle r^4 \rangle$, the average of r^4 for the f electrons. These parameters are discussed below. The secular determinant of the 33×33 matrix so obtained can be factored into one 9×9 and three 8×8 determinants by rearranging rows and columns. The eigenvalues of the matrix are computed by solving for the roots of the factored secular determinants; the eigenvectors are also obtained. This computation was carried out on a 704 electronic computing machine, with a method due to Jacobi, adapted for machine use by Givens [5]. The eigenvalues are shown in figure 1 as a function of D/ζ. The eigenvectors (which are also functions of D/ζ) are not shown, because the effect of their variation with D/ζ can be taken into account more efficiently in ways discussed below.

The matrix $\mu \cdot H$ is calculated in the SLM_SM_L representation, and then transformed for each value of D/ζ to that representation in which $H_c + \zeta L \cdot S$ is diagonal, using the eigenvector matrix of $H_c + \zeta L \cdot S$ for the appropriate value of D/ζ. Then the eigenvalues of $\mu \cdot H$ are calculated with second-order perturbation theory.

The eigenvalues of $H_c + \zeta L \cdot S + \mu \cdot H$ are of the form $W = W_c + W_1 H + W_2 H^2$. Here W_c is the eigenvalue of $H_c + \zeta L \cdot S$, and W_1 and W_2 give the first-order and second-order contributions of $\mu \cdot H$. The values of W_c/ζ, W_1/β, and $W_2\zeta/\beta^2$ are tabulated in table 1, for the eight values of D/ζ for which the calculation has been carried out (β is the Bohr magneton). Each state is designated by a set N of two quantum numbers i and j; i is a label for the irreducible representation of the cubic group [6] of the level W_c, and j indicates the factor of the secular determinant in which the eigenvalue occurs. The original 33×33 secular determinant factors into four determinants. (One basis vector is given, to identify the determinants) D_1: $|M_L = 3,\ M_S = -1\rangle$, D_2: $|-5,\ -1\rangle$, D_3: $|-4,\ -1\rangle$, and D_4: $|4,\ 1\rangle$. D_1 is a 9×9 determinant, the others are 8×8. It turns out that the different states belonging to a degenerate level W_c arise always from different determinants, and further that the set of determinants from which they arise characterizes the irreducible representation of the octahedral group to which the level belongs [6]. Thus nondegenerate levels with $j=1$ belong to Γ_1, and those with $j=2$ belong to Γ_2. Doubly degenerate levels, always with $j=1$ and 2 belong, of course, to Γ_3. Triply degenerate levels with $j=1$, 3, and 4 belong to Γ_4, those with $j=2$, 3, and 4 to Γ_5. The method of assignment is simple. One Γ_1 state must be identified as such; the other assignments can be made by inspection, by noting whether any nonvanishing matrix elements of $\mu \cdot H$ connect Γ_1 with the unidentified

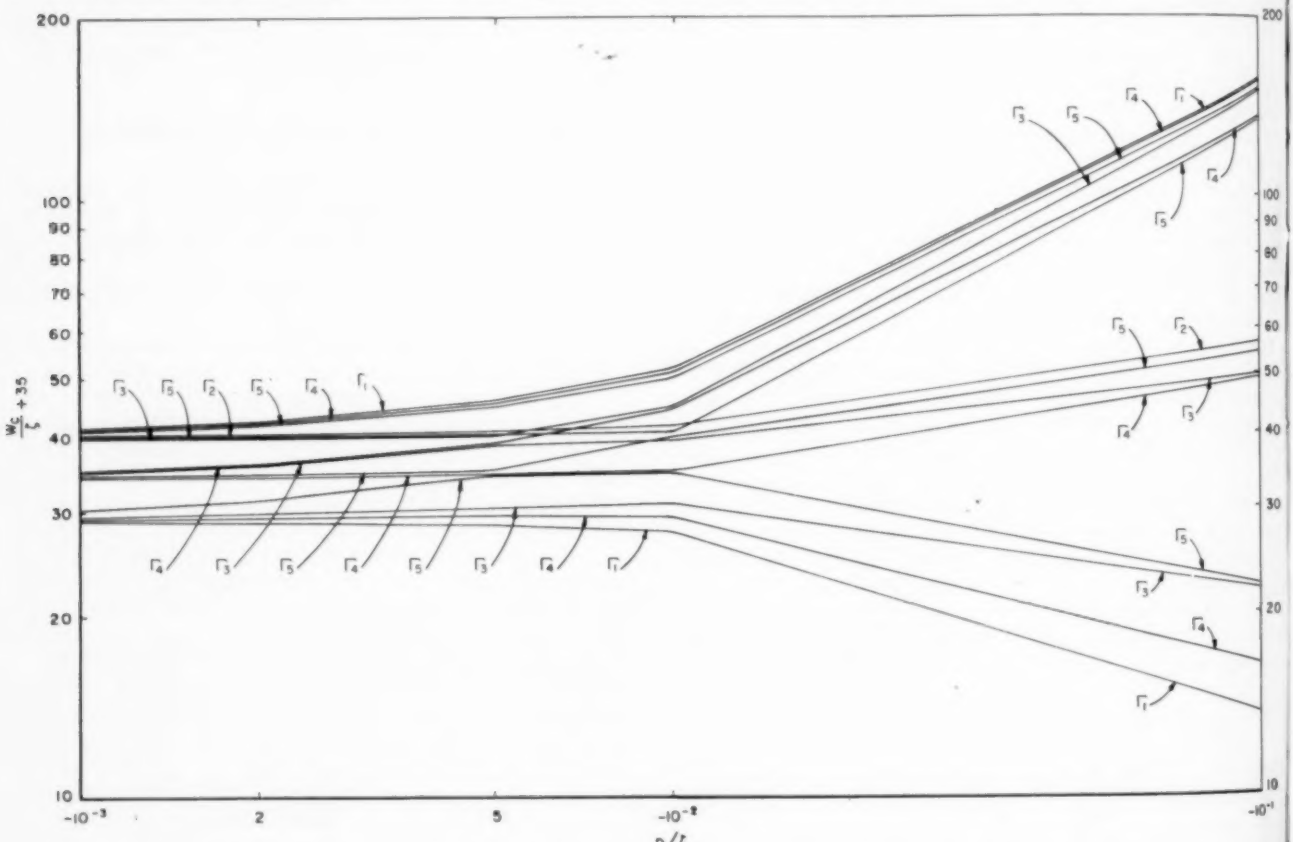

FIGURE 1. *Eigenvalues W_c of crystal-field and spin-orbit coupling as function of D/ζ.*
Calculations are made only for the values shown on abscissa.

TABLE 1. *Coefficients in expansion of energy levels:* $W = W_c + W_1 H + W_2 H^2$

$D/\zeta = -10^{-4}$				$D/\zeta = -2\times10^{-4}$			
N	W_c/ζ	W_1/β	$W_2\zeta/\beta^2$	N	W_c/ζ	W_1/β	$W_2\zeta/\beta^2$
1, 1	−6.0138	0	−133.0	1, 1	−6.0276	0	−67.4
4, 1	−5.9820	0	−125.0	4, 1	−5.9646	0	−61.3
4, 3	−5.9820	−0.404	−12.4	4, 3	−5.9646	−0.411	−6.22
4, 4	−5.9820	.404	−12.4	4, 4	−5.9646	.411	−6.22
3, 1	−5.9592	0	258.0	3, 1	−5.9194	0	129.0
3, 2	−5.9592	0	−37.50	3, 2	−5.9194	0	−18.8
5, 2	−5.8901	0	37.31	5, 2	−5.7801	0	18.7
5, 3	−5.8901	1.998	12.2	5, 3	−5.7801	1.999	6.05
5, 4	−5.8901	−1.998	12.2	5, 4	−5.7801	−1.999	6.05
4, 1	−0.9936	0	−25.5	4, 1	−0.9872	0	−12.4
4, 3	−.9936	−3.013	−253.0	4, 3	−.9872	−3.006	−132.62
4, 4	−.9936	3.013	−253.0	4, 4	−.9872	3.006	−132.62
5, 2	−.9724	0	−75.02	5, 2	−.9454	0	−37.0
5, 3	−.9724	−2.587	221.0	5, 3	−.9454	−2.581	117.0
5, 4	−.9724	2.587	221.0	5, 4	−.9454	2.581	117.0
3, 1	−.9156	0	−1490.0	3, 1	−.8303	0	−789.0
3, 2	−.9156	0	75.06	3, 2	−.8303	0	37.0
4, 1	−.9055	0	1520.0	4, 1	−.8107	0	801.0
4, 3	−.9055	2.506	31.8	4, 3	−.8107	2.505	15.6
4, 4	−.9055	−2.506	31.8	4, 4	−.8107	−2.505	15.6
3, 1	4.9924	0	−25.3	3, 1	4.9848	0	−1.34
3, 2	4.9924	0	−5739.6	3, 2	4.9848	0	−2925.0
5, 2	4.9985	0	5041.9	5, 2	4.9971	0	2569.0
5, 3	4.9985	−0.696	−46.4	5, 3	4.9971	−0.688	−23.2
5, 4	4.9985	.696	−46.4	5, 4	4.9971	.688	−23.2
2, 2	5.0168	0	623.82	2, 2	5.0336	0	309.0
5, 2	5.0823	0	93.97	5, 2	5.1652	0	46.7
5, 3	5.0823	−2.224	−956.0	5, 3	5.1652	−2.230	−478.0
5, 4	5.0823	2.224	−956.0	5, 4	5.1652	2.230	−478.0
4, 1	5.0994	0	−1165.0	4, 1	5.1992	0	−635.0
4, 3	5.0994	−0.586	1000.0	4, 3	5.1992	−0.590	501.0
4, 4	5.0994	.586	1000.0	4, 4	5.1992	.590	501.0
1, 1	5.1146	0	1190.0	1, 1	5.2291	0	636.0

$D/\zeta = -5\times10^{-4}$				$D/\zeta = -10^{-3}$			
N	W_c/ζ	W_1/β	$W_2\zeta/\beta^2$	N	W_c/ζ	W_1/β	$W_2\zeta/\beta^2$
1, 1	−6.0692	0	−27.43	1, 1	−6.1394	0	−14.08
4, 1	−5.9158	0	−25.66	4, 1	−5.8451	0	−13.09
4, 3	−5.9158	−0.4251	−2.586	4, 3	−5.8451	−0.449	−1.37
4, 4	−5.9158	.4251	−2.586	4, 4	−5.8451	.449	−1.37
3, 1	−5.8053	0	52.91	3, 1	−5.6317	0	26.99
3, 2	−5.8053	0	−7.670	3, 2	−5.6317	0	−3.967
5, 2	−5.4507	0	7.475	5, 2	−4.9024	0	3.757
5, 3	−5.4507	2.000	2.405	5, 3	−4.9024	1.998	1.18
5, 4	−5.4507	−2.000	2.405	5, 4	−4.9024	−1.998	1.18
4, 1	−0.9682	0	−4.692	4, 1	−0.9363	0	−2.122
4, 3	−.9682	−2.978	−56.13	4, 3	−.9363	−2.935	−30.90
4, 4	−.9682	2.978	−56.13	4, 4	−.9363	2.935	−30.90
5, 2	−.8685	0	−14.09	5, 2	−.7527	0	−6.546
5, 3	−.8685	−2.578	50.02	5, 3	−.7527	−2.576	27.90
5, 4	−.8685	2.578	50.02	5, 4	−.7527	2.576	27.90
3, 1	−.5695	0	−335.9	3, 1	−.1203	0	−198.0
3, 2	−.5695	0	14.14	3, 2	−.1203	0	6.605
4, 1	−.5243	0	340.7	4, 1	−.0421	0	200.1
4, 3	−.5243	2.501	6.128	4, 3	−.0421	2.492	2.99
4, 4	−.5243	−2.501	6.128	4, 4	−.0421	−2.492	2.99
3, 1	4.9628	0	−4.931	3, 1	4.9280	0	−2.382
3, 2	4.9628	0	−1137.0	3, 2	4.9280	0	−561.5
5, 2	4.9936	0	990.3	5, 2	4.9900	0	485.8
5, 3	4.9936	−0.6639	−9.030	5, 3	4.9900	−0.621	−4.33
5, 4	4.9936	.6639	−9.030	5, 4	4.9900	.621	−4.33
2, 2	5.0840	0	129.1	2, 2	5.1680	0	67.30
5, 2	5.4176	0	18.01	5, 2	5.8490	0	8.557
5, 3	5.4176	−2.258	−196.8	5, 3	5.8490	−2.300	−103.0
5, 4	5.4176	2.258	−196.8	5, 4	5.8490	2.300	−103.0
4, 1	5.5003	0	−257.1	4, 1	6.0076	0	−134.4
4, 3	5.5003	−0.5979	206.0	4, 3	6.0076	−0.614	107.00
4, 4	5.5003	.5979	206.0	4, 4	6.0076	.614	107.00
1, 1	5.5732	0	262.2	1, 1	6.1474	0	137.0

TABLE 1. *Coefficients in expansion of energy levels:* $W = W_e + W_1 H + W_2 H^2$—Continued

$D/\zeta = -2\times10^{-3}$				$D/\zeta = -5\times10^{-3}$			
N	W_e/ζ	W_1/β	$W_2\zeta/\beta^2$	N	W_e/ζ	W_1/β	$W_2\zeta/\beta^2$
1, 1	−6.2820	0	−7.43	1, 1	−6.722	0	−3.262
4, 1	−5.7382	0	−6.910	4, 1	−5.616	0	−3.271
4, 3	−5.7382	−0.504	−0.790	4, 3	−5.616	−0.7050	−0.5133
4, 4	−5.7382	.504	−0.790	4, 4	−5.616	.7050	−0.5133
3, 1	−5.3365	0	14.1	3, 1	−4.7223	0	6.304
3, 2	−5.3365	0	−2.15	3, 2	−4.7223	0	−1.222
5, 2	−3.8105	0	1.92	5, 2	−0.7915	0	0.7243
5, 3	−3.8105	1.991	0.555	5, 3	−.7915	0.4043	−14.86
5, 4	−3.8105	−1.991	0.555	5, 4	−.7915	−.4043	−14.86
4, 1	−0.8705	0	−0.873	4, 1	−.6382	0	−0.2233
4, 3	−.8705	−2.830	−18.4	4, 3	−.6382	−2.494	2.200
4, 4	−.8705	2.830	−18.4	4, 4	−.6382	2.494	2.200
5, 2	−.5600	0	−2.90	5, 2	.0147	0	−0.8934
5, 3	−.5600	−2.571	17.0	5, 3	.0147	−1.071	12.34
5, 4	−.5600	2.571	17.0	5, 4	.0147	1.071	12.34
3, 1	.8211	0	−138.0	3, 1	3.623	0	−39.13
3, 2	.8211	0	2.94	3, 2	3.623	0	−3.4767
4, 1	.9373	0	138.0	4, 1	3.946	0	35.88
4, 3	.9373	2.471	1.46	4, 3	3.946	2.380	0.5397
4, 4	.9373	−2.471	1.46	4, 4	3.946	−2.380	.5397
3, 1	4.8674	0	−1.09	3, 1	4.979	0	3.132
3, 2	4.8674	0	−276.0	3, 2	4.979	0	−291.4
5, 2	4.9917	0	236.0	5, 2	5.069	0	277.1
5, 3	4.9917	−0.543	−1.97	5, 3	5.069	−0.3325	−0.5070
5, 4	4.9917	.543	−1.97	5, 4	5.069	.3325	−.5070
2, 2	5.3360	0	36.4	2, 2	5.840	0	17.88
5, 2	6.7467	0	3.89	5, 2	9.628	0	1.256
5, 3	6.7467	−2.375	−55.9	5, 3	9.628	−2.5010	−26.82
5, 4	6.7467	2.375	−55.9	5, 4	9.628	2.5010	−26.82
4, 1	7.0394	0	−72.7	4, 1	10.228	0	−35.21
4, 3	7.0394	−0.630	58.1	4, 3	10.228	−0.6806	27.61
4, 4	7.0394	.630	58.1	4, 4	10.228	.6806	27.61
1, 1	7.2980	0	74.0	1, 1	10.762	0	35.78

$D/\zeta = -10^{-2}$				$D/\zeta = -10^{-1}$			
N	W_e/ζ	W_1/β	$W_2\zeta/\beta^2$	N	W_e/ζ	W_1/β	$W_2\zeta/\beta^2$
1, 1	−7.4748	0	−1.829	1, 1	−21.447	0	−0.384
4, 1	−5.8051	0	−1.796	4, 1	−18.68	0	−.012
4, 3	−5.8051	−1.0826	−0.4688	4, 3	−18.68	−2.289	−.119
4, 4	−5.8051	1.0826	−.4688	4, 4	−18.68	2.289	−.119
3, 1	−4.1400	0	3.305	3, 1	−13.228	0	.087
3, 2	−4.1400	0	−1.252	3, 2	−13.228	0	−55.54
5, 2	−0.3442	0	−0.3923	5, 2	−12.856	0	55.19
5, 3	−.3442	−2.706	−20.34	5, 3	−12.856	−2.583	−0.064
5, 4	−.3442	2.706	−20.34	5, 4	−12.856	2.583	−.064
4, 1	−.1148	0	−0.0517	4, 1	14.374	0	.041
4, 3	−.1148	−1.972	19.86	4, 3	14.374	−0.470	−.872
4, 4	−.1148	1.972	19.86	4, 4	14.374	.470	−.872
3, 1	4.2067	0	−0.1733	3, 1	14.81	0	0.216
3, 2	4.2067	0	−22.78	3, 2	14.81	0	−1.891
5, 2	4.8578	0	4.865	5, 2	19.424	0	−3.865
5, 3	4.8578	1.454	−0.6913	5, 3	19.424	−0.143	0.972
5, 4	4.8578	−1.454	−.6913	5, 4	19.424	.143	.972
5, 2	5.5857	0	6.340	2, 2	21.8	0	6.010
5, 3	5.5857	0.3332	0.8526	5, 2	99.38	0	0.0443
5, 4	5.5857	−.3332	.8526	5, 3	99.38	0.427	−1.46
2, 2	6.6800	0	12.03	5, 4	99.38	−.427	−1.46
4, 1	9.0480	0	−22.92	4, 1	100.483	0	−0.966
4, 3	9.0480	2.247	0.2085	4, 3	100.483	1.426	.874
4, 4	9.0480	−2.247	0.2085	4, 4	100.483	−1.426	.874
3, 1	9.6933	0	23.06	3, 1	114.018	0	−0.004
3, 2	9.6933	0	0.6781	3, 2	114.018	0	−.0716
5, 2	14.741	0	.5104	5, 2	115.452	0	.1186
5, 3	14.741	−2.582	−15.99	5, 3	115.452	−1.206	−2.00
5, 4	14.741	2.582	−15.99	5, 4	115.452	1.206	−2.00
4, 1	15.712	0	−21.92	4, 1	119.223	0	−6.65
4, 3	15.712	−0.6925	16.48	4, 3	119.223	−0.161	2.67
4, 4	15.712	.6925	16.48	4, 4	119.223	.161	2.67
1, 1	16.555	0	22.33	1, 1	121.247	0	7.67

level. The lowest lying level belongs to Γ_1 and arises from D_1. Matrix elements for $\mu \cdot H$ that connect any eigenvector of D_1 with any vector of the matrices of the other determinants must vanish. Therefore only levels with $j=1$ are thus connected to Γ_1, and hence levels with $j=1$, 3, and 4 belong to Γ_4. Similarly for all other levels.

The results in table I cover a wide range of situations, and allow one to calculate magnetic properties quite readily. The method of presentation of the results permits their adaptation in two ways. First, the eigenvalues can be adapted to any finite nonzero value of the spin-orbit coupling constant ζ. For positive ζ the problem corresponds to the octahedral case with f^2 configuration. (For negative ζ the problem corresponds to the cubic case with f^{12} configuration.) The adaptation is straightforward. Thus for $D/\zeta = -10^{-4}$ and for the state $N=2,3$, $W_c/\zeta = -5.9820$, $W_1/\beta = -0.404$, $W_2\zeta/\beta^2 = -12.4$. Hence $W_c = -5.9820\zeta$, $W_1 = -0.404\beta$, $W_2 = -12.4\beta^2/\zeta$. If $\zeta = 10^3$ cm^{-1}, $W_c = -5.9820 \times 10^3$ cm^{-1}, $W_1 = -0.404\beta$, $W_2 = -12.4\beta^2 \times 10^{-3}$. The second adaptation involves interpolation of the results for values of D/ζ other than those covered here. This can be accomplished by a graphical interpolation of the values in table I. These vary sufficiently slowly to permit interpolation of W_c, W_1, and W_2 for each state.

3. Calculated Magnetic Susceptibility and Discussion of the Results

The magnetic susceptibility per mole, χ_M, of ions with f^2 configuration was calculated [7] for a powder, as a function of temperature and D. The results are plotted as χ^{-1} in figure 2. The results for our calculation for $\zeta = 10^3$ cm^{-1}, and $\zeta = 5 \times 10^2$ cm^{-1} are given for several values of D. Also some results of the theory of Penney and Schlapp [2] (effectively $\zeta = \infty$) are shown. For $D/\zeta = -10^{-1}$, -10^{-2}, and -5×10^{-3}, with $\zeta = 10^3$ cm^{-1}, χ^{-1} is practically independent of temperature up to 300°K, and equals 5,102, 1,080, and 602, respectively.

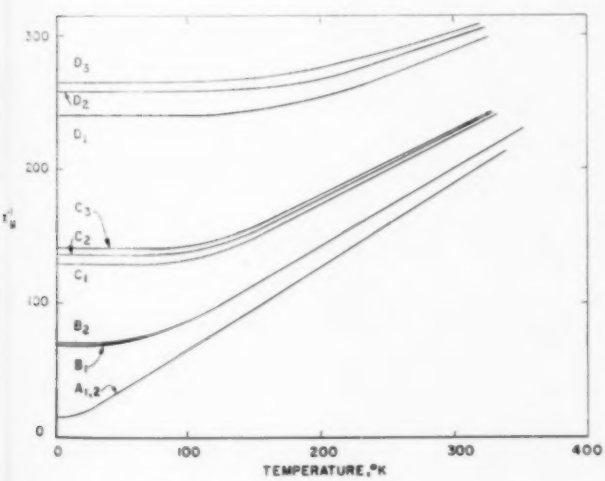

FIGURE 2. χ^{-1} *versus temperature.*

Curves A_k for $D = -0.1$ cm^{-1}; B_k for $D = -0.5$ cm^{-1}; C_k for $D = -1.0$ cm^{-1}; and D_k for $D = -2.0$ cm^{-1}. $k=1$ corresponds to $\zeta = 500$ cm^{-1}, $k=2$ to $\zeta = 10^3$ cm^{-1}. Curves C_3 and D_3 are taken from Penney and Schlapp theory ($\zeta = \infty$), and crystal-field splittings comparable to C_2 and D_2, respectively.

The matrix elements of $H_c + \zeta \vec{L} \cdot S$ are given [2] in terms of the two undetermined parameters ζ and D. The value of ζ in a solid is uncertain, though the free ion value is often a useful first approximation. The correct value of ζ for U^{+4} lies probably [3] between 600 cm^{-1} and 800 cm^{-1}. Thus the calculated susceptibilities reported in this paper bracket the most likely value. Direct calculation, using eigenstates $|f^2\,{}^3H\,M_S M_L\rangle$ obtained by standard methods [8] shows for the regular octahedron that the parameter $D = -\sqrt{2\pi}\epsilon\langle r^4\rangle/(9r_0^5)$, indicating that D is negative.

The calculations reported in this paper agree in a general way with the measurements and calculations of Hutchison and Candela [3] on $[(CH_3)_4N]_2$ U Cl_6. They find a value of $\chi_M^{-1} = 520$, which is independent of temperature over the range measured, and explain this satisfactorily with their theory. Because the calculations reported in this paper always give a nondegenerate groundstate (Γ_1), they also give a temperature independent χ_M^{-1} for sufficiently large crystal-field splittings, and this for any value of ζ. The calculations reported in this paper shed some light on other measurements [9] of powder susceptibilities of compounds containing U^{+4}. These measurements (on $U(SO_4)_2$ $4H_2O$, $U(C_2O_4)_2$ $6H_2O$, UF_4NaF, (γ)$UF_4 2NaF$, and $UF_4 3NaF$) cannot be explained by a theory of the Penney and Schlapp type (i. e., $\zeta = \infty$), nor by the present theory, though the present calculations somewhat improve agreement with the measurements on $U(C_2O_4)$ $6H_2O$. This indicates that the finite value of ζ does not play a very important role in these systems, and that a more realistic crystal-field potential, involving terms of second, fourth, and sixth degree, is required for an understanding of these systems.

The computation of the eigenvalues W and the eigenvectors was carried out on a 704 computer by Miss Irene Stegun of the Computation Section of the Applied Mathematics Division of the National Bureau of Standards. Her help was essential for this study, and is gratefully acknowledged.

4. References

[1] B. Bleaney and K. W. H. Stevens, Repts. Progr. Phys. **16,** 108 (1953).
[2] W. G. Penney and R. Schlapp, Phys. Rev. **41,** 194 (1932).
[3] C. A. Hutchison, Jr., and G. Candela, J. Chem. Phys. **27,** 707 (1957).
[4] R. Schlapp and W. G. Penney, Phys. Rev. **42,** 666 (1932).
[5] W. Givens, Numerical computation of the characteristic values of a real symmetric matrix, Oak Ridge Report ORNL 1574 (1954).
[6] H. Bethe, Ann. Phys. **3,** 133 (1929).
[7] J. H. Van Vleck, The theory of electric and magnetic susceptibilities, ch. VII (Oxford University Press, New York, N. Y., 1932).
[8] E. U. Condon and G. H. Shortley, The theory of atomic spectra, ch. 8 (Cambridge University Press, New York, N. Y., 1935).
[9] C. A. Hutchison, Jr., and C. M. Herzfeld, J. Chem. Phys. **23,** 1650 (1950).

WASHINGTON, April 18, 1958.

U. S. GOVERNMENT PRINTING OFFICE: 1958

THE NATIONAL BUREAU OF STANDARDS

The scope of activities of the National Bureau of Standards at its headquarters in Washington, D. C., and its major laboratories in Boulder, Colorado, is suggested in the following listing of the divisions and sections engaged in technical work. In general, each section carries out specialized research, development, and engineering in the field indicated by its title. A brief description of the activities, and of the resultant publications, appears on the inside of the front cover.

WASHINGTON, D. C.

Electricity and Electronics. Resistance and Reactance. Electron Devices. Electrical Instruments. Magnetic Measurements. Dielectrics. Engineering Electronics. Electronic Instrumentation. Electrochemistry.

Optics and Metrology. Photometry and Colorimetry. Optical Instruments. Photographic Technology. Length. Engineering Metrology.

Heat. Temperature Physics. Thermodynamics. Cryogenic Physics. Rheology. Engine Fuels. Free Radicals Research.

Atomic and Radiation Physics. Spectroscopy. Radiometry. Mass Spectrometry. Solid State Physics. Electron Physics. Atomic Physics. Neutron Physics. Nuclear Physics. Radioactivity. X-rays. Betatron. Nucleonic Instrumentation. Radiological Equipment.

Chemistry. Organic Coatings. Surface Chemistry. Organic Chemistry. Analytical Chemistry. Inorganic Chemistry. Electrodeposition. Molecular Structure and Properties of Gases. Physical Chemistry. Thermochemistry. Spectrochemistry. Pure Substances.

Mechanics. Sound. Mechanical Instruments. Fluid Mechanics. Engineering Mechanics. Mass and Scale. Capacity, Density, and Fluid Meters. Combustion Controls.

Organic and Fibrous Materials. Rubber. Textiles. Paper. Leather. Testing and Specifications. Polymer Structure. Plastics. Dental Research.

Metallurgy. Thermal Metallurgy. Chemical Metallurgy. Mechanical Metallurgy. Corrosion. Metal Physics.

Mineral Products. Engineering Ceramics. Glass. Refractories. Enameled Metals. Concreting Materials. Constitution and Microstructure.

Building Technology. Structural Engineering. Fire Protection. Air Conditioning, Heating, and Refrigeration. Floor, Roof, and Wall Coverings. Codes and Safety Standards. Heat Transfer.

Applied Mathematics. Numerical Analysis. Computation. Statistical Engineering. Mathematical Physics.

Data Processing Systems. SEAC Engineering Group. Components and Techniques. Digital Circuitry. Digital Systems. Analog Systems. Application Engineering.

• Office of Basic Instrumentation.

• Office of Weights and Measures.

BOULDER, COLORADO

Cryogenic Engineering. Cryogenic Equipment. Cryogenic Processes. Properties of Materials. Gas Liquefaction.

Radio Propagation Physics. Upper Atmosphere Research. Ionospheric Research. Regular Propagation Services. Sun-Earth Relationships. VHF Research.

Radio Propagation Engineering. Data Reduction Instrumentation. Modulation Systems. Navigation Systems. Radio Noise. Tropospheric Measurements. Tropospheric Analysis. Radio Systems Application Engineering. Radio Meteorology.

Radio Standards. High Frequency Electrical Standards. Radio Broadcast Service. High Frequency Impedance Standards. Electronic Calibration Center. Microwave Physics. Microwave Circuit Standards.

Recent Publications of the National Bureau of Standards

Periodicals

Journal of Research of the National Bureau of Standards, Volume 60, No. 6, June 1958 (RP2867 to RP2876 incl.). 60 cents. Annual subscription $4.00, $1.25 additional for foreign mailing.

Technical News Bulletin, Volume 42, No. 6, June 1958. 10 cents. Annual subscription $1.00. 35 cents additional for foreign mailing.

Basic Radio Propagation Predictions for September 1958. Three months in advance. CRPL–D 166. Issued June 1958. 10 cents. Annual subscription $1.00, 25 cents additional for foreign mailing.

Circulars

C593. The federal basis for weights and measurements. 30 cents.*

Handbooks

H66. Safe design and use of industrial beta-ray sources. 20 cents.*

Available from the Superintendent of Documents, U. S. Government Printing Office, Washington 25, D. C. The three NBS periodicals are available on a 1-, 2-, or 3-year subscription basis, although no reduction in rates can be made.

**Foreign postage, one-fourth additional.*

UNITED STATES
GOVERNMENT PRINTING OFFICE
DIVISION OF PUBLIC DOCUMENTS
WASHINGTON 25, D. C.
OFFICIAL BUSINESS

PENALTY FOR PRIVATE USE TO AVOID PAYMENT OF POSTAGE, $300 (GPO)

UNIVERSITY OF MICHIGAN
GENERAL LIBRARY
DOCUMENTS DIVISION
1276 ANN ARBOR MICH

Contents

		Page
Carbon-14 carboxy-labeled polysaccharides. Joseph D. Moyer and Horace S. Isbell.	RP2886	71
Heat of formation of sodium calcium aluminate. Edwin S. Newman.	RP2887	75
Thermal degradation of polyacrylonitrile, polybutadiene, and copolymers of butadiene with acrylonitrile and styrene. Sidney Straus and Samuel L. Madorsky.	RP2888	77
On the motion of two cylinders in an ideal fluid. Lloyd H. Carpenter.	RP2889	83
Properties of sodium titanium silicate glasses. Edgar H. Hamilton and Given W. Cleek.	RP2890	89
Wavelengths from thorium-halide lamps. William F. Meggers and Robert W. Stanley.	RP2891	95
An electrical-analog method for transient heat-flow analysis. A. F. Robertson and Daniel Gross.	RP2892	105
Effect of crystal field and spin-orbit coupling on magnetic susceptibility of systems with f^2 electron configuration. Charles M. Herzfeld and Daniel B. Levine.	RP2893	117

[A list of recent NBS publications is given on page 3 of the cover.]

For sale by the Superintendent of Documents, U. S. Government Printing Office, Washington 25, D. C. Price 60 cents (single copy). Subscription price: $4.00 a year; $1.25 additional for foreign mailing.
UNITED STATES GOVERNMENT PRINTING OFFICE, WASHINGTON : 1958